Transcriptional regulation by the BET proteins in the developing and adult brain

Josefa Sullivan

A dissertation submitted to the Graduate Faculty of the Graduate School of Biomedical Sciences, Neuroscience Doctoral Program, in partial fulfillment of the requirements for the degree of Doctor of Philosophy, Icahn School of Medicine at Mount Sinai

Dissertation Adviser: Dr. Anne Schaefer

2019

ProQuest Number: 27741382

![ProQuest logo]

ProQuest 27741382

_____

_____

Approval Page

This manuscript has been read and accepted by the Graduate Faculty of the Graduate School of Biomedical Sciences, in satisfaction of the dissertation requirement for the degree of Doctor of Philosophy.
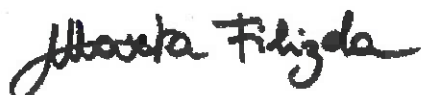
_____ 18th of February, 2020

Dissertation Advisor – Anne Schaefer, M.D., Ph.D. Date

_____ 2/24/2020

Dean – Marta Fillizola, Ph.D. Date

Thesis Committee Members:

Dr. Schahram Akbarian

Dr. Deanna Benson

Dr. Patrizia Casaccia

Dr. Eric Nestler

Dr. Helen Bateup (University of California – Berkeley)

Abstract

The mammalian brain is a highly complex organ that integrates diverse sensory inputs, allowing us to adapt to changes in our environment. The intricate architecture of the brain mimics its diverse functionality and is composed of numerous neuronal and glial subtypes. How this diversity in form and function arises in cells with the same genome is thought to be coordinated by specific programs of gene expression. It is becoming increasingly clear that dysregulation of these transcriptional programs during development and in adulthood has a profoundly detrimental impact on brain health. The induction of cell-type-specific gene networks in peripheral cells is controlled by the bromodomain and extraterminal domain-containing (BET) protein family [1]; however their function in the central nervous system is largely unknown. My dissertation identifies fundamental roles for BET proteins in the developing and adult brain. We show that BETs are epigenetic regulators of neuronal and synaptic genes involved in ASD-like behaviors in mice. Second, we describe the transcriptional control of microglial inflammation by BETs, highlighting the diverse cell type-specific functions of these proteins. Lastly we show that, in mature neurons, BETs promote metabolic gene network expression and inhibition of this network increases neuronal lifespan and survival in response to toxic stimuli. This work provides a comprehensive examination of the role of BET-dependent transcription in the central nervous system and offers a novel strategy for the treatment of neurodegenerative disorders.

Acknowledgments

I am very grateful to the many wonderful scientists, in both academia and industry, I have encountered throughout my doctoral work. You have greatly shaped how I think about science, and it has been a pleasure to work with you. Thank you.

Dr. Anne Schaefer, you have been a dedicated, passionate advisor who has pushed me to see past what was expected to envision what was possible.

Drs. Schahram Akbarian, Deanna Benson, Patrizia Casaccia, and Eric Nestler, thank you for your invaluable feedback and support.

Dr. Alexander Tarakhovsky and his lab members, both past and present, your time and perspectives are greatly appreciated.

Dr. Rab Prinjha, Dr. Huw Lewis and all of our fantastic collaborators at GlaxoSmithKline, thank you for your expert guidance. It has been an honor to work with such a great team.

I came to graduate school to improve professionally, but I never expected to gain such dear friendships. Thank you for the laughs and commiseration over the years. I can't wait to see the great things that you each achieve.

To my family and my husband, Jake, I cannot express how deeply I appreciate your unwavering confidence and support. I look forward to facing whatever the next challenge is because I know that we'll go through it together.

Lastly, this work is dedicated to Helen Nowick Sullivan and Katherine Boyce Patrick.

Contributions

This work was done in collaboration with many gifted scientists to whom I am deeply grateful. Their contributions are listed below:

Huw Lewis, James Gray, Neil Garton, Chun-Wa Chung, Nicholas Smithers, Inma Rioja and Rab Prinjha at GlaxoSmithKline developed I-BET858 and advised this project over the years.

Li Shen, Immanuel Purushothaman, Yong-Hwee Loh, Zichen Wang, and Fan Zhang performed bioinformatics analysis of RNA and CHIP sequencing data.

Jacob Varley helped develop the code used for gene length analysis in Chapter 3.

Ana Badimon assisted with I-BET858 injections and performed behavioral assays on the adult I-BET858 cohort in Chapter 3.

Pinar Ayata performed the microglia TRAP experiment in Chapter 4.

Sarah Veugelen performed hypoxia and $A\beta_{1-43}$ experiments and assisted with westerns in Chapter 5.

Sahil Agarwal generated the survival curve in Chapter 5.

Seahorse metabolic experiments from Chapter 5 were done in collaboration with Maureen Erwin.

Daniel Sevin, Johanna Vappiani, and Nao Iwamoto from Cellzome performed mass spectrometry analysis in Chapter 5.

Table of Contents

List of Figures

Chapter One

General Introduction, Background and Significance

Importance of Transcriptional Networks in the Brain

Gene transcription plays a major role in neuronal development and function. The acquisition of specific gene expression patterns during neuronal differentiation will determine the identity, morphology, and function of different neuron subtypes [2,3]. For example, striatal medium spiny neurons are an intermingled population with nearly indistinguishable morphologies. However, ribosome profiling reveals two distinct cell types with differential transcriptomes [2,4]. Single-cell sequencing further revealed that medium spiny neurons have a higher degree of heterogeneity and exist as a continuous spectrum of functional states based on their transcriptional profiles [5]. This diversification is driven in part by the action of "terminal selector" transcription factors (TFs) that regulate cohorts of genes that drive neuronal identity [6]. In Caenorhabditis elegans, terminal selector TFs have been identified for over two-thirds of the 118 neuron classes [7,8], although more work is required to understand how terminal selectors function in mammalian cells.

Highlighting the relationship between transcription and neurodevelopment, mutations in ubiquitously expressed transcriptional regulators or in non-coding regions have been causally linked to Autism Spectrum Disorders (ASD) [9–12]. Currently, more mutations have been identified in transcriptional regulators than in synaptic genes despite the widely accepted "synaptopathy" hypothesis of ASD [13]. A new theory of ASD etiology is emerging where impaired gene transcription shifts global gene networks rather than a single pathway [14,15]. Proper brain development, therefore, relies on tight

transcriptional regulation of inducible genes to coordinate appropriate subtype specification and circuitry formation. Once developed, these patterns must be maintained appropriately, in neurons and in glia, throughout life to ensure healthy brain function. Loss of this specification can lead to widespread brain dysfunction and degeneration [16–20]. However, there is much that remains unknown about transcriptional regulation in the central nervous system. Before we address specific questions in transcriptional regulation in the brain, we will first detail the molecular mechanisms controlling general transcription.

Principles of Transcription

DNA is the essential molecule in the cell that stores genetic information and passes it along to the next generation. It also provides the template for cellular functions by being transcribed into messenger RNA (mRNA) by RNA polymerases. The ribosome then translates mRNA into proteins of diverse function and localization [21,22]. These fundamental processes lie at the heart of all biological activity, but each poses unique challenges. To fit the length of the DNA strand into the nucleus, DNA is folded into an organized, three-dimensional structure. Aiding this process, 146 base pairs of DNA wrap 1.7 times around a protein complex termed the nucleosome [23]. The nucleosome is an octamer containing two copies of each core histone protein H2A, H2B, H3 and H4 which, due to their overall positive charge, tightly associate with negatively-

charged DNA [24] (Figure 1A). In eukaryotes, a fifth histone, H1, sits at the base of the nucleosome and binds to the entering and exiting DNA. This structure which Kornberg described as looking "rather like beads on a string," is the basic unit of chromatin and compacts DNA by 7-fold [25,26]. Present from archaea to eukaryotes, histones are among the most highly conserved proteins thus illustrating their importance to cellular function. Chromatin exists as a continuum between two major states or phases, tightly compacted heterochromatin or loose euchromatin. In heterochromatin, the beads on the string condense further by a factor of 40 to form the solenoid, a secondary structure which comprises a 30nm fiber of chromatin [26]. The nucleosome, while allowing for DNA compaction, presents a barrier for gene transcription. Heterochromatic DNA is inaccessible to the transcriptional machinery and is therefore transcriptionally inactive.
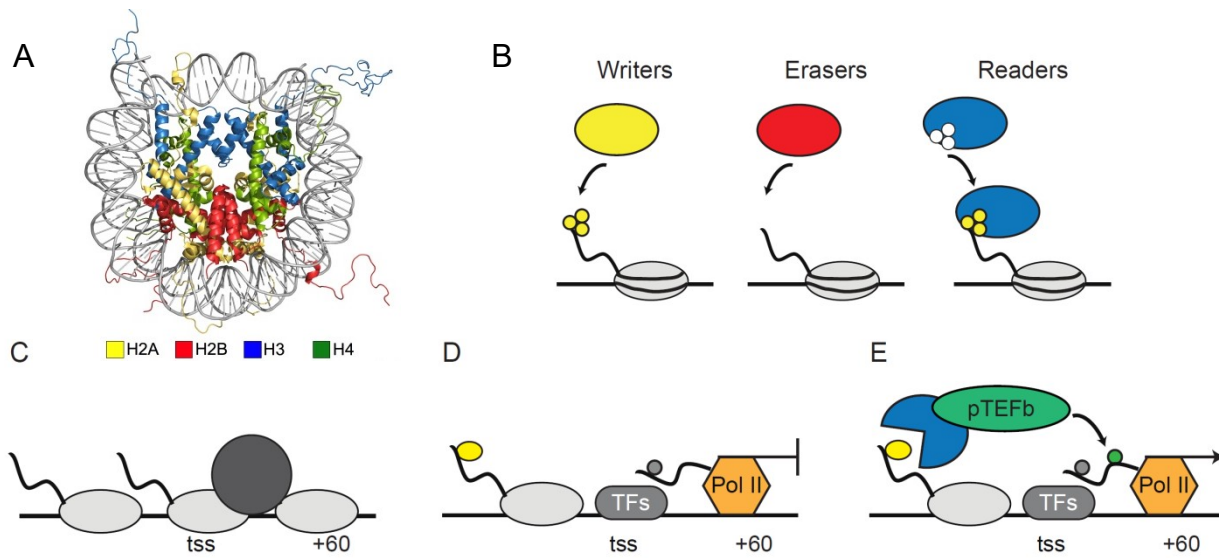
Nucleosomes can also hinder gene transcription in euchromatin and must be cleared or shifted for transcription to proceed. Histones regulate gene transcription through an intrinsically disordered [27], N-terminal domain. This tail can be post-translationally modified with different moieties such as acetyl or methyl groups, to directly or indirectly alter nucleosome compaction [28]. Our knowledge of these modifications continues to evolve as improving technologies identify novel histone marks such as acylation and monoaminylation [29,30]. The first modification identified and perhaps the best understood is histone acetylation [31,32]. Acetylation reduces the overall positive charge of the histone, decreasing the electrostatic interaction with DNA. In

addition to direct structural changes, these modifications serve as a type of code, the

so-called "histone code," for proteins to interact with the chromatin and regulate

transcription [33]. Chromatin-interacting proteins can be grouped into three categories:

writers which add modifications to histone tails [34,35], erasers which remove these marks,

and readers which bind modifications to directly or indirectly modulate transcription [36,37]

(Fig. 1b). Together these proteins control the timing and specificity of gene

transcription in response to diverse cellular stimuli by regulating protein interactions

with the DNA, the most important being RNA polymerases.

Three classes of polymerases transcribe various RNA species, but RNA

Polymerase II (RNAPII) catalyzes the transcription of messenger RNAs from the DNA

template strand. mRNA transcription occurs in three phases: initiation, elongation, and

termination. For gene transcription to occur, the promoter region must be cleared of

nucleosomes to allow for the transcriptional machinery to bind (Fig. 1C). Once the

promoter is free of nucleosomes, general transcription factors can recruit the

polymerase to form the pre-initiation complex. In particular, TFIIH, dissociates the two

DNA strands allowing RNAPII to initiate transcription [38].

Following these events, RNAPII transcribes the first 20-120 nucleotides and then

pauses downstream of the transcriptional start site on the majority of metazoan genes

[39–42] (Fig. 1D). In this initial elongation step, TFIIH phosphorylates the polymerase at

Serine 5 and 7 of its C-terminal domain (CTD) to establish RNAPII pausing [43–45].

Figure 1. Principles of transcriptional regulation. (A) The crystal structure of the nucleosome structure containing two copies of H2A, H2B, H3 and H4. Image credit: OIST. (B) The histone code proposes three types of chromatin interacting proteins. (Left) Writers add post-translational modifications (PTMs). (Middle) Erasers remove these modifications. (Right) Readers bind to histone PTMS to either directly or indirectly regulate transcription. (C-E) Initiation and elongation phases of RNAPII transcription. (C). Initiation begins by the clearing the promoter so transcriptional machinery can bind. (D) TFIIH phosphorylates RNAPII (orange) at Ser5 which causes the polymerase to pause proximal to the promoter. (E) Elongation proceeds after RNAPII is phosphorylated at Ser2 by kinases, usually P-TEFb (green).

The location of the downstream pausing site can vary based on polymerase escape speed and rate of pause factor recruitment as well as other undetermined factors [41]. Two main factors NELF and DSIF also bind to RNAPII to prevent productive elongation [46–49]. RNAPII remains stably paused and associated with the nascent RNA transcript awaiting further signals [50].

Phosphorylation of RNAPII at serine 2 of its CTD is required for elongation to proceed [43,51] (Fig. 1E). Additional phosphorylation of NELF and DSIF is also required to alleviate pausing [52–54]. These phosphorylation events are mainly accomplished by the

positive transcription elongation factor b, P-TEFb. P-TEFb is a heterodimer of Cdk9 and either Cyclin T1, T2, or K which associates within three main complexes: the 7SK/Hexim1 snRNP, the super elongation complex (SEC), and a BET protein, Brd4. The 7SK complex represses transcription by sequestering P-TEFb via its interaction with Hexim1 [55–57]. Up to 90% of the total pool of P-TEFb is sequestered in the 7SK complex [58]. Therefore, active pools of P-TEFb are either associated with Brd4 [59,60] or with SEC [61]. Because interaction with Brd4 prevents P-TEFb from associating with the 7SK/Hexim1 complex, Brd4 can modulate the global levels of active P-TEFb within a cell, which makes it a potent transcriptional regulator [59,60]. This recruitment of P-TEFb to release RNAPII is required for transcriptional elongation to commence throughout the gene body. While much is known about the molecular dynamics of RNAPII function and regulation, many questions still exist as to how exactly a specific transcriptional response is generated by a given stimulus. If the majority of genes have paused RNAPII, what triggers the expression of one gene over another? Additionally, do these regulatory mechanisms, identified in proliferating cells, also function similarly in postmitotic neurons?
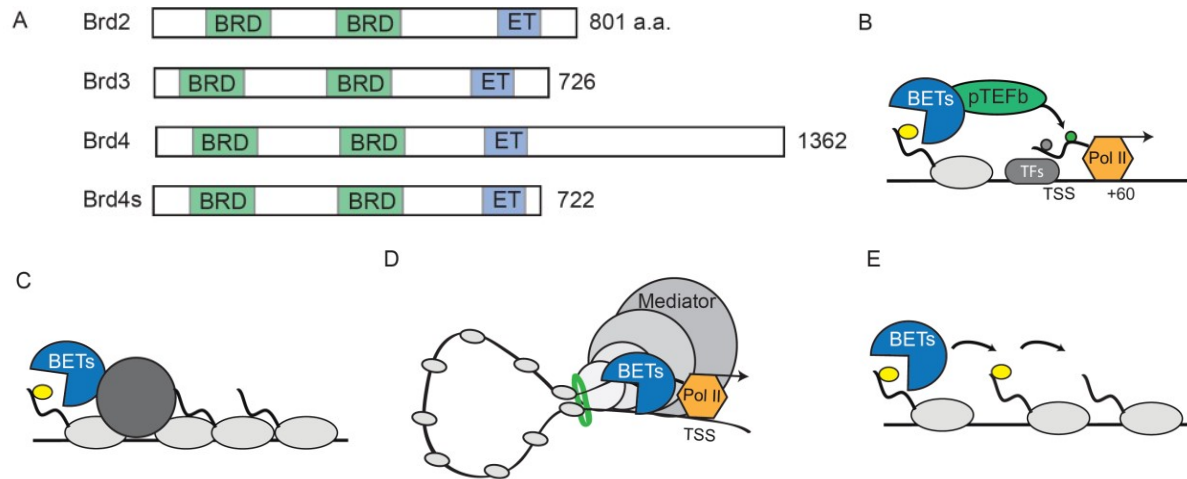
Bromodomains in Transcriptional Regulation

The mammalian bromodomain and extraterminal domain-containing protein (BET) family includes four members, Brd2, Brd3, Brd4, and Brdt, which have diverse roles in the regulation of transcription. While Brdt expression is restricted to the testes,

Brd2, Brd3, and Brd4 are ubiquitously expressed in mouse and human somatic tissues including the brain (Human Protein Atlas available from http://www.proteinatlas.org) [62]. The BET family is approximately 75% identical with each containing two tandem bromodomains, BD1 and BD2, and an extraterminal domain, ET (Fig. 2A) [63]. Notably, the predominant Brd4 isoform has a unique, extended c-terminal domain that may confer additional functions distinct from other BET members [64].

The bromodomain was the first identified chromatin reader domain [36,37] and comprises a ~110 amino acid protein domain that recognizes ε-N-lysine acetylation motifs on histones. Sixty-one bromodomains have been identified across 46 proteins in the human proteome which have diverse roles in the nucleus [65]. While sequences vary across bromodomains, all modules share a left-handed α-helical bundle linked by a loop region of variable length that determines binding specificity. The BET family bromodomains bind to mono-acetylated lysine residues on histone H3 or H4 but have the highest affinity for multiply acetylated regions along histone H4 such as H4K5K8ac [63,66–68]. BET bromodomains can also bind to histone propionylation and butyrylation although with a much weaker affinity [69,70]. In addition to binding to acetylated histones, the BET bromodomains can bind to certain transcription factors that are acetylated at histone-like motifs [71–74]. In these interactions, BET proteins act as a scaffold to stabilize transcription factors at the chromatin by binding to acetylated histones with one bromodomain while simultaneously binding a transcription factor with the other.

Because constitutive loss of Brd2 or Brd4 is embryonically lethal [75,76], small molecule BET inhibitors greatly facilitated our understanding of BET protein function [1,77]. These inhibitors mimic the structure of acetyllysine and prevent BET association with histones within 5 minutes [78]. Interference with acetylated histone binding alters gene expression with remarkable specificity and in a precisely controlled temporal fashion. Second- and third-generation inhibitors are now being developed to specifically target individual bromodomains [79,80] or individual members of the BET family to improve our understanding of BET functions. Alternatively, compounds to ablate BET function through selective protein degradation are now being developed [81–83]. These advances in chemistry can significantly inform our understanding of basic BET function and may

Figure 2. Structure and function of the BET proteins. (A) Three BET proteins, Brd2, Brd3, and Brd4 are expressed in somatic cells. Each member contains two tandem bromodomains (green) and an Extraterminal domain (blue). Brd4 has an extended c-terminus. (B) BETs release paused RNAPII from the promoter either by direct phosphorylation or by recruiting P-TEFb. (C) BETs recruit chromatin remodelers to facilitate transcription. (D) BETs control enhancer-mediated transcription. (E) Brd4 has histone acetyltransferase activity that may contribute to nucleosome eviction.

open new avenues for therapeutic targeting.

So how do BET proteins regulate transcription? As described above, BETs activate transcriptional elongation by recruiting P-TEFb to release paused RNAPII (Fig. 2B); however this is just one mechanism of BET action [59,60]. Brd4 can directly phosphorylate RNAPII to activate transcription independent of P-TEFb [64]. In addition, BET proteins bind to a host of other factors to regulate gene expression including chromatin remodelers like NSD2, JMJD6, and CHD4 [84–86] (Fig. 2C). Regulation at the gene promoter is only a small subset of transcriptional regulation and BETs importantly cooperate in enhancer-mediated transcription [87–93] (Fig. 2D). Within the gene body, prominent BET binding may represent an additional role for BET proteins in transcriptional elongation separate from paused RNAPII release [94]. Indeed, Brd4 has intrinsic histone acetyltransferase activity that facilitates nucleosome eviction [95,96] (Fig. 2E). In summary, multiple roles for BET proteins in the regulation transcription have been identified throughout the genome.

Given the broad pattern of BET binding and the multitude of interaction partners, there are still many remaining questions, including why only a subset of genes is sensitive to BET inhibition [1,97,98]. It also remains to be seen if these principles of BET-dependent transcription which were discovered in highly proliferative cells [89,99], apply to non-dividing cells like neurons or if there are additional mechanisms regulating BET function. Furthermore, little work has been done on the BET proteins in the central nervous system. Currently, it is not even known which genes are direct targets of BET

proteins in neurons let alone in glial cells. In the next section we describe what is currently known about BET protein function in the central nervous system (CNS).

BETs in the Central Nervous System

Within the CNS, BET proteins are expressed in all major cell types, although with some regional variability. Analysis of single-cell sequencing datasets shows that Brd2 mRNA expression is enriched in microglia whereas Brd4 expression is highest in neurons [5]. Mutations in human patients link Brd2 and Brd4 to neurological diseases and emphasize the importance of BET proteins in neuronal development. A variant in Brd4, resulting in a proline deletion, was linked to ASD [12,100]. Loss of Brd2 function may contribute to juvenile myoclonic epilepsy (JME) [101–106].

Evidence from genetic models also identifies a prominent role for BET proteins in brain function. Deletion of *Fsh*, the BET homolog in Drosophila melanogaster, reduces dendritic arborization complexity and decreases action potential frequency [107]. Constitutive Brd4 loss in mice leads to lethality shortly after implantation while heterozygous mice have significant growth defects pre- and postnatally, including severe head malformations [75]. Homozygous loss of Brd2 is also embryonically lethal and is preceded by neural tube malformations [76]. Further supporting a crucial role for BETs in neuronal development, Brd2 heterozygous mice have fewer GABAergic neurons and develop spontaneous seizures [108,109]. These data suggest that loss of Brd2 function

11

during neuronal development critically impairs neuronal subtype differentiation and may disrupt the excitation/inhibition balance in the brain resulting in epilepsy. Together these data highlight the vital role for BET proteins during neurodevelopment, but more work is required to understand the transcriptional and molecular mechanisms by which BETs control brain maturation.

BET expression remains high in the central nervous system after development which suggests a role for BET proteins in adult brain function. Several studies suggest BET-dependent transcription impacts cognition and memory in adult mice; however the precise nature of this regulation remains unclear. BET proteins contribute to addictive behaviors as BET inhibition prevents conditioned place preference for cocaine in mice [110]. BETs are required for appropriate memory formation in the novel object task [111,112], but negatively regulate memory formation in the fear conditioning assay [113]. Together these studies implicate BET proteins in the regulation of learning and memory however more work is needed to clarify the nature of BET-dependent regulation of memory.

Lastly, this protein family can regulate transcription in other cell types, including glia. Pharmacological inhibition of the first bromodomain of BETs in oligodendrocyte progenitors increases differentiation into mature oligodendrocytes [80]. This study is paralleled by the finding that neural progenitor cells increase neurogenesis and decrease astrogenesis after BET inhibition [114]. These studies indicate BET proteins regulate differentiation processes in the central nervous system which agrees with BET function in other tissues [92,97]. BET proteins may also be required for inflammatory gene

expression in microglia although current studies have only investigated BETs in immortalized microglial cell lines which do not adequately reflect the transcriptome of primary microglia [115,116].

Together the literature identifies a potential role for BET-dependent transcription in brain function in neurodevelopment and in the mature brain. In Chapter Three, we identify the BET proteins as critical transcriptional regulators of long, synaptic genes, many of which are risk genes for Autism Spectrum Disorders. Pharmacological inhibition of BET proteins in young mice causes an autism-like phenotype, suggesting the critical role of the BET-controlled gene network in ASD. In Chapter Four, we discuss the BET-dependent initiation of inflammatory gene networks in microglia and address the impact of these gene networks on brain health using two mouse models of neurodegenerative disease. Finally in Chapter Five, we identify a novel role for BET proteins as negative regulators of neuronal survival in the adult brain. Inhibition of BET-dependent transcription initiates a protective state in neurons characterized by decreased metabolic activity, increased protein degradation pathways and increased lifespan. Importantly, we show that pharmacological BET inhibition reduces microglial-mediated inflammation while increasing neuronal resilience to toxic stimuli and therefore has promising therapeutic potential in the treatment of neurodegenerative diseases. Here we identify the genes that require BET proteins for their proper transcription in both the developing and adult brain. Furthermore we generate the first genome-wide dataset of Brd2 and Brd4 chromatin occupancy from neurons. Critically we highlight the

importance of BET proteins in appropriate brain function by showing that inhibition of BET-dependent transcription during postnatal brain development initiates an autism-like phenotype. Lastly, blockade of BET-mediated transcription in adulthood induces a neuroprotective state that preserves brain function during neurodegeneration. In conclusion we find novel roles for BET proteins in the regulation of gene transcription that contribute to diseases both during development and in the adult brain.

Chapter Two

Platform and Methods

Animals

4-week-old male C57Bl/6 mice were purchased from The Jackson Laboratory. Mice were housed at five animals per cage on a 12-hour light/dark cycle (lights on from 0700 to 1900 hours) at constant temperature (23 ºC) with ad libitum access to food and water. All studies were also conducted in accordance with the GSK Policy on the Care, Welfare, and Treatment of Laboratory Animals and were reviewed by the Institutional Animal Care and Use Committee at GSK and/or at the Icahn Schol of Medicine at Mount Sinai where the work was performed.

Cx3Cr1$^{CreErt2/+(Litt)}$; Eef1a1$^{LSL.eGFPL10a/+}$mice were orally gavaged 5 times with tamoxifen to induce the expression of GFP-labelled ribosome. Mice were intraperitoneally injected with I-BET858 (30mg/kg) or vehicle control once daily for two weeks. Four hours after either an acute (1 injection) or chronic (2 weeks) injection, mice were decapitated and used for TRAP.

tetO-Cdk5r1/GFP; Camk2a$^{tTA/+}$ model of Alzheimer's disease uses the Camk2a promoter-driven tetracycline-controlled transactivator system (tTA) to overexpress human p25 fused to GFP in forebrain projection neurons after the removal of doxycycline from the diet. All mice were conceived and raised in the presence of doxycycline until 6-8 weeks of age to avoid the developmental effects of p25 expression.

Brd4$^{fl/fl}$ mice were donated by Dr. Keiko Ozato, and Brd2$^{fl/fl}$ mice were generated by Drs. Enyuan Shang and Debra Wolgemuth who kindly gifted them to us.

In vivo I-BET858 treatment

I-BET858 was developed and validated by GlaxoSmithKline. I-BET858 solutions used for in vivo studies (3mg/ml) were prepared in 10% Kleptose buffer with 5% DMSO (pH 6.5) and maintained at 4ºC. I-BET858 was made fresh daily. Buffers were made fresh each week. 30 mg/kg I-BET858 or vehicle (5% DMSO, 10% Kleptose saline buffer

pH=6.5) was delivered by i.p injection. For acute treatment, 6-week-old mice received a single I-BET858 injection. For chronic I-BET858 treatment in Chapter 3 and 4, 4-week-old mice received a total of 14 i.p. injections (one per day) over two weeks. Gene expression and behavioral changes were assessed in 6 week old mice at 4 h (acute, n=8-10 for behavior, n=2 for gene expression analysis) or 12 h (chronic, n=10 for behavior, n=2 for gene expression analysis) after the (last) I-BET858 injection, respectively. In Chapter 4, the P25 cohort was 8 weeks of age when taken off doxycycline. At 10 weeks of age the cohort was intraperitoneally injected with I-BET858 or vehicle daily for five weeks before behavioral and molecular analysis.

<u>Primary Cortical Neuron Culture</u>

Embryonic day 16 (E16) timed-pregnant female mice were anesthetized with CO_2 and sacrificed by cervical dislocation. In a dissection hood, 24-26 embryos per experiment were collected through an incision of the mother's abdomen, taken out of the amniotic sacs and decapitated in ice-cold Hank's Balanced Salt Solution (HBSS). Using fine scissors and forceps, brains were rapidly dissected and the cortex cleared from meninges and isolated under a dissection microscope. Cortices were collected in ice-cold HBSS and kept on ice until all embryos had been dissected. In a tissue culture hood, HBSS was removed and the cortex tissue digested by 0.25% Trypsin-EDTA for 12 minutes at 37 °C, followed by DNase1 treatment for 10 minutes at 37 °C. The tissue was dissociated by serial trituration with a 25 ml serological pipette, followed by trituration with 10 ml and 5 ml serological pipettes. Cell suspension was washed once with DMEM medium, supplemented with 10% FBS and 1% penicillin/streptomycin and passed through a 40 µM cell strainer before being counted on a hemocytometer. Single cells were seeded on poly-D-lysine (0.1 mg/ml) coated wells at a density of 1×10^6 cells per well on a 12-well plate. Cells were grown in Neurobasal medium, complemented with B27 supplement, N2 supplement, and 0.5 mM L-glutamine and maintained at 37 °C in 5% CO_2 for 1 week. Cultures were treated with DMSO (0.2%), I-BET858 (1 µM, 0.2%DMSO), BDNF (50 ng/ml), or BDNF + I-BET858 for 2 and 12 h on day 7 *in vitro*.

Cultures were washed with phosphate-buffered saline (PBS) on ice and processed for RNA isolation using TRIzol/Chloroform extraction.

Primary Microglia Culture

Postnatal day 0 C57/Bl6 mice were decapitated in ice-cold HBSS. The forebrain was rapidly dissected and treated as above in order to generate a single-cell suspension. 60,000 cells per cm^2 were seeded in vented, Poly-D-lysine coated flasks. Mixed glial cultures were maintained in DMEM containing 10% FBS and 1% penicillin/streptomycin for3 weeks. After three weeks, microglia were isolated by shaking the mixed glial cultures for 4 hours at 360 rpm and re-plated at density on 100,0000 cells/ cm2. Cultures were given 24 hours to settle before treatment. Cultures were pre-treated for 30 minutes with either DMSO (0.01%) or 1 µM I-BET858. After 30 minutes, LPS (100 ng/ml) was added to the cultures. RNA was isolated with Trizol LS according to the manufacturer's recommendations after 1, 4 and 12 hours of LPS treatment.

Axion Recordings

A 48-well multielectrode array plate (Axion) was coated with 0.1% PEI for 1 hour at 37ºC and washed four times with deionized water. Plates were dried overnight at room temperature in a sterile hood. Plates were incubated with 20 ug/ml laminin for one hour at 37 ºC before cells were seeded onto the plate. Primary cortical neurons were plated 50,000 per well. Plates were equilibrated on the Axion Maestro system at 37 ºC for 5 minutes before each 10-minute recording session. Baseline activity was recorded at day 7 before cells were treated with either I-BET858 (1 µm) or DMSO. Electrical activity was recorded every day until day 21 and then at regular intervals until activity was no longer detected.

<u>RNA Isolation</u>

For *in vitro* gene expression analysis, neuronal culture plates were washed once with PBS, and TRIzol was added directly to cultures to isolate RNA (n=3 per group). For in vivo gene expression analysis, mice were anesthetized with CO_2 and decapitated. The striata from two control and acute or chronic I-BET treated mice were rapidly dissected on ice and frozen in liquid nitrogen. RNA extraction from frozen samples was performed using TRIzol/Chloroform according to manufacturer's instructions (Invitrogen Corporation, Carlsbad, CA). RNA was precipitated overnight at -80ºC in isopropanol with 0.15 M sodium acetate, washed twice with 70% ethanol, air-dried, and resuspended in RNase-free water. RNA samples were purified using Rneasy Micro columns (Qiagen) with on-column DNAse treatment as specified by manufacturer. RNA integrity was assayed using nanodrop and RNA Pico chip on Bioanalyzer 2100 (Agilent, Santa Clara, CA) for quality RIN>9.

<u>Microarray analysis</u>

Total RNA samples were prepared for microarray analysis, as described previously. Briefly, total RNA was converted to cDNA using the Superscript GeneChip Expression 3'-Amplification Reagents Two-Cycle cDNA Synthesis Kit (Affymetrix) and the GeneChip T7-Oligo(dT) primer. Affymetrix Mouse Genome 430 2.0 arrays were used in all experiments. Mouse Genome 430 2.0 arrays were scanned using the GeneChip Scanner 3000 (Affymetrix, Santa Clara, CA) and globally scaled to 150 using the Affymetrix GeneChip Operating Software (GCOS v1.4). Three biological replicates were performed for each experiment. GeneChip CEL files were imported into GeneSpring GX 13.0 (Agilent Technologies, Santa Clara, CA), processed with the GC-RMA algorithm, and expression values on each chip were normalized to that chip's 50th percentile. Statistical analysis was carried out to determine which genes are differentially expressed in BDNF-, I-BET858-, or BDNF, I-BET858-treated neurons as compared to the DMSO control. Genes were filtered for a raw expression level of > 20 and a fold change of > 2, followed by moderate t-test with a p-value cutoff of 0.05. P-values were

adjusted using the Benjamini-Hochberg correction. Gene expression changes are shown using Volcano plots where the corrected p-value ($-\log_{10}$) is plotted versus fold-change ($\log_2$). Heatmaps were created by hierarchical gene clustering on entities using the Euclidean distance metric and Ward's linkage rule using GeneSpring GX 13.0.

RNA Sequencing

Double-stranded cDNA was generated from 1-5 ng purified RNA using the Nugen Ovation V2 kit (NuGEN, San Carlos, CA) following manufacturer's instructions. 500 ng of cDNA per sample were sonicated to obtain fragments of 200 bp using Covaris-S2 system (Duty cycle: 10%, Intensity: 5.0, Bursts per second: 200, Duration: 120 seconds, Mode: Frequency sweeping, Power: 23W, Temperature: 5.5ºC - 6ºC, Covaris Inc., Woburn, MA). These fragments were then used to produce sequencing libraries with the TruSeq DNA Sample kit (Illumina, San Diego, CA, USA). The quality of the libraries was ensured using the 2200 TapeStation (Agilent). Duplexed libraries were sequenced on HiSeq 2000, typically yielding on average 60 million, 100 bp long single-end reads per sample (Illumina). All samples were mapped at a rate of 79-80%. After filtering out adaptor and low-quality reads, reads were mapped using TopHat (version 2.0.8) to the mm9 mouse genome. The Cufflinks/Cuffdiff suite was used to estimate gene-level expression values as fragments per kilobase of exon model per million mapped fragments (FPKM). Differentially expressed autosomal genes between control and acute I-BET858 or chronic I-BET858 libraries were determined using a p-value <0.05 and fold change of >2. Values with an FPKM less than 0.5 were excluded.

Gene List Statistics

Overlaps between gene sets were tested for statistical significance using the χ^2 test by using GraphPad Prism 5.01. The total number of expressed genes in neurons as measured by microarray (25,788) was used to calculate the χ^2 test for all lists generated by microarray. For RNA sequencing data, the total number of protein-coding genes in the mouse genome according to Mouse Genome Informatics (24,979) was

used for the χ^2 test. The ASD candidate gene list (n=1193) was obtained from the SFARI homepage (Basu et al., 2009) and supplemented with the list from (King et al., 2013).

Pathway analysis

Bioinformatic network and pathway analyses of I-BET858 suppressed genes have been performed using the Database for Annotation, Visualization and Integrated Discovery (DAVID) version 6.7 (david.abcc.ncifcrf.gov/) or using the KEGG Pathways from Enrichr (https://amp.pharm.mssm.edu/Enrichr/). Representative biological pathways from the top 25 enriched categories are shown. Pathway enrichment was calculated as –log10 p-value. The p-value cut-off (0.05) for significance is indicated by the red dashed line in Chapter 3 and black arrowhead in Chapters 4 and 5.

Gene Length Analysis

Gene Symbols were annotated with their gene start and end (in bp) using the mm9 database. Gene length was then calculated from these values. Replicate symbols were filtered out. To determine the relationship between fold-change (e.g., I-BET858 vs DMSO) and gene length, the $\log_2$ fold-change was plotted versus length for all genes expressed in neurons. Pearson correlation coefficients and p-values were calculated from the resulting scatter plot using linear regression. Genes were binned by length, and a sliding window was employed to calculate the average of the log2 fold-changes for the genes within each length window (in vitro: window 200, step 40; in vivo: window 800, step 20). For the BDNF induced, I-BET858 suppressed gene list, different parameters were necessary due to the significantly smaller list size (625 genes, window: 80, step: 1). To assess changes in gene expression levels in regards to length, raw microarray values were transformed using $\log_{10}$ and plotted versus length for each condition. A running average was calculated as above using window size of 400 and a step size of 20. The code used to generate expression versus length plots can be found at https://github.com/GeneExpressionScripts/ibet858_expression_plots.

Chromatin Immunoprecipitation with Sequencing

Primary cortical neuronal cultures were washed once with PBS then fixed for 10 minutes with a 1% formaldehyde solution in PBS with protease inhibitors (Sigma #P8340) at room temperature. Fixation was quenched, adding glycine to a final concentration of 0.125M (5 minutes, room temperature). Fixed cells (1×10^7) were resuspended in 1 ml of lysis buffer (50mM Hepes KOH, pH7.5, 140mM NaCl, 1mM EDTA, 10% glycerol, 0.5% NP-40, 0.25% Triton X-100) and 10 µl of protease inhibitor cocktail (PIC). Samples were rotated for 10 minutes at 4 ºC then spun at 1350g at 4 ºC for 10 minutes. Pellets were resuspended in 1 ml of lysis buffer 2 (10mM Tris-HCl pH8.0, 200mM NaCl, 1mM EDTA, 0.5mM EGTA) and 10 µl PIC.). Nuclei (5×10^6) were sonicated in lysis buffer 3 (10mM Tris-HCl pH8.0, 100mM NaCl, 1mM EDTA, 0.5mM EGTA, 0.1% Na-Deoxycholate, 0.5% N-Lauroylsarcosine) at 4 ºC for 5 cycles of 30 seconds ON/ 30 seconds OFF using the Diagenode bioruptor. After, 30 µl of 10% Triton-X100 was added to each sample and then spun for 15 minutes at 20,000g at 4 ºC. Sonication efficiency was checked by running the samples on a 2% agarose gel to confirm enrichment for fragments from 200-500 bps.

Streptavidin M-280 dynabeads were blocked with 0.5% BSA solution and coupled to 7 µg of antibody (Brd4 #Ab84778, Brd2 Bethyl #A302-583A, Pol2 Ser5 #Ab5408) for at least 8 hours at 4 ºC with rotation. Antibody-coupled beads were then added to sonicated chromatin (2×10^7 cells for Brd2/Brd4, 1×10^7 for Pol2) and incubated overnight at 4 ºC. After washing the IPs eight times with wash buffer (50mM Hepes-KOH pH7.6, 100mM LiCl, 1mM EDTA, 1% NP-40, 0.7% Na-Deoxycholate) and once with TE buffer (10mM Tris-HCl, 1mM EDTA, 50mM NaCl), Chromatin was eluted from magnetic beads in 200 µl elution buffer (50mK Tris-HCl pH8.0, 10mM EDTA, 1% SDS) for 45 minutes at 65 ºC. Samples were de-crosslinked overnight at 65 ºC, and proteins and RNA were removed by incubating with RNAse and Proteinase K. Samples were purified using the Qiagen PCR purification kit according to the manufacturer's protocol.

Samples were end-repaired using the End-IT DNA End-Repair Kit (#ER0720). After 45 minutes of incubation, samples were purified using the Qiagen PCR Clean up kit as described above. Samples were adenylated using a reaction mix (200μM dATP, 1x Klenow buffer NEB2, Klenow Fragment (3` to 5` exo-), NEB M0212L) and incubating at 37 ºC for 30 minutes. After, samples were purified as above except using the Minelute columns to minimize sample loss. Adapters were ligated to samples using a reaction mix containing T4 DNA ligase buffer, Solexa adapter oligo mix and 1200 units of T4 DNA ligase. The samples were incubated according to the following PCR program: 1) 20 ºC for 15 minutes, 2) 4 ºC for 2 hours, 3) 0.1C/second to 16 ºC, 4) 16 ºC for 20 minutes, 5) 0.1 ºC/second to 4 ºC, 6) back to step 2 for 6 cycles. Samples were purified using the Minelute kit as described above. Samples were amplified using a reaction mix containing the Phusion HF buffer, 300 μM dNTP mix, 3% DMSO, diluted Solexa primers 1.0 and 2.0, and 1 unit of Phusion polymerase. Samples were amplified according to the following program: 1) 30 seconds at 98 ºC, 2) 18 cycles of: 10 seconds at 98 ºC, 30 seconds at 65 ºC, 30sec at 72 ºC, 3) 5 minutes at 72 ºC. Prepared samples were then sequenced on the HiSeq 2000 platform by Rockefeller's Genomic Core Facility. Bioinformatic analyses were performed by the Shen Lab. Briefly, raw sequencing data were processed by using Illumina bcl2fastq2 Conversion Software v2.17. The ChIP-seq data were first checked for quality using the various metrics generated by FastQC (v0.11.2;ttp://www.bioinformatics.babraham.ac.uk/projects /fastqc). Raw sequencing reads were then aligned to the mouse mm9 genome using the default settings of Bowtie (v2.2.0). Only uniquely mapped reads were retained, and the alignments were subsequently filtered using the SAMtools package (v0.1.19) to remove duplicate reads. Peak-calling was performed using MACS (v2.1.1) with default settings. Annotation of called peaks and differential regions to their genomic features (promoters, gene bodies, intergenic, etc.) was performed using region-analysis (v0.1.2), and read alignment profile plots and heatmaps were generated using ngsplot (v2.47) and Multiple Experiment Viewer 4.8. Bioinformatic analysis of RNA and Chip sequencing was done in collaboration with Dr. Yong-Hwee E. Loh, Aarthi Ramakrishnan, and Dr. Li Shen.

All behavioral tests were performed between 7AM and 7PM. For all behavioral experiments, experimenters were blinded to the treatment of the animals. GraphPad Prism version 5.01 for Windows (Graph-Pad Software) was used for statistical analysis of the data. Samples corresponding to data points that are more than 2 standard deviations from the sample mean were excluded from analyses. All procedures were conducted in strict accordance with the National Institutes of Health Guide for the Care and Use of Laboratory Animals and were approved by the IACUC at Icahn School of Medicine at Mount Sinai.

Locomotion, exploratory, and thigmotaxis/anxiety behaviors were measured using the open field analysis as previously described [117]. Mice were assessed for 60 minutes, and data were collected in 5-minute intervals (n=10). Locomotor activity was assessed by total distance traveled (m), anxiety-like behavior was defined by counts of rearing (number of vertical episodes in counts), and the ratio of the distance moved in the center versus the periphery (thigmotaxis), and stereotypical behavior (time spent). Mice were tested in the open field 4 h after acute (n=8) and 12 h after chronic (n=10) I-BET858 or vehicle treatment.

Memory and learning in mice acutely treated with I-BET858 or vehicle (n = 10) were analyzed using a standard fear conditioning paradigm (Med Associates, St. Albans, VT) as described previously [117]. Briefly, a mouse was placed in the test chamber (house lights on) and allowed to explore freely for 2 minutes. White noise (80 dB) was then presented for 30 seconds, co-terminating with a mild foot shock (2 seconds, 0.7 mA). Two minutes later the same sequence of auditory cue-shock pairing was repeated. The mouse was removed from the chamber 30 seconds later and returned to its home cage. Freezing behavior was continuously recorded during the time spent in the test chamber. Mice were injected with either I-BET858 (30 mg/kg) or vehicle 10 minutes after the training. Twenty-four hours later, the mouse was placed back into the test chamber for 5 minutes and freezing behavior was recorded (context test). Two hours later, the

mouse was tested for freezing in response to the auditory cue. Environmental and contextual cues were changed for the auditory cue test. The auditory cue test was divided into two phases: 3 minutes in the absence of the auditory cue and 3 minutes of the auditory cue. The time freezing during each test was converted to a percentage of freezing value.

Social preference and social memory was performed as previously described (Ellegood and Crawley, 2015) using a plexiglass chamber divided into three-compartments. The two edge compartments contained an empty wire cup. Mice were habituated to the testing room for at least 1 hour prior to the experiment. Stimulus mice (6-8 week old C67Bl/6 males) were housed in separate areas of the animal facility and had no prior contact with the test mice. Stimulus mice were habituated to the wire cup prior to testing. For the sociability test, the test mouse was introduced to the middle chamber and allowed to freely explore to all three compartments for 10 minutes. Then, the mouse was restricted to the middle chamber using dividers while a novel object (Lego) was placed under the wire cup in one chamber and an unfamiliar mouse in the other. The test mouse was then allowed to investigate the whole apparatus for 10 minutes. After, the mouse was again restricted to the middle chamber while the object was replaced by a second, unfamiliar mouse. The test mouse was allowed 10 minutes to investigate. Data were acquired using the Ethovision system (Noldus) to automatically track motion while manual scoring was used to quantify time spent sniffing the stimuli. Counter-balancing was used to control for potential left-right preferences. Social preference index = $(\frac{Time_{targe} - Ti_{object}}{Time_{total}} \; x \; 100)$. Social novelty index = $(\frac{Time_{new} - Time_{old}}{Time_{total}} \; x \; 100)$.

Olfaction was tested by exposing mice (n=5) to a small amount of palatable food (Cinnamon Toast Crunch cereal) once per day for two days. Mice were deprived of food overnight before the test. A clean cage was filled with roughly 3 inches of fresh bedding, and the stimulus food was buried in the bedding until it was not visible. Mice

were then placed in the cage one at a time and allowed to freely explore. The latency to localize and retrieve the food was measured. Bedding was mixed in between trials and tested mice were placed in a new holding cage until all cage-mates had been tested. After this, all mice were returned to their original cage, and ad libitum food access was restored. All mice retrieved the food within 2 minutes.

Accession numbers

The data discussed in Chapter 3 have been deposited in NCBI's Gene Expression Omnibus (GEO) and are accessible through GEO SuperSeries accession number GSE72149. Data from Chapters 4 and 5 will be deposited during manuscript submission.

LDH Assay

LDH activity was measured using the Pierce LDH Cytotoxicity Assay Kit. Culture media was incubated with an equal volume of LDH master mix and incubated for 30 minutes at room temperature in the dark. After, the same volume of stop reagent was added, and the absorbance was measured at 490 and 680 nm. Maximum LDH measurements were obtained by adding lysis buffer to release the total amount of LDH in the sample. LDH release is calculated as a percent of the maximum.

Propidium Iodide Assay

Propidium iodide (1 mg/ml, Life Technologies #P3566) was added to each culture well at a final concentration of 0.5 µg/ml. Cultures were incubated for 30 minutes at 37 °C then washed with PBS. Cells were then fixed with 4% paraformaldehyde in PBS for 15 minutes at room temperature. After fixation, cells were washed with PBS and then mounted using mounting media containing DAPI.

Immunostaining

Mice were anesthetized with ketamine (120 mg/kg) and xylazine (24 mg/kg) and perfused transcardially with 10 ml PBS and 40 ml 4% paraformaldehyde (Electron

Microscopy Sciences). Fixed brains were removed and dehydrated in 5%, 15% and 30% sucrose in PBS. Following dehydration, brains were frozen in Neg-50 (Thermo Scientific) on dry ice and stored at −80 °C until further processing. Brains were cut using a cryostat and 25-μm sections were mounted on Superfrost Plus microscope slides (Fisher Scientific). Slides were stored at −80 °C until staining. Slides were washed with PBS, permeabilized with PBS + 0.2% Triton X-100 (PBST) and blocked with 2% normal goat serum in PBST for one hour at room temperature. Slides were incubated with primary antibodies (BRD4, 1:500, ab84776, Abcam; BRD2, 1:200, 5848, Cell Signaling; IBA1, 1:500, 019-19741, Waco; MAP2, 1:500, 4542, Cell Signaling; NeuN, 1:500 MAB377, Millipore) in 2% normal goat serum in PBST overnight at 4 °C. Slides were washed in PBST and incubated in Alexa Fluor-conjugated secondary antibodies (Alexa Fluor 488-, 546-, and 568- and 647-labeled goat anti-mouse, goat anti-rat, goat anti-chicken, goat anti-rabbit or donkey anti-goat IgGs (H+L); 1:500, Thermo Scientific) in 2% normal goat serum in PBST for 1 h at RT. Slides were washed and cover-slipped using Prolong Gold anti-fade with DAPI (Invitrogen) and dried overnight. Imaging was performed using a Zeiss LSM 780 Confocal Microscope (Zeiss, Oberkochen, DE). For single plane images, 4.6 μm images were acquired at 20x/.8 or 40x/1.3 objectives 0.6 or 1x zoom. Image processing was performed using Zen 2011 software (Zeiss).

Immunoblotting

Mice were anesthetized with CO_2 followed by decapitation, and the region of interest was rapidly dissected and frozen in liquid nitrogen and stored at -80 °C until further processing. Samples were sonicated at 4 °C in a 1% SDS solution supplemented with Trichostatin A (500 ng/ml), protease and PhosStop phosphatase inhibitors (Roche, Switzerland), and boiled for ten minutes. The protein concentration was determined using a BCA protein assay kit (ThermoFisherScientific, USA) according to the manufacturer's instructions. Protein samples were diluted in equal volume of 2X LDS sample buffer (Invitrogen) and supplemented with DTT to a final concentration of 200 mM (Sigma). Lysates were separated on 4–12% NuPAGE Bis-Tris precast denaturing

gels (Invitrogen) and transferred onto PVDF membranes in Mini Gel Tank at 25 V for 2 h. Membranes were blocked with 5% milk–TBST or 5% BSA-TBST for 1 h at RT. Membranes were then probed with primary antibodies diluted in 5% milk–TBST or 5% BSA-TBST solution overnight at 4 °C. Primary antibodies: anti-ACTB (1:10,000, ab8227, Abcam, milk), anti-Brd4 (1:1000, A301-985A100, Bethyl, milk), anti-GAPDH (1:1000, ab9485, Abcam, milk), anti-GFP (1:1000, ab6556, Abcam, milk), anti-LC3B (1:1,000, 2775, Cell Signaling, BSA), anti-mTOR (1:1000, 2983, Cell Signaling), anti-NEUN (1:1000, MAB377, Millipore, milk), anti-PSD95 (1:1000, milk), anti-p-S6K (1: 1000, 9234, Cell Signaling, 5%BSA), anti-S6K (1:1000, 2708, Cell Signaling, milk). Membranes were then washed and probed with horseradish-peroxidase-conjugated anti-mouse (Life Technologies, 31438, 1:10,000) or anti-rabbit IgG secondary antibody (GE, NA934V, 1:10,000) for 1 h at RT. Membranes were developed using enhanced chemiluminescence substrate (PerkinElmer, USA, 509049326) and exposed on film.

Mass Spectrometry

Cell culture plates (2 x 10^6 cells per well n =7-8 per group) were washed with 75 mM Ammonium bicarbonate, pH 7.4, warmed to 37 °C. Plates were quenched on liquid nitrogen for 10 seconds and then placed on dry ice. 1 ml of 70% Ethanol in MS-grade water was warmed to 75 °C and added to each well. Plates were incubated in a 75 °C water bath for 3 minutes, shaking gently every minute. After 3 minutes, plates were placed on dry ice and once cooled, supernatants were lyophilized using the speed vacuum and stored at -80 °C. Samples were shipped on dry ice to Cellzome, a GSK company specializing in metabolomics, who processed the samples for mass spectrometry and performed the initial analysis annotating metabolites. We used a semi-quantitative approach that determines the metabolite levels relative to a control rather than absolute concentrations. All detected ions were used for statistical analysis regardless of how many samples they were detected. This allows for the identification of low-abundant metabolites that may be present in only a subset of samples.

Comparison of untreated neuron cultures to vehicle-treated cultures revealed no effect of vehicle on the cellular metabolome.

Seahorse Mitochondrial Stress Test

In this assay, two fluorescent probes that detect the concentration of oxygen or protons are added to the culture media. Cellular metabolism causes rapid changes in the concentration of these molecules in the media, which can be detected by changes in sensor fluorescence. The oxygen consumption rate (OCR) indicates mitochondrial respiration and the extracellular acidification rate (ECAR) is largely due to glycolysis. Certain pathways can be analyzed by the sequential addition of inhibitors to the media and measuring ensuing changes to the OCR and ECAR. First baseline readings are measured to give an understanding of basal metabolic rates. Then the last step of oxidative phosphorylation, the ATP synthase, is inhibited by oligomycin to determine how much oxygen is being used for ATP production. FCCP is next added to decouple the electron transport chain from the ATP synthase by increasing proton permeability of the membrane which drives oxidative phosphorylation to its maximum. Lastly, complex I is inhibited by rotenone to completely shut down mitochondrial respiration. Any oxygen that is consumed after rotenone is due to other cellular processes such as fatty acid metabolism. On the day of the assay, cultures were washed times with artificial CSF (aCSF) [120 mM NaCl, 3.5 mM KCl, 1.3 mM $CaCl_2$, 1 mM $MgCl_2$, 0.4 mM KH_2PO_4, 5 mM HEPES, 0.4% BSA, 10 mM Sodium-pyruvate, 15 mM Glucose], and incubated at 37 °C without CO_2 for one hour prior to assay. Oxygen Consumption Rate (OCR) was measured using the Seahorse XFe24 Analyzer (Agilent), under basal conditions and after the sequential addition of 2 mM oligomycin, 4 mM FCCP [carbonyl cyanide p-(trifluromethoxy) phenylhydrazone], 0.5 mM rotenone (R) and 4 mM antimycin A (A). Metrics were calculated according to the following equations. All values were calculated per well and normalized to cell number for each experiment. Each experiment (n=3) was normalized to the average of all control values.

Basal Respiration = $OCR_{baseline} - Lowest\ OCR_{R+A}$

Maximum Respiration = $Highest\ OCR_{FCCP} - Lowest\ OCR_{R+A}$

ATP Production= $Lowest\ OCR_{oligomycin} - Basal\ Respiration$

Proton Leak = $OCR_{baseline} - Lowest\ OCR_{R+A}$

Coupling Efficiency = $\dfrac{Atp\ Production}{Basal\ Respiration}\ x\ 100$

Statistics

Data was analyzed using GraphPad Prism version 5.01. Significant differences between experimental groups were determined using the Student's t-test for two groups or One-Way ANOVA for three or more groups with Tukey posthoc multiple comparisons. Repeated measures ANOVA was used to assess the significance of data collected over time such as survival curves (Chapter 5, Fig. 1). Before testing for differential effects, data were first checked for normality using the Kolmogorov-Smirnov test. If the data were not normally distributed, this was corrected by using the Mann-Whitney test for the comparison of two independent groups or the Kruskal-Wallis test for analyses containing three or more groups. Second, data variances were tested for equivalence using the f-test. If variances failed the f-test, this was accounted for by using the Welch correction for the Student's t-test for two independent groups. Groups were determined to be significantly different if the analysis yielded a p-value less than 0.05. Samples corresponding to data points that are more than 2 standard deviations from the sample mean were excluded from analyses as outliers. Culture experiments were independently replicated a minimum of twice with biological triplicates.

Chapter Three

BET Inhibition causes an Autism-like phenotype in young mice

Abstract

Studies investigating the causes of autism spectrum disorder (ASD) point to genetic, as well as epigenetic, mechanisms of the disease. Identification of epigenetic processes that contribute to ASD development and progression is of major importance and may lead to the development of novel therapeutic strategies. Here, we identify the bromodomain and extraterminal domain-containing proteins (BETs) as epigenetic regulators of genes involved in ASD-like behaviors in mice. We found that the pharmacological suppression of BET proteins in the brain of young mice, by the novel, highly specific, brain-permeable inhibitor I-BET858 leads to selective suppression of neuronal gene expression followed by the development of an autism-like syndrome. Many of the I-BET858–affected genes have been linked to ASD in humans, thus suggesting the key role of the BET-controlled gene network in the disorder. Our studies indicate that environmental factors controlling BET proteins or their target genes may contribute to the epigenetic mechanism of ASD.

Introduction

The search for the cause of autism spectrum disorder (ASD) revealed the disease's associations with numerous genes mutations. Many of the ASD candidate genes encode proteins that control neuronal network formation and function [118]. A significant fraction of ASD associated genes, however, encode rather ubiquitous regulators of gene expression [9]. The latter finding underscores the possibility of an epigenetic etiology of ASD, where aberrant control of gene expression rather than gene mutations, can lead to abnormal neuronal development and function.

One of the major challenges for testing the role of abnormal gene regulation in brain function is the lack of experimental models where changes in gene expression can be achieved in a controlled fashion and without the generalized negative impact on neuronal development, survival and function. This obstacle could be potentially overcome by utilizing brain-permeable compounds that regulate transcription in a selective and time-dependent fashion. Pharmacological suppression of well-defined transcriptional processes would allow one to determine the impact of acute or chronic transcriptional de-regulation on animal behavior at any developmental time point and would also enable the identification of genes affected by the temporal impairment of these processes.

Previous studies describe the pharmacological modulation of transcription by BET inhibitors [1]. In humans and mice, somatic cells, including neurons, express three independent BET proteins: Brd2, Brd3 and Brd4 [119]. All three BET proteins contain two
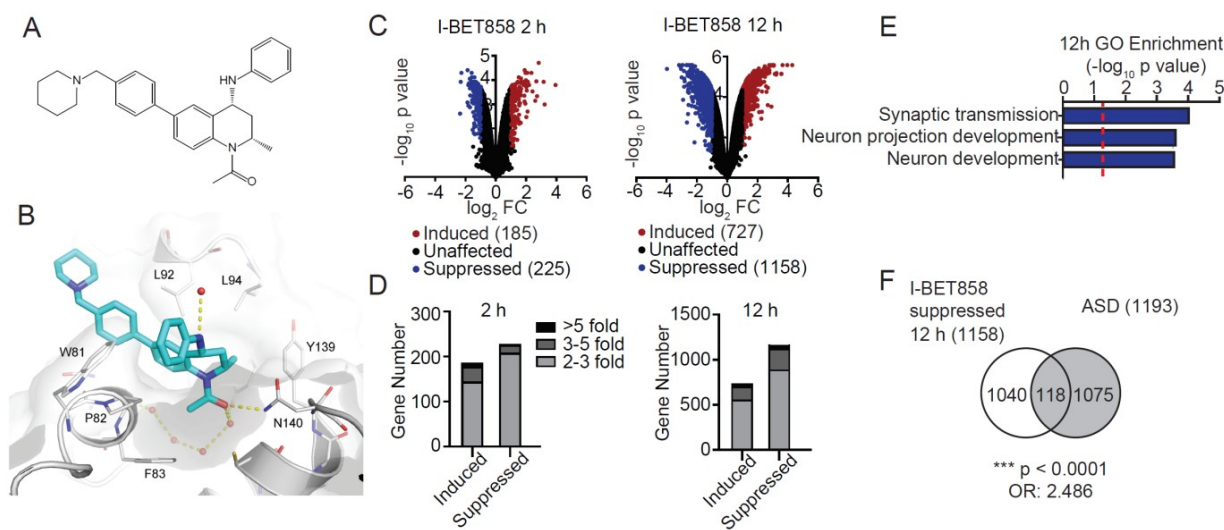
N-terminal bromodomains (BD1, BD2) that recognize acetylated lysines within the N-terminal domain of histone H4 as well as other lysine acetylated proteins [63]. The binding of the BET bromodomain to acetylated lysines on histone H4 initiates a chain of biochemical and molecular events that leads to the formation of elongation-competent transcriptional complexes containing RNA Polymerase II phosphorylated at serine 2 [120]. Pharmacological inhibitors of BET proteins such as I-BET [1] or JQ1 [77] bind with high specificity to the acetyl-lysine-binding pocket of the tandem bromodomains of all members of the BET family. The inhibitor binding prevents BET protein association with acetylated histone H4 and affects gene transcription [1,121]. However, despite the widespread BET binding to numerous genes, the impact of the BET inhibitors on gene expression in various cell types is surprisingly limited [1,89,99]. The mechanism of the selective effect of BET inhibitors on gene expression is not well understood. Our earlier studies showed that susceptibility to I-BET in activated macrophages correlates with the gene's dependence on SWI/SNF-mediated chromatin remodeling [1]. Other studies have suggested a link between the susceptibility to BET inhibitors and BET-association with specific enhancer clusters (super-enhancers) [88]. Loss of function mutations in *fs(1)h*, the single BET in Drosophila, leads to decreased dendritic arbor complexity and impaired mechanosensitive response in sensory neurons [107]. Additionally, a de novo deletion mutation in Brd4 has been identified in ASD patients [12]. Together these studies suggest a critical role for BET proteins during neuronal development.

In order to address the impact of BET suppression on neuronal gene expression and brain function, we identified a novel, brain-permeable I-BET (I-BET858) in collaboration with GlaxoSmithKline. Here we provide evidence for the selective impact of BET protein functions on neuronal gene expression *in vitro* and *in vivo*. We show that I-BET858 treatment preferentially suppressed genes associated with neuronal differentiation and synaptic function and had no effect on neuronal housekeeping or early response genes. The suppressive effects of I-BET858 correlated directly with gene length. A significant number of I-BET858 suppressed genes, including genes of extended length, are potential ASD candidate genes in humans [14,122]. Furthermore, suppression of specific neuronal genes by I-BET858 in young mice led to the development of an autism-like syndrome. Our findings describe for the first time a pharmacologically-induced model of ASD and point to the selective I-BET858 suppressed genes as potential key contributors to ASD in mice.

Results

Identification of a novel brain-permeable BET inhibitor.

Brain permeability is a crucial factor in assessing the impact of BET inhibitors on neuronal gene expression and associated behaviors. To investigate the effects of BET inhibition within the central nervous system, we identified a novel BET inhibitor compound with higher brain permeability than the original I-BET151 and I-BET762. Through in silico assessment of ~1000 potential brain-penetrant BET inhibitor compounds, we identified the novel tetrahydroquinoline class (THQ) [123] compound I-BET858 (Fig. 1A). I-BET858 displayed an appropriate profile for progression into *in vivo* rodent models based on its calculated physicochemical properties, pharmacokinetics,

Figure 1. Effect of the brain-permeable inhibitor of BET proteins (I-BET858) on gene expression in primary neurons *in vitro*. (A) Chemical structure of I-BET858. (B) X-ray structure of I-BET858 (blue) bound to the acetylated lysine (Kac) recognition pocket of BRD4-BD1 (red spheres, water network; yellow dashed lines, hydrogen bonds). The WPF shelf (W81, P82, F83), as well as the asparagine N140 essential for acetylated lysine (Kac) binding, are labeled accordingly. (C and D) Gene expression in primary cortical neurons treated with I-BET858 (1 µM) for 2 and 12 h was analyzed using microarray analysis (n = 3/group, experiment was performed in duplicate). (C) Volcano plot shows the genes that are significantly suppressed (P < 0.05; >2-fold; blue) or induced (red) after I-BET858 treatment. (D) Bar graph shows the number and fold gene expression changes. (E) Gene Ontology (GO) enrichment of I-BET858–induced (top) or suppressed (bottom) genes (-$\log_{10}$ p-value; red line, P = 0.05). (F) Venn diagram shows the overlap between I-BET858–suppressed genes and ASD-associated genes. Statistics: χ^2 test, ***, P < 0.0001; OR, 2.486.

BET inhibitory activity in cell-based assays, and enhanced brain penetrance (data not shown). The binding mode of I-BET858 to BRD4-BD1 was determined by X-ray crystallography (Fig. 1B). The curvature of the THQ template complements that of the BET proteins and results in high affinity of I-BET858 for the BET subfamily with >1000 fold selectivity over 34 other bromodomain-containing proteins (data not shown) [124].

Selective impairment of neuronal gene expression by pharmacological BET inhibition in vitro.
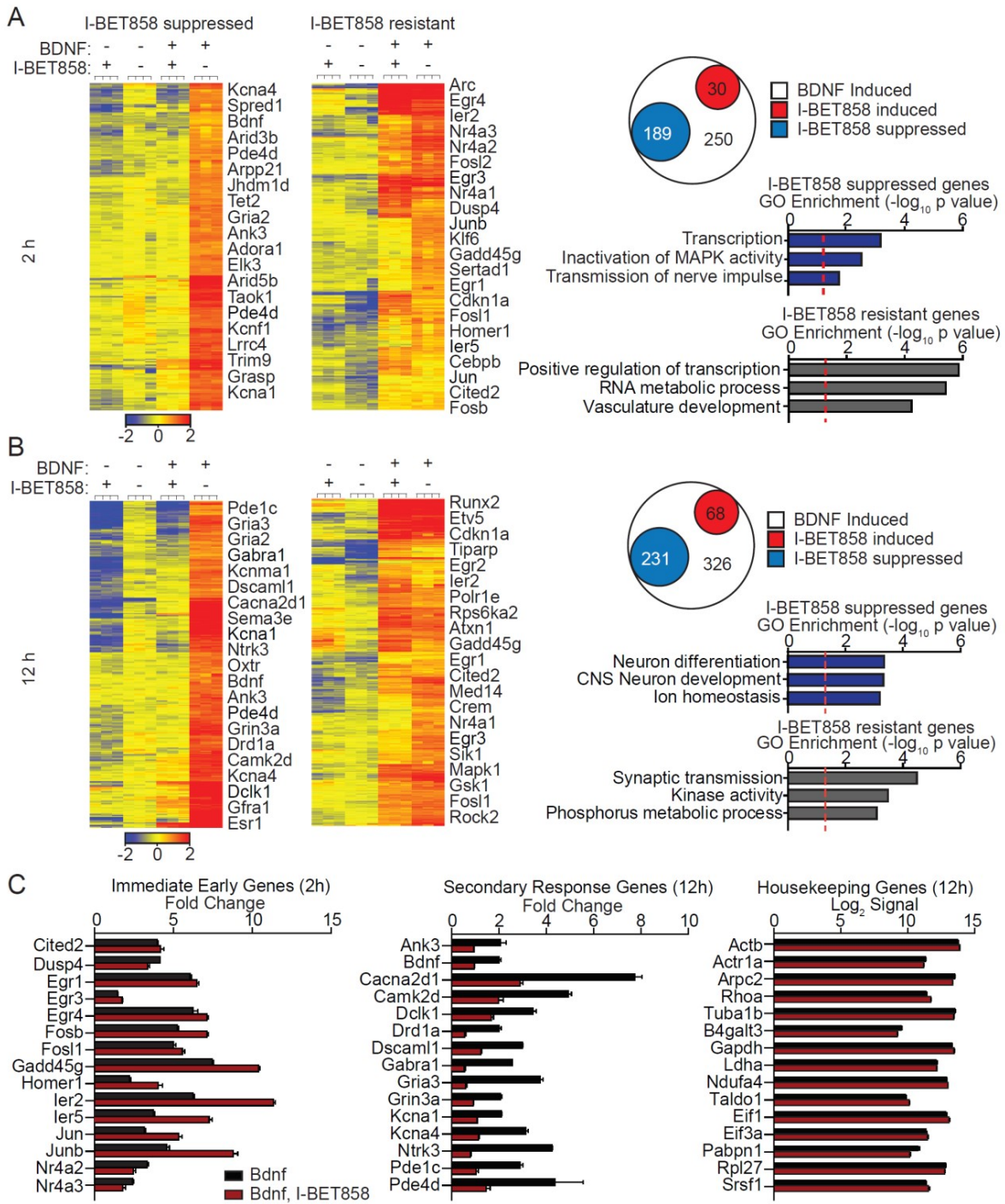
The impact of I-BET858 on neuronal gene expression was initially assessed *in vitro*. Primary cortical neurons isolated from E18 mouse brain were grown in an *in vitro* culture system for 7 days followed by the treatment with I-BET858 at a concentration of 1 µM. As in other cell types treated with I-BET or JQ1 [1,89,99], the treatment of primary cultured neurons with I-BET858 led to a time-dependent up- and down-regulation of numerous genes (Fig. 1C, D). Opposite to gene induction, the down-regulation of gene expression by BET inhibitors has been shown to correlate directly with BET-association at the gene loci prior to the BET inhibitor treatment and loss of BET-association following exposure to the inhibitors [1]. Therefore, in our studies, we focus exclusively on genes that are suppressed by I-BET858.

Treatment of primary cortical neurons with I-BET858 results in time-dependent changes in gene expression, characterized by the moderate (2.75 fold on average) down-regulation of 225 and 1158 genes at 2 and 12 h after I-BET858 treatment, respectively (Fig. 1C, D). Notably, I-BET858 preferentially affected genes controlling synaptic transmission, neuronal development, and morphogenesis (Fig. 1E). Moreover, ~10% of the suppressed genes (118/1158, p < 0.0001, OR: 2.486) were previously identified ASD risk genes (combined lists from Basu et al., 2009; King et al., 2013) in humans (Figure 1F). Several of the ASD candidate genes that showed strong suppression in response to I-BET858, such as *Met, Gabra1, Cntn6, Pde4b, Npas2, Cdh10,* and *Foxp1*, have been shown to play an important role in neuronal development and function in circuits relevant to core behavioral domains of ASD [125–128]. The brain-specific deficiency of Foxp1-expression was recently shown to impair neuronal development, causing autistic-like behaviors in mice [125].

The ability of I-BET858 to modify gene expression in neurons was further demonstrated by the profound yet selective effect of I-BET858 on the expression of genes induced by the brain-derived neurotrophic factor (BDNF) (Fig. 2A, B). The BDNF-controlled genes play a crucial role during brain development and are essential for normal neuronal function and survival [129]. Treatment of primary cortical neurons with BDNF resulted in the induction of numerous genes that regulate neuronal maturation, axogenesis, synapse formation and synaptic transmission in neurons. The BDNF-induced transcriptional changes followed a well-defined temporal pattern with the

induction of early response genes, such as *Egr1-4, Fos, FosB, Ier2-5, Jun, JunB, Nr4a2/3*, within 20 minutes after BDNF stimulation [130]. The expression of these immediate early genes (IEGs) was followed by the induction of secondary/late response genes that control the specific BDNF-induced changes in neuronal morphology and function [130,131].
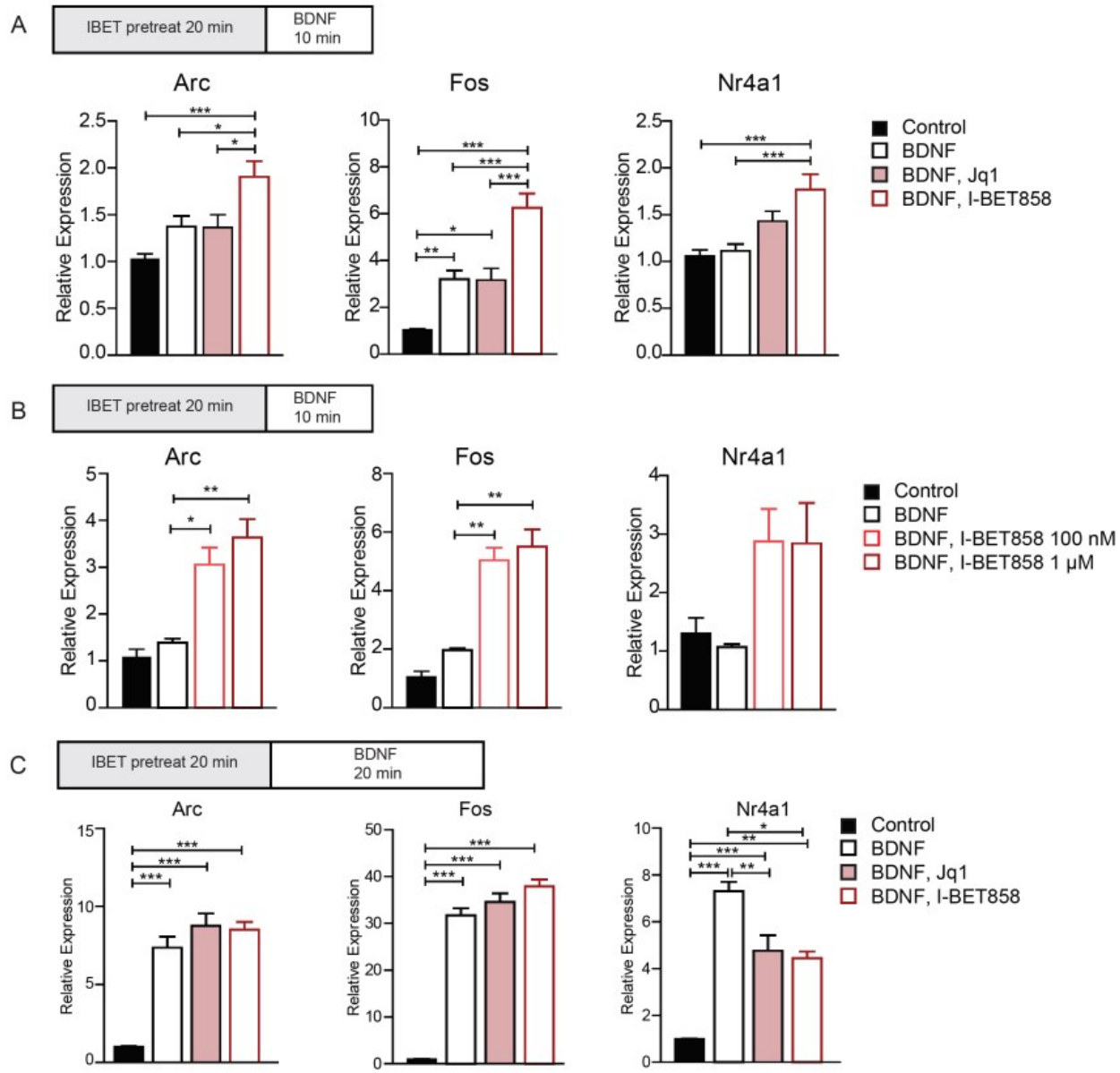
We found that treatment with I-BET858 at 1 µM resulted in a highly selective and time-dependent suppression of gene expression in BDNF-stimulated cortical neurons (Fig. 2A, B). I-BET858 had no impact on housekeeping gene expression but specifically affected the expression of a selected group of BDNF-induced neuronal genes at 2 and 12 h after BDNF treatment (Fig. 2A–C). Many BDNF-inducible and I-BET858– suppressed genes were regulators of important neuronal processes, including neuronal transmission via ion channels (such as *Cacna2d1, Kcnma1,* and *Kcna1/4*), neurotransmitter receptor signaling (*Drd1a, Gabra1, Gria1-3, Grin3a,* and *Pde1c/4d*), and dendrite and axon development (*Ank3, Bdnf, Camk2d, Dscaml1, Dclk1, Ntrk3,* and *Sema3a*; Fig. 2A–C).

Figure 2. I-BET858 effect on BDNF-inducible gene expression *in vitro*. Heat maps show normalized expression values using microarray analysis for all BDNF-inducible and I-BET–suppressed (left, more than twofold) or I-BET–resistant (right) genes in cortical neurons at 2 h (A) and 12 h (B) after treatment (n = 3/group; experiment was performed in duplicate). Selected genes are indicated. Circle plot shows the number of BDNF-inducible genes that are unchanged (white), significantly suppressed (blue), or induced (red) more than two-fold after I-BET858 treatment.

40

Decreased synaptic gene expression following BET inhibition has been linked to impaired immediate early gene (IEG) induction [111]. However, we observed the expression of IEGs, such as *Arc, Dusp1/4, Egr1-4, Fosb, Homer1, Ier2/5, Junb, Nr4a1/2/3,* and *Srf* in response to BDNF treatment after 2 and 12 h were increased by I-BET858 (Fig. 2A-C). To better assess rapid IEG induction, neurons were pretreated with I-BET858 (1μM) or JQ1 (250 nM) for 20 minutes before a 10- or 20-minute BDNF (50 ng/mL) stimulation. We confirmed that I-BET858, in fact, potentiated the induction of *Arc, Fos,* and *Nr4a1* after 10 of BDNF stimulation (Fig. 3A). Potentiation of IEG expression was observed in a concentration-dependent manner (1 μM and 100 nM) (Fig. 3B). After 20 minutes, when IEG induction is strongest, neither JQ1 nor I-BET858 impaired *Arc* or *Fos* induction; however *Nr4a1* was decreased in both conditions (Fig. 3C). These results indicate apparent differences between the two BET inhibitors which should be considered when comparing datasets. These data also suggest that I-BET858 treatment in neurons does not generally disrupt BDNF-induced neuronal signal responses or subsequent IEG induction, but specifically represses the transcription of a selected group of secondary/late response genes in response to BDNF treatment (Fig. 2A-C).

Figure 2. Continued. Bar graphs display selected GO enrichments (-log10 p-value; red line, P = 0.05). (C) I-BET858 effect on the expression of selected immediate-early (left) or secondary (middle) BDNF-inducible genes or housekeeping genes (right) is shown.
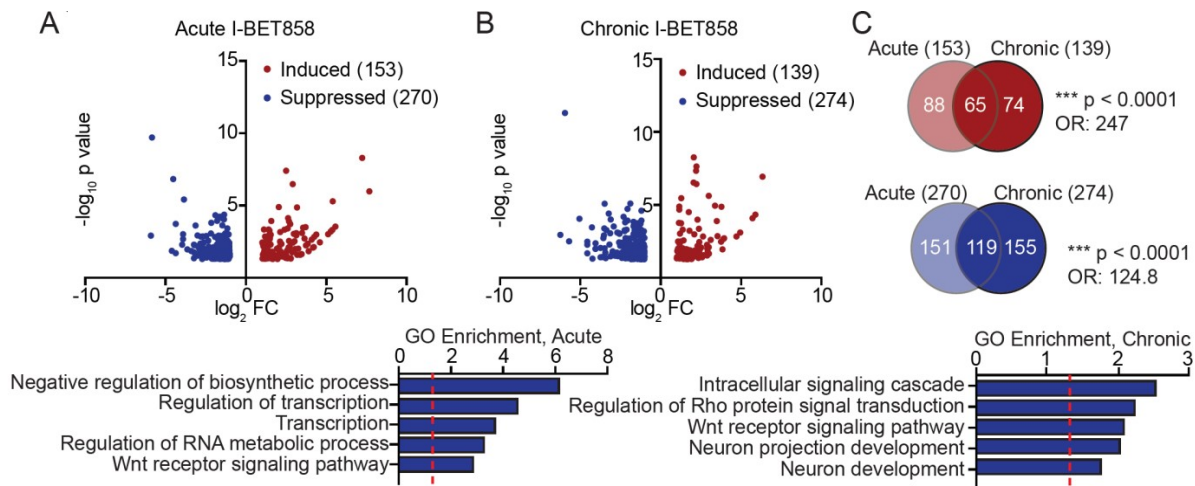
Figure 3. Immediate early gene expression after acute BET inhibition *in vitro*. (A-B) Effect of BET inhibition on *Arc, Fos,* and *Nr4a1* expression after BDNF stimulation (50ng/ml, 10 minutes) in primary cortical neurons at day 7 *in vitro*. (A) I-BET858 (1μM) but not JQ1 (250 nM) increases immediate early gene expression after 10 minutes of BDNF stimulation (n=9-18, three independent experiments). (B) *Arc, Fos,* and *Nr4a1* expression after BDNF stimulation two, independent concentrations of I-BET858 (1μM, 100nm, n = 3) (C) IEG expression after 20 minutes of BDNF stimulation (n = 3). One-Way ANOVA *p<0.05, **p<0.01, ***p<0.001.

Selective impairment of neuronal gene expression by pharmacological BET inhibition in vivo.

The development of the brain permeable I-BET858 allowed us to address for the first time the impact of pharmacological suppression of BET proteins on gene expression in neurons *in vivo*. We found that I-BET858 entered the mouse brain shortly after an intraperitoneal (i.p.) injection (data not shown). A single acute i.p. administration of I-BET858 at 30 mg/kg allowed I-BET858 detection in the brain at a concentration of >1 μM lasting for eight hours after the injection (data not shown). The tissue concentration of 1 μM matched the concentration of I-BET required for the therapeutic impact during systemic inflammation [1].

In our initial studies, we addressed the impact of acute and chronic I-BET858 administration on gene expression in the striatum. We chose the striatum because of 1) its relatively homogenous neuronal population with 90% of striatal neurons being D1 or D2 receptor-expressing medium spiny neurons, 2) the well-known pattern of medium spiny neuron gene expression [2], 3) the well-established role of the striatum in animal behavior, and 4) the contribution of impaired striatal function to neuronal disorders including ASD [132–134].

Figure 4. Selective effect of I-BET858 on gene expression *in vivo*. Volcano plots show genes that are significantly suppressed (blue) or induced (red) more than twofold after acute (A) or chronic (B) I-BET858 treatment in the mouse striatum using RNA sequencing analysis (n = 2). Bar graphs display selected GO enrichments (bottom; -$\log_{10}$ p-value; red line, P = 0.05). (C) Venn diagrams show the overlap of genes after acute or chronic I-BET858 treatment. Statistics: χ^2 test, ***, P < 0.0001; OR. 247 and 124.8.

Acute I-BET858 treatment resulted in the suppression of 270 genes 4 h after a single i.p. injection (Fig. 4A). The chronic administration of I-BET858 for 2 weeks did not affect the total number, but rather the pattern of affected genes (Fig. 4B, C). About 45% of genes suppressed by acute I-BET858 (119/270) remained down-regulated 12 h after chronic daily I-BET858 injections, while 155 genes were suppressed by I-BET858 only after long-term treatment (Fig. 4C, p < 0.0001, OR: 124.8). A significant fraction of the *in vivo* I-BET858 suppressed genes (69/270 after acute, 51/274 after chronic, p < 0.0001, OR: 7.701 and 5.042) overlapped with the I-BET858-repressed genes in primary neurons *in vitro*. Most importantly, acute and chronic I-BET858 treatment resulted in significant down-regulation of 34 genes that have been previously implicated in ASD (p= 0.0025, OR: 1.755). Several of the I-BET858-suppressed ASD-associated genes included potent transcriptional regulators, such as the histone lysine demethylase

44
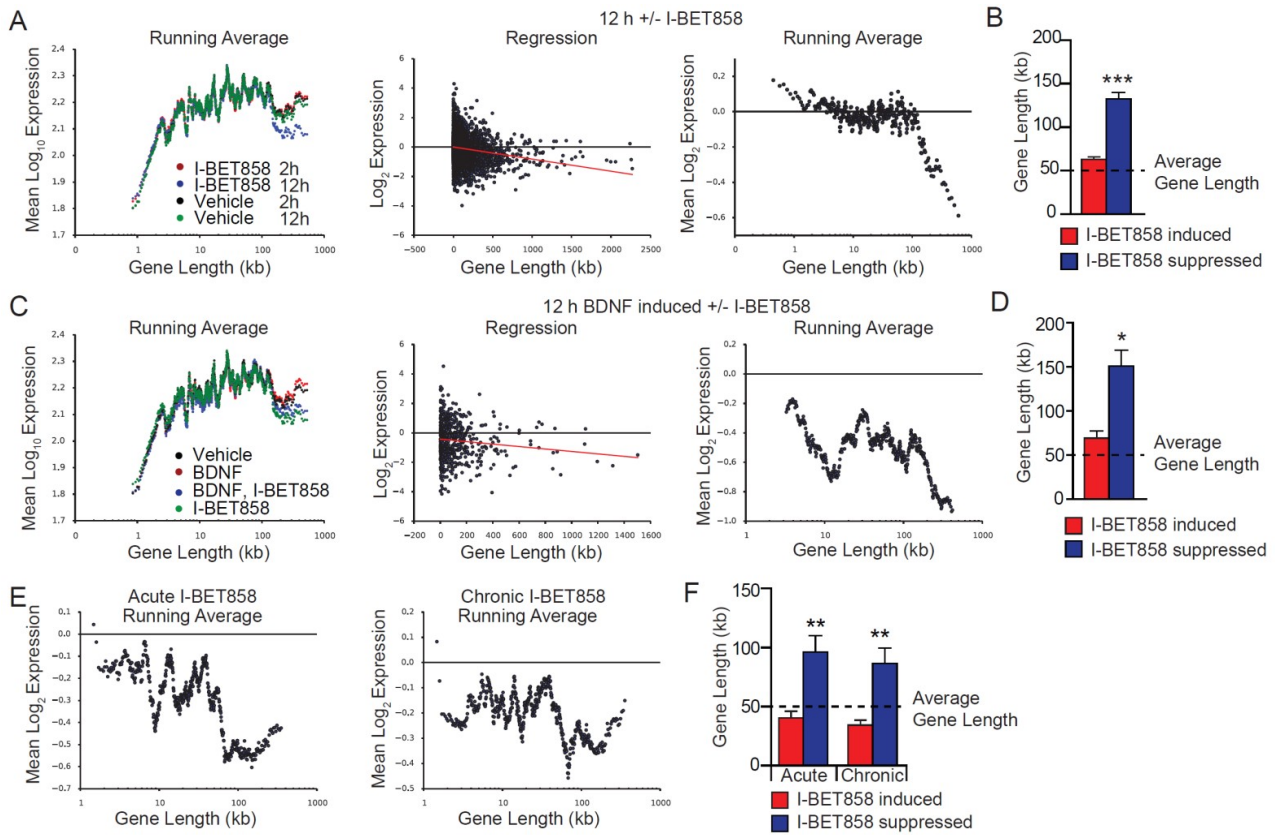
Phf2, the Set-domain binding protein *Setbp1*, and the transcription *factors Foxp1, Nr4a2, Zbtb20, and Tcf3*. The latter finding points to BET proteins as transcriptional regulators of gene-controlling chromatin circuits that can broaden the impact of BET inhibition on gene expression in neurons. This may, in part, explain the distinct patterns of genes only altered with chronic dosing (Fig. 4C). Similar to our *in vitro* studies, *in vivo* administration of I-BET858 had no impact on housekeeping gene expression (data not shown) but preferentially suppressed genes involved in neuronal development, dendrite and synapse formation and function (Fig. 4B).

I-BET858 mediated gene suppression correlates with gene length.

Earlier studies revealed a link between gene length and human ASD risk genes [14,135]. Remarkably, many of the genes suppressed by I-BET858 were on average significantly longer than the unaffected genes (Fig. 5). Treatment with I-BET858 for 12 h, but not for 2 h, of *in vitro* cultured, non-stimulated neurons suppressed preferentially extra-long genes > 100 kb with a correlation between gene length and reduced expression (Fig. 5A, Pearson's r = -0.147877, p < 0.0001). The average gene length of I-BET858 suppressed genes was ~130 kb and exceeded by ~2.5 fold the average length of genes (~50 kb) expressed in these neurons (Fig. 5B). Notably, 20% of the I-BET858 suppressed genes (194/1158) were extremely long genes that range in length from 200-2000 kb. In accordance with previous data pointing to a possible correlation

between extra-long gene length and human ASD risk genes, [14] we found that 42 of the 100 longest I-BET858 repressed genes were potential ASD candidate genes (p < 0.0001, OR: 15.44). A similar correlation between gene length and susceptibility to I-BET858-mediated transcriptional suppression was observed in BDNF-treated neurons (Fig 5C, D). BDNF treatment led to a slight increase in the expression of long genes > 100 kb that were also strongly and specifically suppressed by I-BET858 treatment (Fig. 4C, Pearson's r = -0.119946, p=0.004). The gene length of I-BET858 suppressed genes was ~3 fold higher than the average length of genes expressed in these neurons (Fig. 5D).

The strong correlation between gene length and I-BET858 susceptibility was also observed *in vivo* (Fig 5E). Similar to *in vitro* cultured neurons, I-BET858 suppressed gene transcripts in the mouse brain *in vivo* were on average ~2 fold longer than those induced or unaffected by I-BET858 (Fig. 5F). Furthermore, 18 (acute) and 13 (chronic) of the 100 longest I-BET858 repressed genes *in vivo* were ASD candidate genes (p < 0.0001, OR: 4.428; p < 0.001, OR: 3.001). These genes include the transcriptional regulators *Foxp1, Npas2, Phf2, Setbp1, Tcf3, Zbtb20*, and the neuronal signaling and adhesion proteins *Antxr1, Cdh10, Cdh11, Grm1, Lamb1, Nrg1,* and *Slitrk5,* many of which were similarly controlled by I-BET858 in cultured neurons *in vitro*. The preferential impact of I-BET858 on long genes in neurons may reflect the known role of BET proteins in regulation of transcriptional elongation [58,136].

Figure 5. I-BET858–mediated gene suppression correlates with gene length *in vitro* and *in vivo*.
(A) Distribution of gene expression levels versus gene length in primary neurons after 2 h (red) or 12 h (blue) I-BET858 or vehicle treatment (2 h, black; 12 h, green) using microarray analysis ($n = 3$). Linear regression of $\log_2$ gene expression fold changes (middle) and running averages (right) are shown (Pearson's r = -0.147877, red line; P <0.0001). (B) Bar graph shows average gene length of I-BET858–induced (red) or –suppressed (blue) genes after 12 h using microarray analysis ($n = 3$); dashed line, average neuronal gene length. (C) Distribution of gene expression versus gene length in primary neurons after 12-h treatment with BNDF (red), vehicle (black), I-BET858 (green), or BDNF + I-BET858 (blue) using microarray analysis ($n = 3$) is shown. Linear regression (middle) and running averages (right) of log2 expression fold changes of 12-h BDNF induced genes ± I-BET are shown (Pearson's r = -0.119946, red line; P = 0.004). (D) Bar graph shows average gene length of I-BET858–induced (red) and –suppressed (blue) BDNF-inducible genes after 12 h. (E) Distribution of gene expression versus gene length using RNA-seq analysis of mouse striatum ($n = 2$) after acute (left) or chronic (right) I-BET858 treatment are shown. (F) Bar graph shows average gene length of I-BET858–induced (red) and –suppressed (blue) genes after acute and chronic I-BET858 treatment, respectively. Statistics: two-tailed unpaired Student's *t* test, error bars represent SEM. *, P < 0.05; **, P < 0.01; ***, P < 0.0001.

It is possible that the successful generation of a nascent transcript for long genes exceeding 100 kb is more susceptible to perturbation of elongation efficiency as compared to shorter genes.

In addition to its role in releasing paused PolII, Brd4 can evict nucleosomes from the chromatin through its own histone acetyltransferase activity [95]. Higher nucleosome content can slow the rate of RNAPII transcription which is tightly coupled to splicing events [137]. Therefore we reasoned that I-BET858 may cause alternative splicing events by slowing the rate of elongation possibly from the loss of P-TEFb recruitment or by increased nucleosome occupancy along long genes. Indeed we identified a number of genes (213 in acute and 196 in chronic) that were alternatively spliced in the presence of I-BET858 in vivo. Of these, 44 were shared between acute and chronic conditions. Additional ASD risk genes, including *Fmr1, Nsd1, Mll3,* and *Tsc2*, were alternatively spliced after BET inhibition (25/213 in acute and 27/196 in chronic). Interestingly, exon 3 of *Brd2* was skipped in acute I-BET858 tissues. Very few genes that were alternatively spliced after acute (7/213) or chronic (5/196) I-BET858 were also down-regulated at the mRNA level.

Given the role of Brd4 in enhancer-mediated gene expression [88,92], we used Chip Seq datasets previously generated in our lab to determine if the I-BET858-sensitive genes were located near and presumably targets of enhancers. These 1034 regions were then annotated to the closest gene as an attempt to understand the targets of enhancers. A minor fraction of BET sensitive genes (6%, 71/1158) were identified as putative target genes of enhancers (H3K4me1+, H3k27ac+ sites) including *Gria1* and *Whsc1*. While this analysis can approximate the contribution of enhancers to our observed gene expression changes, a chromatin conformation capture assay such as Hi-

C would be required to confirm that these enhancer elements interact with the promoters of our I-BET858-sensitive genes and that this association is lost after BET inhibition. Based on this analysis, it seems unlikely that the BET-mediated recruitment of enhancers regulates the expression of long, synaptic genes.
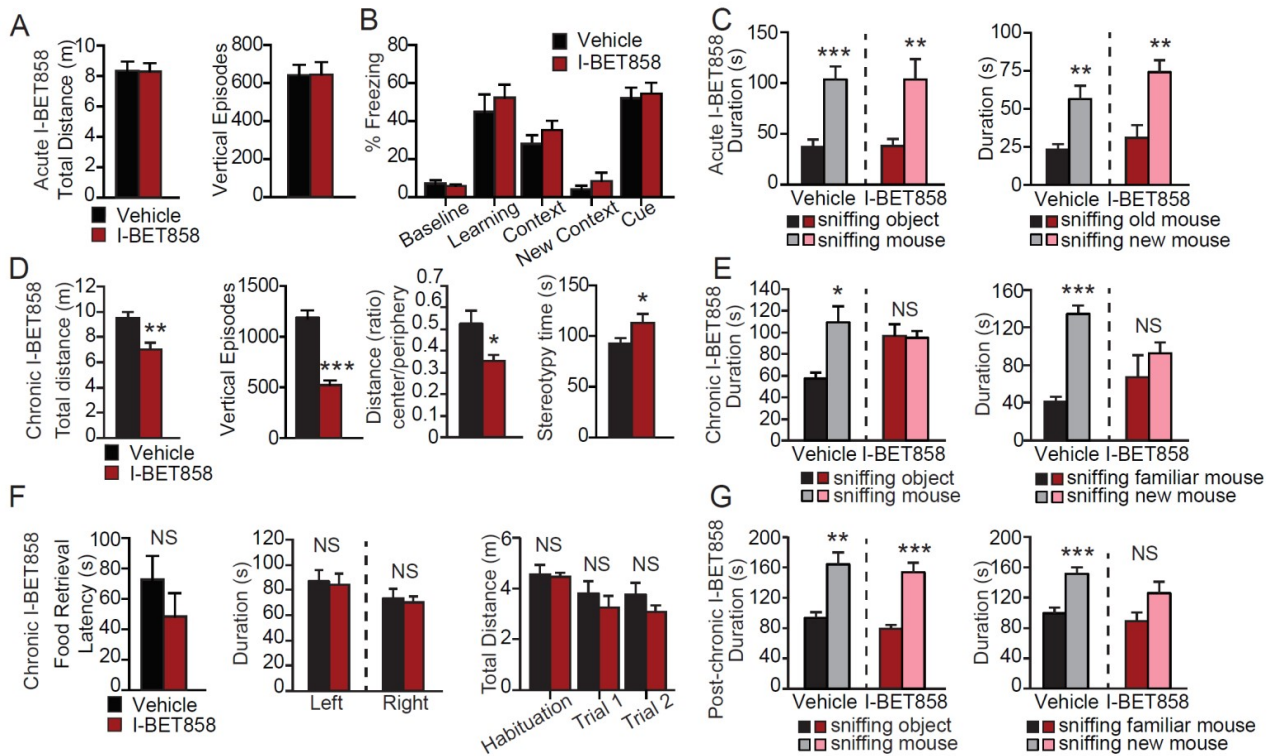
I-BET858 treatment induces autism-like behavior in mice.

The selective impact of BET protein inhibition on neuronal gene expression and the preferential I-BET858-dependent inhibition of long genes suggested that treatment with I-BET may lead to the development of ASD-like behaviors in mice. The key behavioral symptoms of ASD in humans include abnormal social interactions, communication deficits, anxiety, and repetitive behaviors. A combination of alterations in social behaviors, anxiety, and repetitive behaviors are, therefore, frequently used to diagnose autism-like phenotypes in mice [133,138].

The impact of acute I-BET858 on mouse behavior was determined by assessing basal motor activity, anxiety-like behaviors, social interaction, and memory (Fig. 6). We did not observe any signs of distress, anxiety, or other behavioral or motor abnormalities in mice of various ages acutely treated with I-BET858 (Fig. 6A, data not shown). Acute I-BET858 treatment also did not affect memory formation in mice. A single injection of I-BET858, after training mice in a fear-conditioning paradigm, had no

effect on mouse memory of the foot-shock associated context or auditory cue 24 h later as compared to vehicle-injected controls (Fig. 6B).

Contrary to acute BET inhibition, chronic daily I-BET858 administration starting at 4 weeks of age led to the development of behavioral abnormalities consistent with an autism-like syndrome (Figure 6D, E). Following 2 weeks of chronic I-BET858 treatment, 6-week-old mice displayed reduced explorative motor activity and heightened anxiety-like behavior in the open field (Fig. 6D). I-BET858 treated mice also spent slightly more time engaging in stereotypic behaviors as compared to their vehicle-treated controls (Fig. 6D). Using the three-chamber social approach task that is commonly used to reveal ASD-like social deficits in mice [138], we found that chronic (Fig. 6E), but not acute (Fig. 6C), 6-week-old I-BET858 treated mice displayed greatly reduced sociability. When tested for their preference to explore a novel mouse versus an inanimate novel object, the chronic I-BET858-treated mice spent equivalent amounts of time sniffing the mouse and the object, unlike vehicle-treated littermates that preferred to explore the novel mouse (Fig. 6E). In addition to the reduced sociability, chronic I-BET858 treated mice showed a significant reduction in their preference for social novelty. Preference for social novelty requires functional social recognition and is defined as the test mouse spending more time exploring/sniffing a novel mouse than a familiar mouse. Opposite to vehicle-injected mice, chronic I-BET858 treated mice displayed no significant preference in exploring a novel mouse over a familiar mouse (Fig. 6E). Importantly, the observed effects on social preference in the I-BET858 treated mice were not due
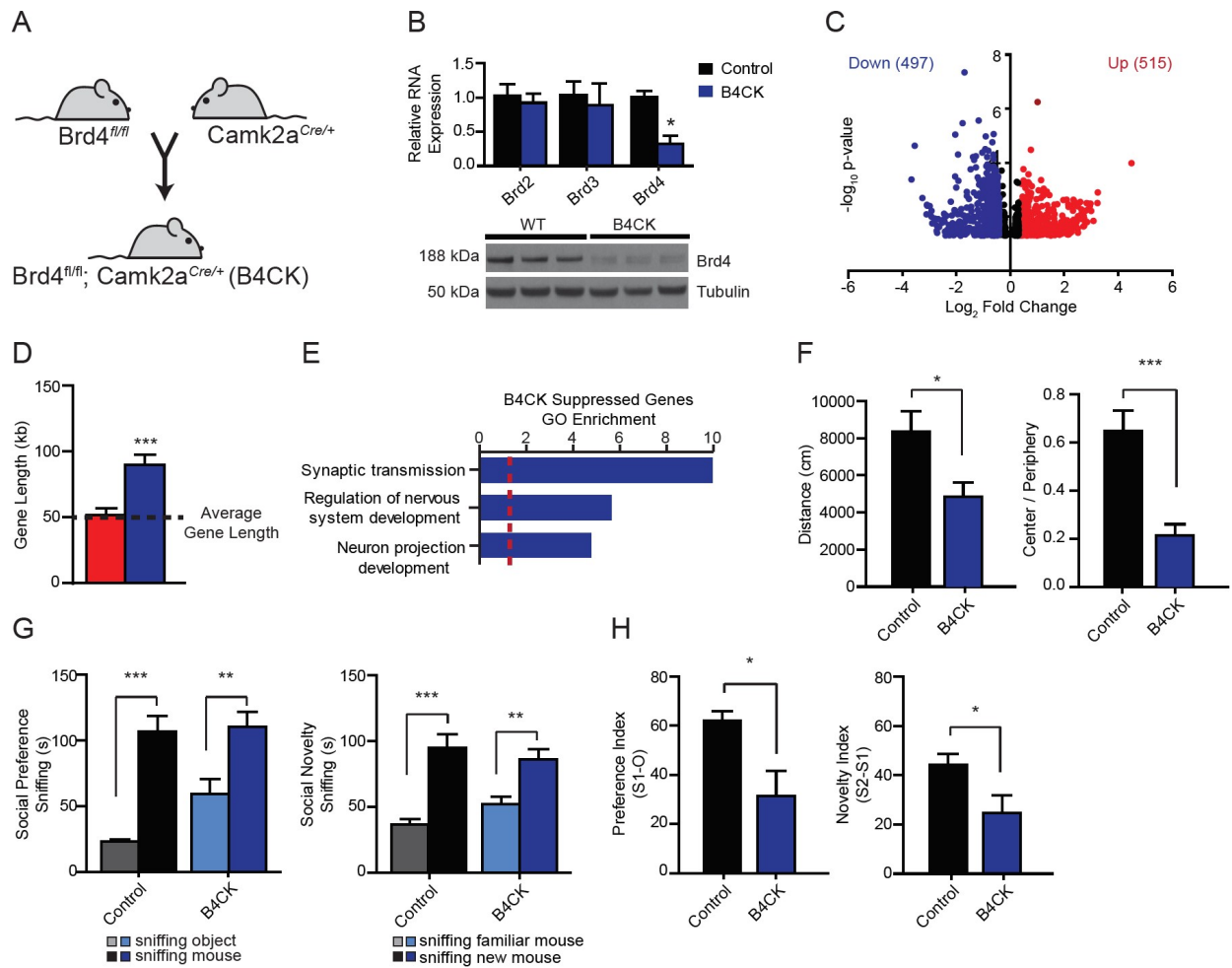
Figure 6. I-BET858 treatment induces an autism-like syndrome in mice. (A–C) Effects of acute I-BET858 treatment on motor activity and exploration in the open field (A; n = 8 mice per group), memory (B; n = 10), and social interaction (C; n = 8) in mice are shown. (D and E) Effects of chronic I-BET858 treatment on motor activity, anxiety, and stereotypic behavior in the open field (D; n = 10), social behavior (E; n = 10), hidden food retrieval (F; n = 5), left versus right bias and total distance moved during the social interaction paradigm (n = 10) in mice are shown. (G) Social behavior in mice 5 mo after chronic I-BET858 treatment is shown (n = 5). Statistics: Student's t test, error bars represent SEM. *, P < 0.05; **, P < 0.01; ***, P < 0.0001.

to defective olfaction or reduced overall explorative activity in the three-chamber assay; I-BET858-treated mice displayed no differences in hidden food retrieval, no left versus right bias differences, and no reduction in velocity, total distance moved, or time spent sniffing/exploring during the social interaction paradigm (Fig. 6F, data not shown) as compared to control vehicle-injected mice. Notably, social behavioral deficits were partially reversed in mice after a recovery period of 5 months (Fig. 6G).

Neuronal Brd4 may mediate the development of social behaviors

Of the BET proteins, Brd4 is the most likely candidate for the mechanistic action of I-BET858. I-BET858 has the highest affinity for Brd4 suggesting it may preferentially inhibit Brd4 activity first [139]. Brd4 binds to the promoters of key neurodevelopment regulators *Bdnf* and *Gria1* and regulates their expression in an activity-dependent manner [110,111]. Finally, a deletion mutation in Brd4 has been identified in ASD patients, strongly suggesting a role for Brd4 in the development of social behaviors [12]. These data indicate that Brd4 may be a critical transcriptional regulator of extra-long synaptic genes required for proper brain development.

To test this hypothesis, Brd4 was deleted specifically from forebrain neurons at postnatal day 14 by crossing the Brd4$^{fl/fl}$ mouse line to the Camk2a$^{Cre/+}$ line hereafter referred to as B4CK (Fig. 7A). Decreased levels of Brd4 mRNA and protein were observed in the forebrain at six weeks of age (Fig. 7B) which is consistent with a specific loss of Brd4 in neurons but not glial cells. Importantly, Brd2 and Brd3 mRNA levels did not change after Brd4 depletion, suggesting that the BETs may have non-redundant functions.

Figure 7. Brd4 regulates the transcription of long, synaptic genes in vivo. (A) Brd4^{fl/fl} mice were crossed to Camk2a[Cre/+] mice to delete Brd4 specifically from forebrain neurons at two postnatal weeks. (B) Brd4 mRNA and protein are reduced in the forebrain of B4CK mice (n = 3). (C) Volcano plots show genes that are significantly suppressed (blue) or induced (red) more than 1.25 fold at 6 weeks in the B4CK mouse striatum using bulk RNA sequencing analysis (n = 3). (D) Bar graph shows average gene length of genes induced (red) or suppressed (blue) in the striatum of B4CK mice; dashed line, average neuronal gene length (Mann Whitney test, ***p<0.0001). (E) Bar graphs display selected GO enrichments (-$\log_{10}$ p-value; red line, P = 0.05). (F-H) Effect of Brd4 neuronal loss on motor activity and exploration in the open field (F; two-tailed unpaired Student's t-test, *p<0.05, ***p<0.0001) and social interaction (I-J; two-tailed unpaired Student's t-test, *p<0.05, **p<0.01, ***p<0.0001) are shown (n = 7-11 per group).

Brd4 loss from neurons suppressed the expression of 497 genes in the striatum

and approximately 15% of these genes (46/497 Acute p<0.0001, OR: 11.0, 35/497

Chronic p <0.0001, OR: 7.68) were also regulated by I-BET858 *in vivo* (Fig. 7C). As

53

previously observed with I-BET858, long, synaptic genes were selectively down-regulated after neuronal loss of Brd4 (Fig. 7D, E). Of these, 46 genes were previously identified ASD risk genes (p<0.0001, OR: 2.075) including *Cntnap2/3, Kcnd2,* and *Cdh9*. Additionally, essential medium spiny neuron identity genes were decreased after Brd4 deletion (91/502, p<0.0001, OR: 13.33) including *Drd1a, Drd2*, and *Adora2a*, suggesting that loss of Brd4 may interfere with striatal neuron development. Together, these data indicate that Brd4 regulates the expression of long, synaptic genes implicated in ASD.

To understand if Brd4 loss also resulted in an autism-like phenotype similar to I-BET858, we assessed behavioral changes in the B4CK mice (Fig. 7). Similar to I-BET858-treated mice, B4CK explored less in the open field assay and exhibited decreased thigmotaxis (Fig. 7F). However elevated plus-maze activity was similar to wild-type littermate controls indicating that loss of Brd4 in forebrain neurons did not increase anxiety-like behaviors (data not shown). When tested in the three-chamber sociability assay, B4CK mice exhibited overtly normal social preference and social novelty behaviors (Fig. 7G). Because the total sniffing time varied between experimental groups (data not shown) the preference indexes were calculated as below to more accurately compare between groups:

O – object　　　　　S1 – social target 1　　　　S2 – social target 2

$$Social\ Preference\ Index = \frac{Sniff\ Time_{S1} - Sniff\ Time_O}{Total\ Sniff\ time}\ x\ 100$$

$$Social\ Novelty\ Index = \frac{Sniff\ Time_{S2} - Sniff\ Time_{S1}}{Total\ Sniff\ time}\ x\ 100$$

Accounting for these differences revealed that neuronal loss of Brd4 led to impaired

social behaviors in mice (Fig. 7H). While this phenotype is not as robust as that

observed with I-BET858, it suggests a role for Brd4 in postnatal brain development.

Together these data indicate loss of Brd4 from neurons reproduces the effects of I-

BET858 on neuronal gene expression and partially reproduces the autism-like

phenotype, although to a lesser extent.

Discussion

Autism spectrum disorder (ASD) confines a group of complex

neurodevelopmental disorders characterized by repetitive behaviors and social

interaction deficits. While the classic ASD etiology focused on altered synaptic

development and function, recent genetic studies of ASD patients revealed the

importance of epigenetic regulators of gene transcription in the disease etiology

[9,11,140,141]. In support of this, several genetic mouse models lacking these chromatin

regulators develop ASD-like phenotypes [117,125,142,143]. These findings suggest the

possibility of a novel, epigenetic mechanism of ASD where alterations in gene

transcription may lead to abnormal neuronal development and circuit formation.

Despite the ubiquitous expression of these chromatin regulators, ASD symptoms

are primarily centered in the central nervous system. The proposed vulnerability of the

brain to impaired transcription has been linked to an enrichment in the expression of long genes in the human and mouse brain as compared to any other organ [14,144]. These long genes encode synaptic proteins and ion channels, including those that have been linked to ASD [14,135]. Transcription of genes of extended length is likely to be more sensitive than that of short genes and may require additional regulatory mechanisms to ensure proper transcriptional fidelity. In support of this, long genes harbor unique expanded enhancer domains and are particularly dependent on the topoisomerase, Top2b which assists the elongation phase of transcription [14,145]. It is therefore essential to understand the mechanisms that regulate transcriptional elongation in neurons during development.

Here we identify the BET proteins as critical transcriptional regulators of extra-long synaptic genes linked to ASD. Inhibition of this family causes an autism-like phenotype in juvenile mice which includes increased anxiety and repetitive movements and impaired social behaviors. We show that impaired transcriptional elongation significantly alters neuronal development and supports the notion that neuronal gene expression is uniquely sensitive to changes in transcriptional efficiency. Furthermore, neuronal loss of Brd4 primarily leads to decreased expression of extra-long genes sensitive to pan-BET inhibition and partially mimics the autism-like phenotype in mice. Recent work showed increased Brd4 expression in the Fragile X mouse model of ASD [146]. Taken together with our data, this suggests that the gene dosage of Brd4 may be critical for neuronal function with either too little or too much disrupting neuronal

development. While this strongly suggests control of postnatal brain development by Brd4, it is possible that other BET protein members also contribute to the ASD-like phenotype. Future experiments will focus on specifically deleting Brd2, alone and with Brd4, from neurons to understand the distinct roles for BET proteins in the development of social behaviors. Additionally, the observed phenotype induced by I-BET858 may not be neuron-intrinsic and may require loss of BET activity in glia or even in the peripheral organs which can be addressed by taking advantage of the newly generated floxed Brd2 and Brd4 mouse lines. Genetic models may not be sufficient, however, to fully recapitulate the effects of pharmacological BET inhibition as systemic clearance of the injected drug will likely lead to a cyclic ON/OFF binding pattern of BET proteins over time. It is, therefore, possible that permanent loss of the Brd4 protein may alter gene expression in a manner different than that of differential chromatin binding after I-BET858.

It has been proposed that the effects of BET inhibition on neuronal gene expression are due to impaired immediate early gene (IEG) induction [111]. However, we and others observe that BET inhibition potentiates IEG induction [1,110,113]. To explain this phenomenon, we propose that the transcriptional machinery, displaced from synaptic genes by I-BET858, redistributes along the chromatin and binds to accessible promoters which are mainly IEGs. After BET inhibitors displace the BET complex from the chromatin, the released P-TEFb would then be able to incorporate into either the Super-elongation complex which activates transcription or the inhibitory Hexim1/7SK complex.

However, BET inhibition can also lead to the dissociation of P-TEFB from the Hexim1/7SK complex [147]. As a result, the newly released P-TEFB incorporates into the super elongation complex (SEC) and induces expression of Hexim1 mRNA to maintain transcriptional homeostasis [148]. In accordance with this model, we see increased Hexim1 expression after I-BET858 treatment. In conclusion, we propose that the increase in IEGs after BET inhibition is caused by an increased association of P-TEFb with the super elongation complex. This phenomenon would then be mechanistically distinct from the BET-dependent down-regulation of long, synaptic genes implicated in ASD.

In summary, our findings reveal a crucial role of BET proteins in the regulation of selected genes that control normal neuronal development and function. The significance of BET proteins in the regulation of mouse behavior is underscored by the development of an ASD-like syndrome in mice treated with brain permeable I-BET858. The data also suggest that environmental factors that have the ability to affect BET protein function or BET target gene expression may contribute to ASD. The pharmacological induction of ASD-like symptoms in mice provides a valuable tool for the identification of genes that may play a pivotal role in disease development or for the development of novel drugs targeting ASD. Moreover, our studies suggest that the pharmacological control of BET proteins or BET-dependent gene expression regulation could be used not only for modeling of autism-like behaviors, but possibly for the correction of aberrantly expressed genes in ASD and other neurodevelopmental disorders.

Chapter Four

Balancing microglial states in neurodegeneration

through BET inhibition

Abstract

As postmitotic cells, neurons are incapable of replacing themselves and, while adult neurogenesis can occur [149,150], this limited capacity cannot compensate for large-scale neuronal loss during neurodegeneration. It is, therefore, of the utmost importance to understand the cellular and molecular mechanisms that cause neuronal death and dysfunction. Recent genetic studies have identified a causal role for microglia, the brain's immune cells, in neurodegenerative diseases such as Alzheimer's disease (AD) [151–154]. Microglia, which exist in diverse functional states that reflect their microenvironment, can enter a pro-inflammatory state after brain injury or infection by dramatically shifting their morphology, transcriptome, and function. This inflammatory activity, which is initially beneficial, can have deleterious effects on tissue health if left unchecked. In peripheral macrophages, the bromodomain and extraterminal domain-containing (BET) protein family of transcriptional regulators control the induction of pro-inflammatory cytokines in response to danger signals [1,155]. Here we show that, analogous to their role in macrophages, BET proteins regulate the expression of pro-inflammatory genes in microglia *in vitro* and *in vivo*. Furthermore, pharmacological BET inhibition decreases microgliosis, prevents brain atrophy, and rescues fear memory in an Alzheimer's mouse model. These data identify BET proteins as critical regulators of pathological microglial activation and demonstrate a novel, therapeutic potential for BET inhibition in neurodegenerative disease.

Introduction

Microglia, the resident macrophages of the central nervous system, are derived from myeloid progenitors in the yolk sac, unlike other brain cells which are neuroectodermal [156–159]. As such, microglia perform unique roles to maintain brain function during homeostasis and disease. These highly dynamic cells continually survey the brain parenchyma [160] to sense changes in the environment with a multitude of cell-surface receptors [161–163]. In a homeostatic state, microglia perform many neurotrophic functions to promote proper neuronal development and function including synaptic pruning [164,165], secretion of growth factors [166–168], and phagocytosis of dead and dying cells [17,169,170]. These homeostatic functions are critical for the maintenance of proper brain health [17].

If an injury or infection is sensed, microglia initiate an inflammatory response which involves a dramatic, comprehensive change in morphology and function. To facilitate this transition, homeostatic gene networks are down-regulated while inflammatory gene networks are induced [171,172]. Microglia-mediated inflammation initially aids tissue recovery but can exacerbate or even initiate neuronal death if not correctly regulated [169,173,174]. Hyperactive microglial activity has been implicated in almost all major neurodegenerative diseases [175,176]. Postmortem AD tissue, as well as many other neurodegenerative diseases, also shows increased microglial proliferation and expression of pro-inflammatory cytokines such as MHC II, Il-1β, and TNF [175–179]. In Alzheimer's disease (AD), microglia [180–183] generate increased levels of pro-inflammatory

cytokines. These cytokines, which can be triggered by Aβ plaques [184,185] or dying neurons, can themselves cause neurodegeneration [169,173,174]. Furthermore, mutations in microglia-enriched molecules such as TREM2 [151,152], C1R [186], and CD33 [153,154] have been identified as risk factors for late-onset Alzheimer's disease, indicating a significant role for microglia in AD pathology. Understanding the mechanisms that regulate the pro-inflammatory microglial state is therefore crucial to the development of novel therapeutic strategies for neurodegenerative disorders.

In peripheral macrophages, the induction of inflammatory gene networks is regulated by the BET protein family [1,95]. These BET proteins bind to acetylated lysine residues on histones H3/H4 and recruit factors that allow for the full elongation of mRNAs by RNAPII [59,60]. Inhibition of the BET-dependent inflammatory gene expression profile in peripheral macrophages can completely prevent death from sepsis, a pathologically hyperactive immune response [1]. In microglial cell lines, BET inhibition attenuates the induction of several pro-inflammatory genes after lipopolysaccharide, a bacterial wall component [115,116]. Moreover, BET inhibition in the retina prevents cytokine expression and increases neuronal survival after NMDA stimulation, suggesting that blockade of BET-dependent inflammation may be beneficial for neuronal health [187]. Based on this data, we hypothesized that BET proteins regulate inflammatory gene expression in microglia and that BET inhibition may be a potential therapeutic strategy to restrain hyperactive microglial activation during neurodegeneration.
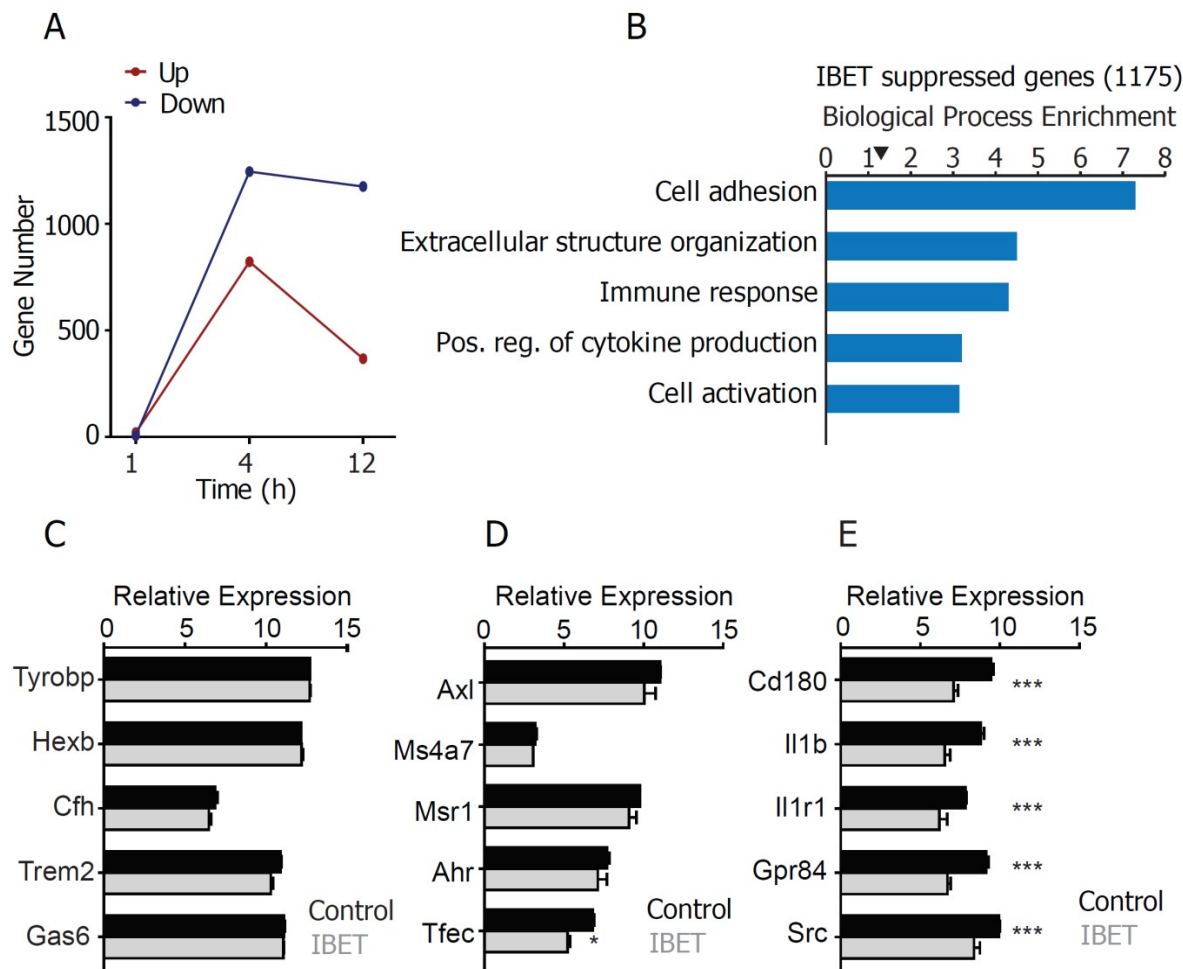
Using the brain-permeable BET inhibitor, I-BET858, we confirm that BET proteins control the inflammatory activation of microglia by LPS *in vitro*. Moreover, we show that chronic BET inhibition in an AD mouse model prevented the expression of key inflammatory mediators without negatively impacting homeostatic gene expression profiles. Furthermore, chronic administration of I-BET858 decreased microgliosis, preserved hippocampal neuron numbers, and significantly rescued memory in an AD mouse model. These data excitingly identify BET inhibition as a promising therapeutic strategy for the treatment of neurodegenerative disease.

Results

BETs regulate LPS-mediated microglial activation *in vitro*
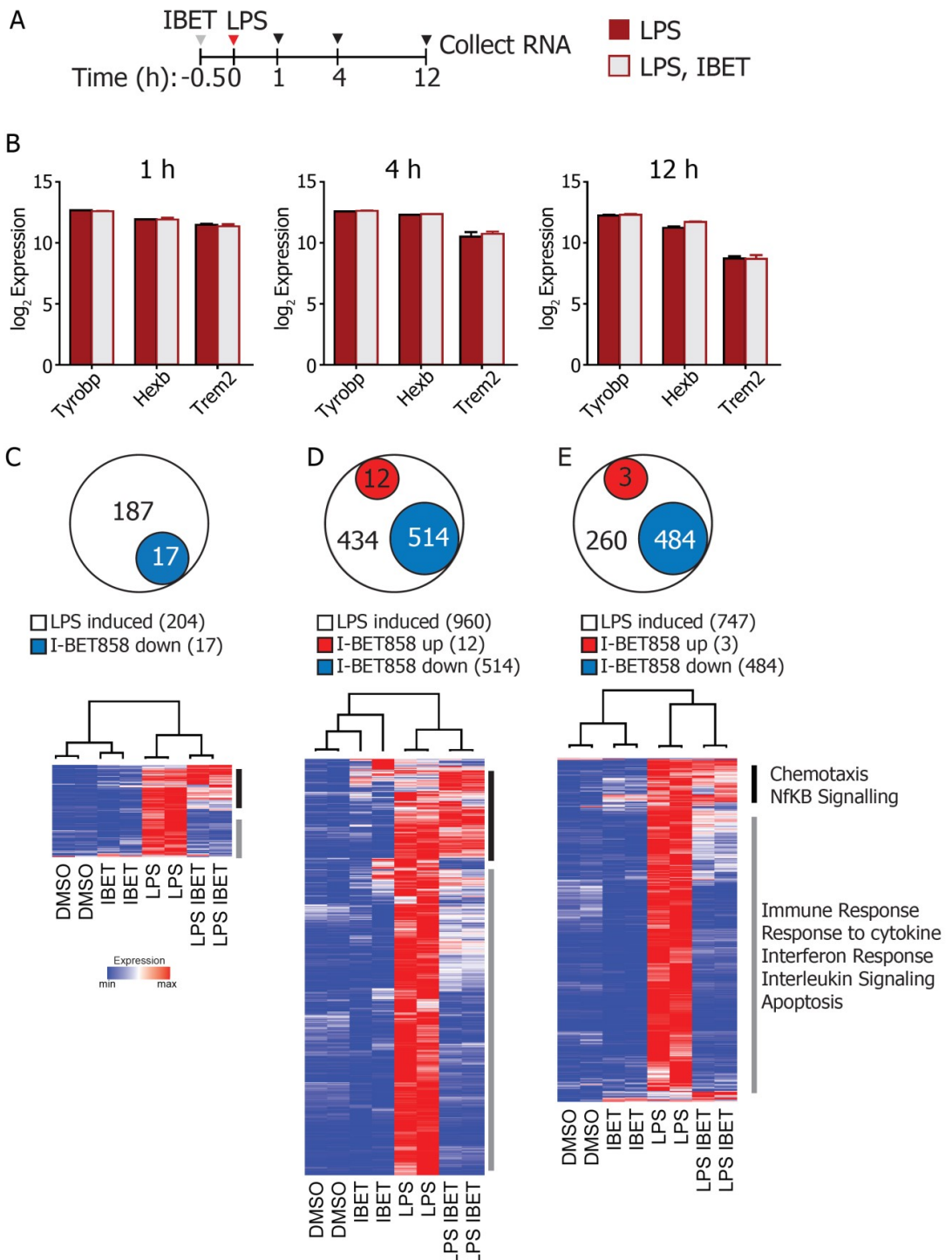
To test the role of BET proteins in microglial gene expression, primary microglia cultures from mouse forebrain were treated with the brain-permeable BET inhibitors I-BET858 (1μM) for 1, 4, or 12 hours (Fig. 1A). While the loss of BET activity in macrophages negatively impacts differentiation and proliferation [188], *Hexb, Cfh, Fcrls,* and *Fcer1g* expression was unaffected by I-BET858 indicating microglial differentiation is unaffected (Fig. 1C, data not shown). Likewise phagocytosis genes, whose expression is tightly regulated by the Polycomb Repressive Complex 2 (PRC2) in microglia [17], were mostly unaffected by I-BET858 treatment at all time points (Fig. 1D). However, we found that I-BET858 suppresses genes enriched for immune response, cell adhesion,

and cell activation pathways (Fig. 1B). These genes encode regulators of every step of the pro-inflammatory response from signal recognition (*Ccr5, Il1r1, and Tlr2/3/7*), to signal transduction (*Irak2, Src, and Traf1*) and cytokines (*Il1b*) (Fig. 1E) suggesting that BETs are required for the maintenance of an inflammatory state in microglia *in vitro*.

Figure 1. Transcriptional effect of BET inhibition in primary microglia. (A) Number of genes significantly suppressed (blue) or induced (red) more than two fold by I-BET858 (1 μM) in primary forebrain microglia after 1, 4, or 12h (microarray, n = 2, experiment performed in triplicate). (B) Down-regulated genes at 4 h are enriched for immune response and cell activation pathways (-$\log_{10}$ p value, arrow indicates significance cutoff p = 0.05) (C-E) Expression of microglia identity genes (C), phagocytosis (D), and pro-inflammatory genes (E) after BET inhibition in primary microglia. (Statistics: moderated t-test with Benjamini-Hotchberg correction, *p<0.05, ***p<0.0001)

However, microglia are highly dynamic cells that initiate an inflammatory gene program in response to tissue damage or infection. To understand if BET proteins regulate the induction of pro-inflammatory gene networks, primary microglia were stimulated with lipopolysaccharide (LPS), a component of bacterial cell walls. In macrophages, the robust increase in cytokine and chemokine production following LPS exposure was dependent on BET-mediated transcription. LPS caused a time-dependent increase in pro-inflammatory gene expression in microglia (Fig. 2C-E). Specifically, proliferation (*Cdk6, Cdk14*), cell death (*Casp1/4/7/12, Bid, Fas*) and cytokine production pathways (*Nfkb1/2, Il1a/b, Ifnb1, Tnf*) were strongly and rapidly induced by LPS in primary microglia. BET inhibition did not negatively impact microglial lineage or survival after LPS stimulation as *Tyrobp, Hexb,* and *Trem2* was unaffected by I-BET858 (Fig. 2B). I-BET858 had little effect on gene induction at 1 h, a timepoint which primarily reflects immediate early gene transcription (Fig. 2C). This indicates that BET inhibition does not prevent microglia from sensing and responding to LPS. In contrast, BET proteins selectively regulated the main effectors of the inflammatory response as BET inhibition suppressed the majority of genes (514/960 at 4 hours and 484/747 at 12 hours) induced by LPS (Fig 2D,E). BET inhibition specifically decreased the expression of inflammatory genes (*Il6, Cd33, and Nlrp3*), interferon response genes (*Ifnb, Irf2/9, Mx1*) and cell death mediators (*Bid, Casp1/4/7/12, Traf1*). Notably, a proportion of genes were insensitive to I-BET858 and enriched for chemotaxis (*Ccl2/3/4/5, Cxcl1/2*) cell proliferation (*Csf1, Kitl*) and NFkB (*Rel, Relb, Nfkb1/2*) pathways, similar to previous findings in peripheral macrophages[1].
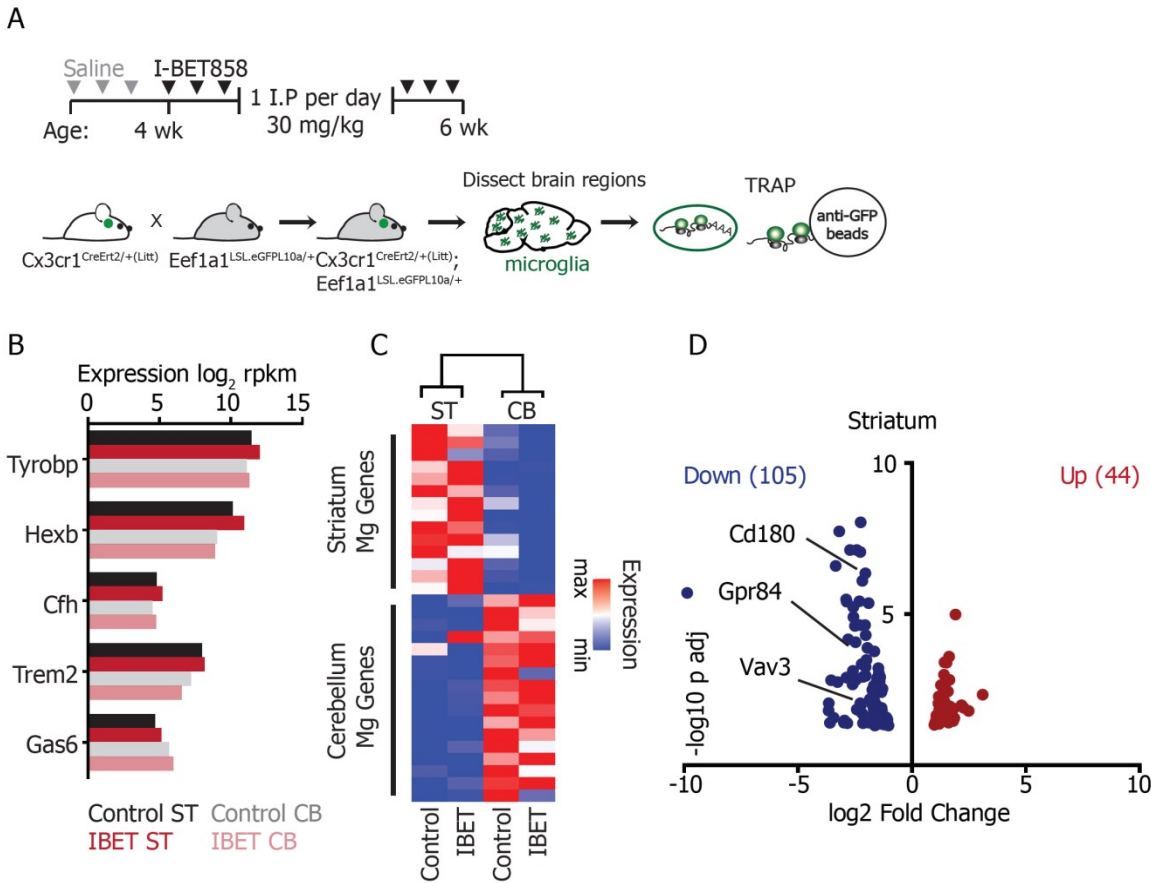
Figure 2. I-BET858 effect on LPS-inducible gene expression _in vitro._ (A) Primary forebrain microglia pretreated with I-BET858 (1 µM) for 30 minutes were exposed to lipopolysaccharide (LPS, 100 ng/mL) for 1, 4, or 12h. RNA was isolated for microarray analysis (n=2 per group, experiment done in triplicate). (B) Expression of microglial identity genes after LPS stimulation at 1, 4, or 12h. (C-E) Circle plots show the number of LPS-inducible genes that are unchanged (white), significantly suppressed (blue), or induced (red) more than twofold after I-BET858 treatment. Heat maps show normalized expression values using microarray analysis for all LPS-inducible genes in primary microglia at 1 h (C), 4 h (D) and 12 h (E) after treatment (n = 2/group; experiment was performed in triplicate). Significantly enriched pathways are indicated.

In summary, we conclude that BETs do not impact signal-induced migration or proliferation of microglia but instead specifically regulate the induction and maintenance of the pro-inflammatory cascade in microglia *in vitro*. These results, contrasted with those described in Chapter 3, reflect the unique specificity of BETs in different cell types. Furthermore, these data indicate I-BET858 may be a potential therapeutic approach to selectively suppress hyper-inflammatory microglia during neurodegeneration.

Loss of BET function in vivo does not disrupt homeostatic microglia functions

While these data are highly indicative of a role for BETs in inflammation, cultured microglia do not fully recapitulate gene expression profiles of microglia *in vivo*. To better understand the role of BET-dependent transcription *in vivo,* the microglia transcriptome was isolated using Translating Ribosome Affinity Purification (TRAP) after chronic I-BET858 administration. TRAP is an ideal method because it prevents the induction of immediate early and pro-inflammatory genes caused by other isolation protocols which can occlude homeostatic transcriptional profiles[17]. Cx3Cr1[CreErt2/+(Litt)]; Eef1a1[LSL.eGFPL10a/+] mice were injected once daily intraperitoneally with I-BET858 (30 mg/kg) for two weeks before TRAP was performed on the striatum (ST) and cerebellum (CB, Fig. 3A). As observed *in vitro*, microglial lineage was maintained after chronic BET

Figure 3. Effect of chronic BET inhibition on microglial transcriptomes *in vivo*. (A) Cx3Cr1 CreErt2/+(Litt); Eef1a1 LSL.eGFPL10a/+ mice were injected daily with I-BET858 (30mg/kg, i.p.) or vehicle for two weeks before TRAP was performed by Pinar Ayata on the striatum (ST) and cerebellum (CB). RNA was isolated for RNA sequencing (n=2 per group). (B) Expression of microglial identity genes after BET inhibition (C) Heatmaps show normalized expression of region-specific microglial genes in cerebellar or striatal microglia *in vivo*. (D) Volcano plot shows all genes significantly (p adj <0.05) induced (red) or suppressed (blue) by chronic I-BET858 administration in striatal microglia.

inhibition as indicated by expression of *Hexb, Fcrls,* and *Fcer1g* in both striatal and

cerebellar microglia (Fig 3B). Moreover, region-specific microglial heterogeneity was

maintained at the transcriptional level after chronic BET inhibition *in vivo* (Fig. 3C). This

is especially relevant to the therapeutic potential of I-BET858 because the loss of these

region-specific gene expression signatures is highly detrimental to brain function [17].
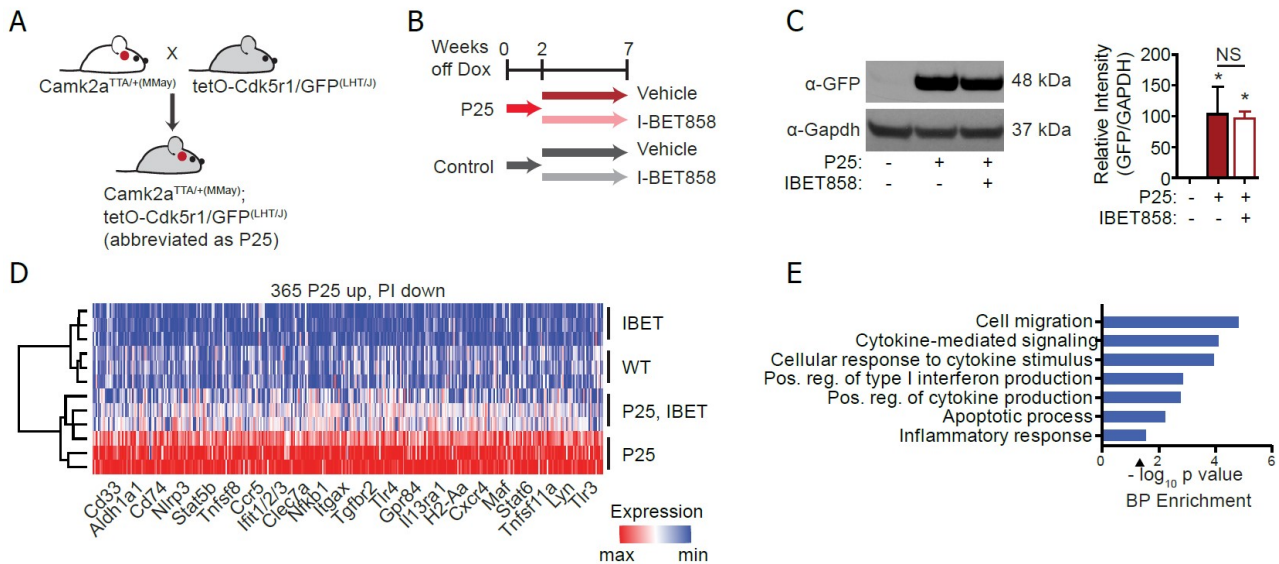
Furthermore, while chronic BET inhibition resulted in modest changes in striatal microglial gene expression *in vivo,* inflammatory genes such as *Ccr5*, *Cd180, Gpr84,* and *Wdfy1* were suppressed by I-BET858 (Fig. 3D). This suggests that there may be low levels of inflammation occurring in the healthy brain and strongly supports a role for BET proteins in the regulation of inflammatory gene transcription *in vivo*. BET inhibition may, therefore, be a viable strategy to prevent neurodegeneration caused by excessive microglial-mediated inflammation.

BET inhibition rescues microgliosis and neurodegeneration in vivo

To understand if I-BET858 can prevent pathological microglial activation and subsequent neuronal damage *in vivo* , two neurodegenerative mouse models were chosen, the p25 model of Alzheimer's and the R6/2 model of Huntington's disease. These models exhibit transcriptomic, cellular, and behavioral phenotypes reminiscent of the respective human diseases. Additionally, these models have a rapid onset of symptoms which minimizes the amount of drug required for the study and the duration of daily intraperitoneal injections received by the animals. In the p25 model, inducible overexpression of human p25 closely mimics the pathology and symptoms seen in AD patients [189–192]. Increased p25 levels increase Aβ accumulation, neurofibrillary tangles and neuron loss similar to AD. In this model, microglia rapidly proliferation and inflammatory genes are dramatically increased in the hippocampus as early as 2 weeks

after p25 induction[193]. This "microgliosis" is followed by severe hippocampal neuron loss, brain atrophy and cognitive deficits after six to seven weeks of transgene expression [189,194–196]. Importantly, microgliosis in this model precedes cognitive deficits[193], placing hyperactive microglia as a critical contributor to the etiology of degeneration which makes it an ideal model to test the role of BET-dependent transcription in the pathological, inflammatory activity of microglia.

In support of the possible protective effect of BET inhibition *in vivo*, we found that chronic I-BET858 treatment (30mg/kg, i.p.) in the P25 neurodegenerative mouse model, administered daily for five weeks starting two weeks after initiating the pathology was associated with a significant reduction in microglial inflammatory gene expression (Fig. 4). Notably, I-BET858 administration did not affect transgene expression at the protein or RNA level, despite being driven by the Camk2a promoter (Fig. 4A-C, data not shown). Of the 2536 genes induced by P25 overexpression in the hippocampus, BET inhibition significantly suppressed 365 (χ^2, p<0.0001, OR: 11.44). These genes enriched for interferon, cytokine production, and apoptosis pathways and included key mediators of the inflammatory response such as *Ccr5*, *Cd33*, *Nlrp3, and Nfkb1 (*Fig. 4D-E)*. Furthermore, histological analysis for IBA1 revealed a 47% decrease in microglia numbers (P25: 713.9 ± 106 Iba1$^+$ cells per mm^2, I-BET858, P25: 332.9 ± 12.6 Iba1$^+$ cells per mm^2) in the dentate gyrus of P25 mice treated with I-BET858 (Fig. 5A, C). Together these data show that BETs are required to drive a pro-inflammatory
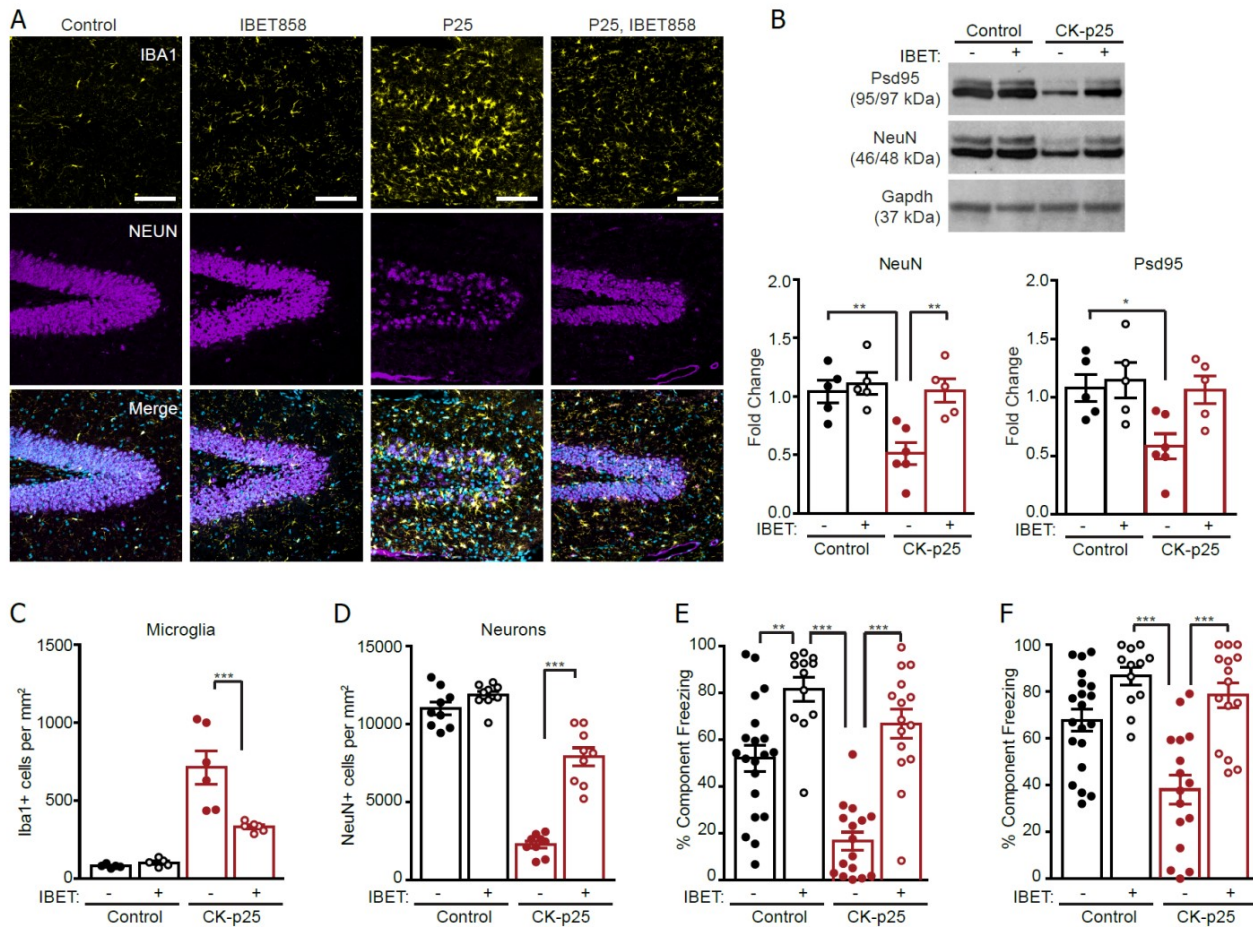
Figure 4. Selective effect of I-BET858 on inflammatory gene expression *in vivo*. (A) The P25 neurodegenerative mouse model was generated by crossing Camk2a$^{Tta/+}$ line with the tetO-Cdk5r1/GFP transgenic mouse line. (B) Transgene overexpression was induced at 8 weeks of age by the removal of doxycycline from the diet. After two weeks, mice were injected daily with I-BET858 (30 mg/kg, i.p.) or vehicle for five weeks. Total RNA was then isolated from the hippocampus and sequenced (n=3 per group). (C) Western blot and quantification of GFP to measure transgene expression (n=3-5, One-Way ANOVA with Tukey's multiple comparisons, *p<0.05). (D) Heatmap shows normalized expression of 365 genes induced by P25 overexpression that are significantly suppressed by I-BET858. (E) Pathway enrichment of the 365 genes from D (arrow indicates significance cutoff of p =0.05).

state in microglia and that BET inhibition is a viable strategy to restrain the pathological activation of microglia *in vivo.*

Perhaps even more important than the decrease in microglial-mediated inflammation was the simultaneous rescue of neuronal function and survival, both at the cellular and molecular level. Neuron density in the dentate gyrus was almost restored to wild type levels (10981 ± 414.6 NeuN$^+$ cells per mm^2) after BET inhibition (Fig. 5A, D). P25, I-BET858 mice (7880 ± 587 NeuN$^+$ cells per mm^2) had a 3.5-fold higher neuronal density than p25 mice (2254 ± 223.8 NeuN$^+$ cells per mm^2, Fig. 5A, D).

Increased neuron density and synapse integrity were also observed at the protein level as indicated by a complete rescue to wild-type levels of Psd95 (Fold Change, Control: 1.00 ± 0.11, P25: 0.54 ± 0.10, P25, I-BET858: 0.98 ± 0.11) and NeuN (Fold Change, Control: 1.00 ± 0.09, P25: 0.49 ± 0.09, P25, I-BET858: 1.01 ± 0.09) in the total hippocampus of P25 mice after I-BET858 treatment (Fig. 5B). In accordance with this data, there was a significant rescue (10%) of brain atrophy in the p25 model after I-BET858 treatment (Percent Control Weight, P25: $73.06 \pm 1.63\%$, P25, I-BET858: $83.42 \pm 1.08\%$, data not shown).

Moreover, the cellular and molecular changes in response to I-BET858 treatment were associated with a complete rescue of the memory deficits observed in P25 mice (Fig. 5E, F). I-BET858-treated P25 mice tested in the classical fear conditioning paradigm displayed wild-type levels of freezing in response to the conditioned context and cue. The pro-cognitive effect of I-BET858 were observed in both the healthy and diseased brain, suggesting a broader therapeutic impact of BET inhibition than on inflammation alone. Importantly, the therapeutic potential of I-BET858 was not limited to the aggressive P25 model. Chronic BET inhibition in the R6/2 Huntington's mouse model increased the median lifespan by over five weeks from 89 days to 127 days (n = 9-13, Log-rank (Mantel-Cox)Test: $p < 0.05$, data not shown). Together these data indicate that BETs control the pro-inflammatory activation of microglia *in vivo* and that suppression of this pathway can preserve neuronal health and function during neurodegeneration.

Figure 5. Cellular and behavioral changes in a neurodegeneration model after BET inhibition. (A,C,D) Immunofluorescence of IBA1 (yellow, quantified in C) and NEUN (purple, quantified in D) in the dentate gyrus after 7 weeks of P25 transgene expression (scale bar=100 µM, n=2-3 images per animal, 3-5 animals per group). (B) Western blotting for NEUN and PSD95 in the hippocampus with quantifications below (One-Way ANOVA, n= 5-6 per group, *p<0.05, **p<0.01). (E-F) Percent time freezing during Contextual (E) and Cued (F) recall one week after classic fear conditioning (One-Way ANOVA, n = 12-20 per group, **p<0.01, ***p<0.001).

Discussion

Microglia perform many functions necessary for healthy brain homeostasis such as tissue remodeling and neurotrophic support. These cells rapidly switch their functional program to an activated, pro-inflammatory state after brain injury or

infection. This transition is essential for the elimination of pathogens and the removal of dead or dying brain cells. However, excessive microglial activation can be devastating for the brain and is thought to exacerbate neurodegeneration. Such a complete shift in the cellular state requires dynamic gene regulatory networks, but little is known about the mechanisms underlying transcriptional control in microglia. Understanding the molecular mechanisms that regulate the excessive pro-inflammatory activation of microglia may elucidate new therapeutic strategies for the treatment of neurodegenerative diseases. Here we show that the BET proteins are critical mediators of pro-inflammatory gene expression in microglia. Pharmacological inhibition of these proteins *in vitro* and *in vivo* prevented the induction of inflammation without disrupting microglia lineage or region-specific transcriptomes which are required to maintain proper brain health. Most importantly, we show that BET inhibition can rescue symptoms of neurodegeneration in two distinct mouse models, emphasizing the therapeutic potential of I-BET858.

This study relies on systemic pharmacological inhibition of the BET proteins, which are ubiquitously expressed and therefore BET function may be affected in many different cell types throughout the body. While I-BET858 suppresses microglial activation and increases neuronal survival and function in a neurodegenerative mouse model, the mechanism remains unclear. To test if the rescue effect was driven by a decrease in microglial-mediated inflammation, we hypothesized that depleting microglia from the brain may recapitulate the effects of I-BET858. This was achieved in wild-type

mice through the pharmacological inhibition of the colony-stimulating factor receptor 1 (CSF1R) [197]. However, microglia in the P25 model escaped CSF1R inhibition and were present at twice the number as controls (Average ±SEM, Wild type: 81.9 ± 5.4, P25, CSF1Ri: 170.3 ± 18.2, data not shown). Therefore the contribution of microglia should be assessed using other methods to deplete microglia such as the targeted diphtheria toxin mouse models or by conditional deletion of individual BET proteins in microglia using the Cx3Cr1 inducible Cre line.

It is possible that the neuroprotective effect of I-BET858 may be a multifactorial process that has beneficial impacts on several cell types. In support of this, BET inhibition stimulates neurogenesis *in vitro* [114] which, if also occurring *in vivo*, could compensate for neuron loss in the P25 mouse model of AD. Additionally, I-BET858 may prevent glial-mediated inflammation by disrupting the instructive communication between microglia and astrocytes or oligodendrocytes [198,199]. Lastly, given its pro-cognitive effect in wild-type animals which we and others have observed [113], BET inhibition may also increase neuronal survival intrinsically (addressed in Chapter 5). Future work should delineate the potential protective effects of BET inhibition in the different cell populations using both pharmacological and genetic deletion models.

Additionally, the current study measured transcriptional changes after BET inhibition in the P25 neurodegeneration using bulk RNA-sequencing. Fluorescence activated nuclei sorting followed by sequencing would better address the effect of BET inhibition on cell-type specific transcriptomes *in vivo*. This technique would more

precisely define the mechanism by which I-BET858 increases neuronal survival and cognition during neurodegeneration.

Previous studies have addressed the therapeutic potential of BET inhibition in neurodegeneration, although with variable outcomes. The majority of these studies use the BET inhibitor, JQ1, which is rapidly cleared from the brain [200]. Prolonged JQ1 treatment in the 3xTg mouse model of Alzheimer's disease did not have any effect on memory deficits perhaps due to the intermittent treatment schedule and the timing relative to behavioral testing [201]. In support of our data, JQ1 treatment enhanced fear memory in wild type mice and rescued cognitive deficits in the APP/PS1–21 mouse model of Alzheimer's disease [113]. BET inhibition also modestly improved recovery after spinal cord injury [202], ischemic stroke [203], and delayed the onset of experimental autoimmune encephalomyelitis [204]. Nevertheless, the data presented here show a more substantial neuroprotective effect of BET inhibition, which is likely due to the superior specificity and bioavailability of I-BET858.

In summary, we find that the BET proteins are required for the induction of a pro-inflammatory transcriptional program in microglia *in vitro* and *in vivo*. Inhibition of this gene network *in vivo* does not disrupt homeostatic microglial gene networks but rather can ameliorate neurodegeneration in response to excessive microglial activation. We, therefore, conclude that BET inhibition, specifically I-BET858, represents a novel and exciting treatment strategy for a broad range of neurodegenerative disorders.

Chapter Five

BET proteins negatively regulate neuronal survival

Abstract

Preservation of postmitotic neurons throughout an organism's life is critical for the proper maintenance of neuronal circuitries and cognition. The unique vulnerability of these cells may arise from the high metabolic demand required to maintain large cell size and the ion gradients necessary for neuronal activity [205,206]. Paradoxically, decreasing nutrient availability and cellular metabolism increases neuronal survival in response to toxic stimuli [207–210]. However, the impact of gene transcription, which is intimately coupled to cellular metabolism, on neuronal longevity is not well understood. We identified a novel role for the bromodomain and extraterminal domain-containing (BET) protein family of transcriptional regulators in neuronal survival. Suppression of BET-dependent transcription resulted in a progressive decline in glycolysis and mitochondrial respiration and an induction of protein degradation pathways. This metabolic switch resulted in a neuroprotective state that is highly reminiscent of that caused by caloric restriction. Moreover, pharmacological BET inhibition increased neuronal lifespan *in vitro* and resilience to toxic stimuli *in vitro* and *in vivo*. Together these data identify BET proteins as negative regulators of neuronal survival and illustrate the therapeutic potential of BET inhibition in the treatment of a broad range of neurodegenerative diseases.

Introduction

Neurons, which execute functions critical for organism survival, are among the most vulnerable cell types. After circulation stops, irreversible neuronal damage occurs within minutes [211–213] whereas other cell populations can survive much longer, even for days [214]. Within the brain, specific neuronal populations are more susceptible than others, including the Purkinje cells, neurons in CA1 of the hippocampus, and Layers III and V of the cortex [215–218]. This vulnerability arises in part due to the extreme metabolic demand of maintaining large cell size, including mRNA [219] and protein synthesis [220], and ion gradients required for synaptic transmission [206,221,222]. Although only 2% of total body weight, the brain consumes 20% of the body's oxygen and 25% of total glucose [205].

Despite the brain's high level of nutrient consumption, neuronal metabolism is inversely correlated with neuronal survival[223]. Indeed, increasing either cell size[224] or glycolytic rate [225] in neurons promotes cell death. This paradox is highlighted by the effectiveness of neuroprotective strategies that decrease nutrient availability and cellular metabolism such as caloric restriction (CR) [207,208,226–228] or pharmacological CR mimetics such as mTOR inhibitors [229–232]. The beneficial effects of CR and its mimetics are thought to be caused by decreased metabolism [233] and associated reactive oxygen species [234] and concomitant increase in protein clearance pathways such as autophagy [235]. These interventions induce a cellular state where anabolic processes, including protein translation, mitochondria biogenesis, lipid synthesis, and ATP production via

glycolysis and oxidative phosphorylation, are suppressed. In turn catabolic pathways like autophagy are activated to generate nutrients from the self.

While it is well known that inhibition of protein synthesis and cell metabolism increases cell survival, less is known about how gene transcription, another energetically consuming anabolic process, impacts cell survival. Transcription is intimately connected with cellular metabolism in that chromatin-modifying enzymes require metabolites as co-factors or substrates to post-translationally modify histone tails which regulate the rate of gene transcription [236]. These modifications, such as histone acetylation, change in response to metabolite availability, importantly linking cellular metabolism to epigenetic regulation [237–242]. Furthermore, transcription rates decrease when nutrients are scarce [243–246], presumably to minimize energy consumption and increase survival. While complete blockade of RNAPI-mediated transcription is highly detrimental to neuronal survival [247], inhibiting the P-TEFb-dependent subset of transcription increases neuronal survival suggesting that specific gene networks may regulate longevity [248–250]. While P-TEFb inhibitors do not have optimal specificity, the recruitment and activity of P-TEFb is governed by the BET protein family which is easily targeted pharmacologically. Therefore we hypothesized that BET inhibition may reveal a novel role for transcription in neuronal longevity.

In support of this hypothesis, mTOR inhibition and caloric restriction decrease specific histone acetylation marks that are recognized by the BET proteins [251–254]. Moreover, Brd2 and Brd4 mRNA expression is reduced in the brains of mice after caloric

restriction suggesting modulation of BET-dependent transcription may be neuroprotective [255]. Further evidence suggesting a beneficial impact of loss of BET activity, a Crispr-Cas9 screen in human cells identified Brd2, a member of the BET family, as a putative negative regulator of neuronal survival [256]. Together, these data suggest that lowering BET-dependent transcription may have a positive effect on neuronal survival.

Here we show that pharmacological inhibition of the BET family of transcriptional regulators significantly increases neuron survival at baseline and in response to toxic stimuli. This is accomplished by inhibiting gene networks that control protein synthesis and ATP production while inducing protein degradation and pro-survival pathways. We propose that BET inhibition induces a protective state reminiscent of that which occurs after mTOR inhibition. These data describe a novel role for the BET proteins as negative regulators of survival and have direct therapeutic implications for neurodegenerative disease.
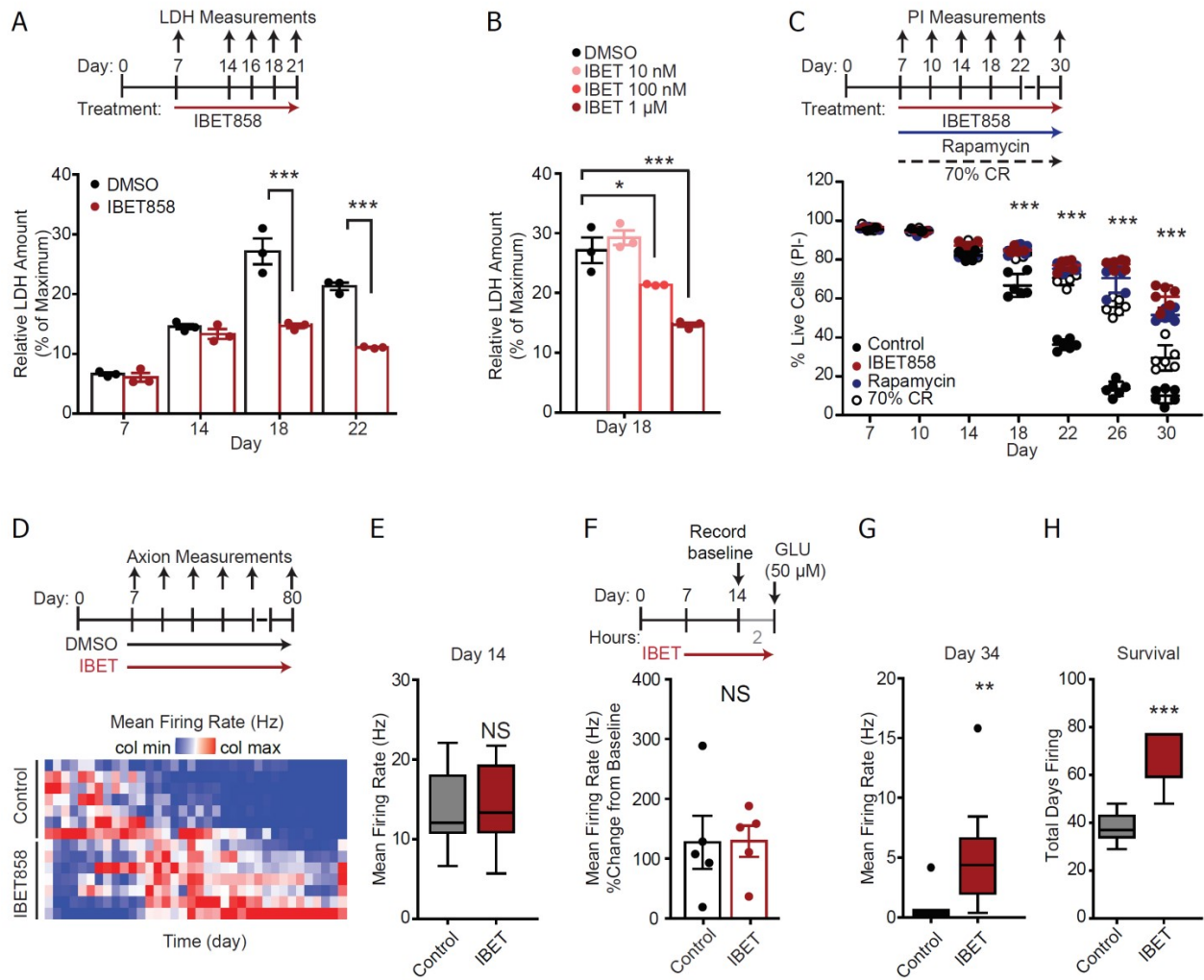
Results

BETs negatively regulate neuronal survival in vitro

In order to understand the effect of chronic BET inhibition on neuronal survival, primary cortical mouse neurons were cultured in the presence or absence of the brain-permeable BET inhibitor I-BET858 (1 µM). Lactate dehydrogenase (LDH), which is

released during cell death as membranes become permeable, was equivalent between conditions until day 18 *in vitro* which suggests I-BET858-treated neurons live longer *in vitro* than control-treated neurons (Fig. 1A; %Maximum LDH at Day 18: Control: 27.1 ± 2.16%, I-BET858: 14.7 ± 0.36%). The decrease in LDH activity occurred in a concentration-dependent manner indicating the increase in survival may be specific to the inhibition of the BET proteins (Fig. 1B). While these results suggest I-BET858 increases neuronal lifespan, LDH activity is an indirect measure of cell death and can be affected by other factors such as metabolic changes or LDH mRNA expression. Therefore, in order to confirm these findings, neuronal survival was directly quantified over time using the membrane-impermeable dye, propidium iodide (PI), which increases in fluorescence 20-30 fold after intercalating into DNA [257]. PI staining confirmed that BET inhibition significantly extended neuronal lifespan (Fig. 1C). While only 10% of primary cortical neurons were alive at day 30, 60% of I-BET858-treated neurons had survived (Fig. 1C). Compared to other well-known, pro-longevity treatments, I-BET858 increased neuronal survival to a greater extent than either the mTOR inhibitor rapamycin (20 nM), or caloric restriction (Fig. 1C; Percent Survival at Day30: I-BET858: 60.9 ± 2.32%, Rapamycin: 51.5 ± 1.27%, CR: 29.4 ± 2.67%).
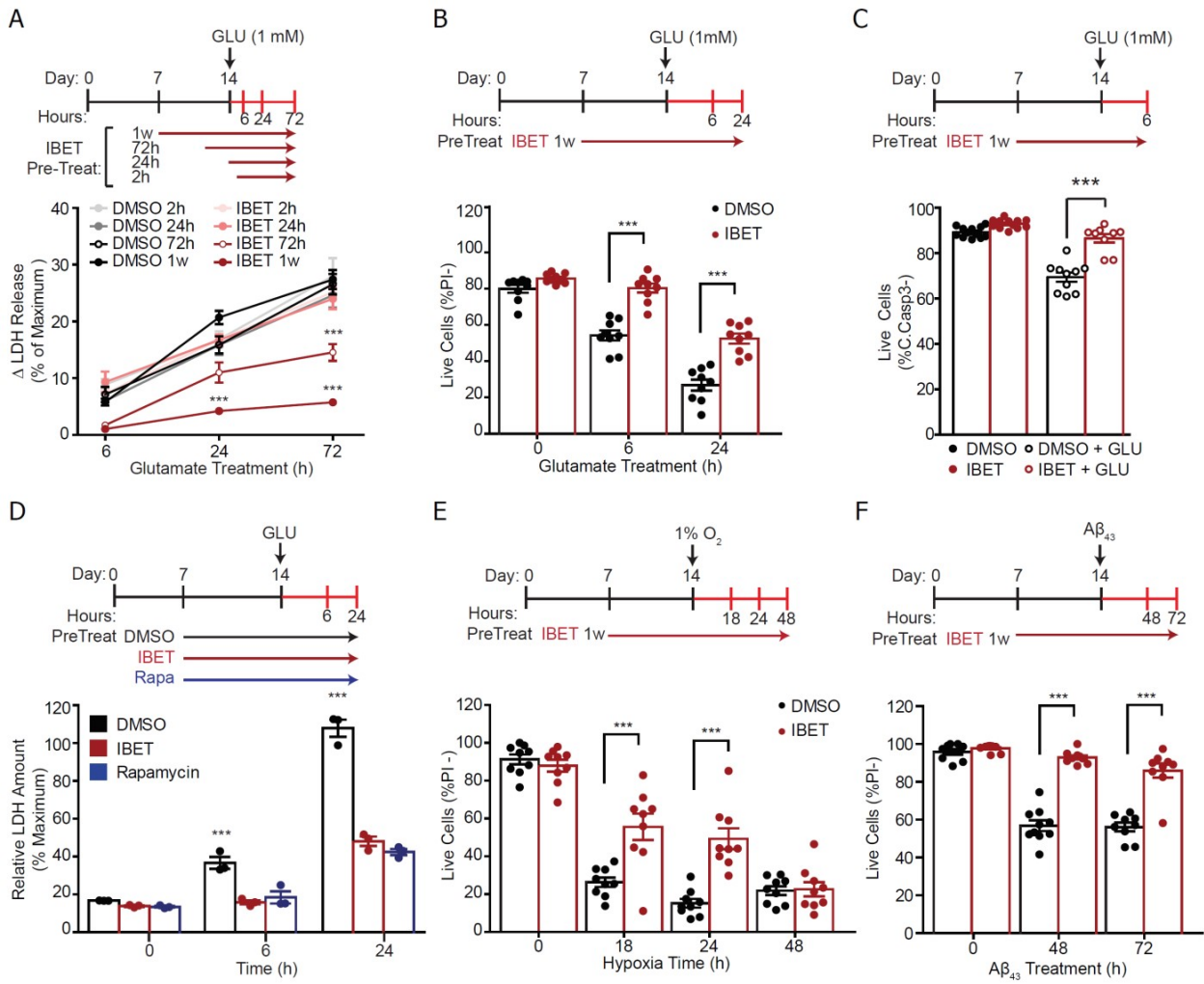
However, increased survival does not guarantee appropriate neuronal function throughout the lifespan of the neuron. Therefore to determine the effect of chronic BET inhibition on electrical activity, neurons were cultured on a microelectrode array in the presence of I-BET858 (1μM, Fig. 1D-H).

Figure 1. BET proteins negatively regulate neuronal survival. (A) LDH release was measured over time in primary cortical mouse cultures treated with I-BET858 (1 µM). Two-way ANOVA with repeated measures and Bonferroni multiple comparison, ***$p < 0.0001$, n = 3 (B) Dose-dependent release of LDH after I-BET858. One-Way ANOVA with Tukey multiple comparison, * $p < 0.05$, ***$p < 0.001$, n = 3. (C) Number of propidium iodide negative cells in primary cultures treated with vehicle, I-BET858 (1 µM), Rapamycin (20 nM), or 70% caloric restriction. Two-way repeated measures ANOVA with multiple comparisons. (D) Heatmap shows mean firing rate (Hz) normalized by column in neuronal cultures over time. (E) Mean firing rate (Hz) of control and I-BET858-treated neurons at day 14. Student's t-test, n = 7- 14. (F) Percent change in mean firing rate (Hz) compared to baseline activity in primary cortical mouse neurons immediately after glutamate stimulation (50 µM). Two-tailed Student's t-test, n = 5 (G) Mean firing rate (Hz) of control and I-BET858-treated neurons at day 34. Two-tailed Mann-Whitney test, n = 7- 14, ** $p < 0.01$. (H) Number of days that the mean firing rate was greater than zero per condition. Two-tailed Mann-Whitney t-test, n = 7- 14, *** $p < 0.001$.

In agreement with the BET-dependent expression of glutamatergic and synaptic genes described in Chapter 3, I-BET858 initially decreased neuronal firing rate (Fig. 1D). Notably, firing rates were equivalent between conditions at day 14 when primary cortical neuronal activity is at the maximum (Fig. 1E, Control: 13.8 ± 1.94 Hz, I-BET858: 14.2 ± 1.30Hz). Furthermore, glutamatergic signaling activity was intact after BET inhibition, as comparable increased firing rates were observed in both I-BET858-treated and control neurons after an acute glutamate (50 µM) stimulation (Fig. 1F, Percent Baseline Firing Rate, Control: 127.4 ± 44.37%, I-BET858: 129.3 ± 26.20%, Student's t-test p = 0.55). Most importantly, neuronal activity was maintained throughout the prolonged lifespan of I-BET858-treated neurons, indicating that neurons retain their functionality (Fig. 1G, H) (Days Firing, Control: median 37.57, IQR 34-43, I-BET858: median 77, IQR 59.25-77). Therefore, BET inhibition significantly increased neuronal survival without any detrimental effect on neuronal activity *in vitro*.

In addition to increasing neuronal lifespan, I-BET858 treatment (1µM) led to a time-dependent increase in neuronal resilience to glutamate (1 mM) excitotoxicity (Fig. 2A). While moderate protection was observed after 72 hours, extended I-BET858 treatment (1 week) conveyed significant protection against excitotoxicity-induced neuronal death (Fig. 2A). Indeed more neurons survived after 6 (Percent PI negative, Control: 54.2 ± 2.80%, I-BET858: 80.29 ± 2.51%) and 24 hours (Percent PI negative, Control: 26.78 ± 3.08%, I-BET858: 52.45 ± 2.74%) of excitotoxic glutamate treatment (Fig. 2B, Two-way repeated-measures ANOVA with multiple comparisons, ***p<0.001).
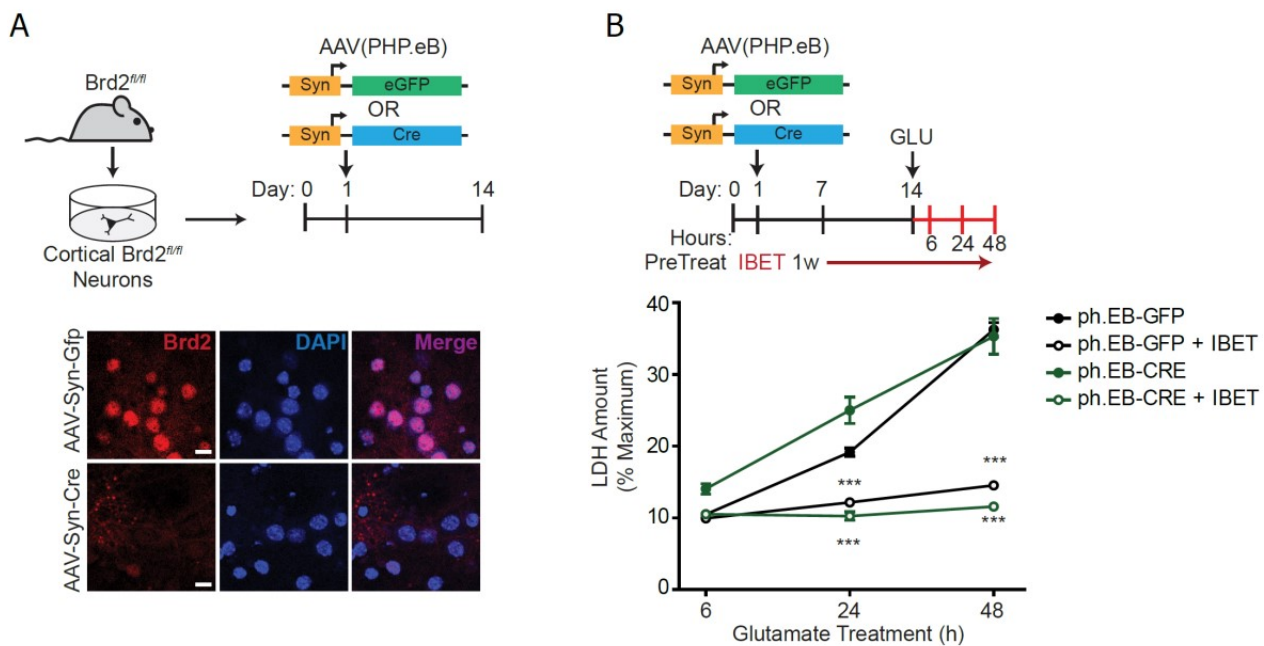
Figure 2. BET inhibition protects neurons from toxic stimuli. (A) Primary cortical neurons were pre-treated with either I-BET858 (1 µM) or control for 2, 12, 72 or 168 hours before glutamate exposure (1 mM) at day 14. LDH release was measured 6, 24, and 72 hours after initial glutamate exposure. Two-way repeated measures ANOVA with multiple comparisons, n = 3 per group, *** $p < 0.001$. (B) Percent of cells that are propidium iodide negative 6 and 24 hours after 1 mM glutamate exposure. Two-way repeated measures ANOVA with multiple comparisons, n = 3 per group, *** $p < 0.001$. (C) Cleaved caspase 3 immunofluorescence in primary cortical neurons 6 hours after 1 mM glutamate exposure. Two-way ANOVA with Bonferroni posttests, n = 3 per group, *** $p < 0.0001$. (D) Primary cortical neurons were pre-treated for one week with either I-BET858 (1 µM), Rapamycin (20 nM) or control before glutamate exposure (1 mM) at day 14. LDH release was measured 6 and 24 hours after initial glutamate exposure. Two-way repeated measures ANOVA with Bonferroni posttests, n = 3 per group, *** $p < 0.001$. (E, F) Percent of cells that are propidium iodide negative after (E) 18, 24, and 48 hours of hypoxia (1% O_2) and after (F) 48 and 72 hours of Aβ_{1-43} oligomer exposure (10 µM). Two-way repeated measures ANOVA with multiple comparisons, n = 3 per group, *** $p < 0.00$. Experiments were repeated a minimum of three times.

Cleaved caspase-3, a marker of apoptosis, immunofluorescence confirmed that increased numbers of I-BET858-treated neurons (Control: 69.49 ± 2.05%, I-BET858: 86.58 ± 1.90%, Two-way ANOVA ***$p < 0.001$) survive an acute glutamate exposure (6h, 1 mM) (Fig. 2C). This finding indicates that BET inhibition prevents neuronal death in response to toxic stimuli. The significant neuroprotection afforded by I-BET858 was equivalent to that observed after rapamycin treatment (20 nM, Fig. 2D). Furthermore, BET inhibition initiated a broad neuroprotective state that increased neuronal resistance to various toxic stimuli, including hypoxia (1% O_2, Fig. 2E) and $A\beta_{1-43}$ oligomers (10 μM, Fig. 2F). Together these data demonstrate that BETs negatively regulate neuronal survival and suggest a therapeutic potential for BET inhibition in neuronal aging and degeneration.

Effect of neuron-specific deletion of BETs on glutamate toxicity

Notably, I-BET858 is a pan-BET family inhibitor which displaces all three BET proteins from the chromatin. The individual protein family members have distinct interaction partners and may have unique, alternative functions [64,71,97]. To understand which BET mediates the neuroprotective mechanism of I-BET858, the survival of Brd2- or Brd4-deficient neuronal cultures was measured after exposure to excitotoxic levels of glutamate (Fig. 3). Primary neuronal cultures were generated from either Brd4^{fl/fl} mice or the newly developed Brd2^{fl/fl} mouse line (a kind gift from Drs. Debra Wolgemuth and

Enyuan Shang). On day 1, cultures were infected with either with AAV (PHP.eB)-Synapsin-Cre or AAV (PHP.eB)-Synapsin-GFP to overexpress Cre recombinase or GFP specifically in neurons. Complete culture infection was confirmed visually by GFP expression and by the loss of protein (Fig. 3A, data not shown). BRD2 and Brd4 immunofluorescence showed total loss of the protein from neurons by day 7, matching the time point previously used for I-BET858 administration. In three independent experiments, neuronal loss of Brd2 did not protect neurons from glutamate toxicity and did not impact the protective effect of I-BET858 (Fig. 3B). In two preliminary experiments, neuron-specific deletion of Brd4 increased neuronal survival after
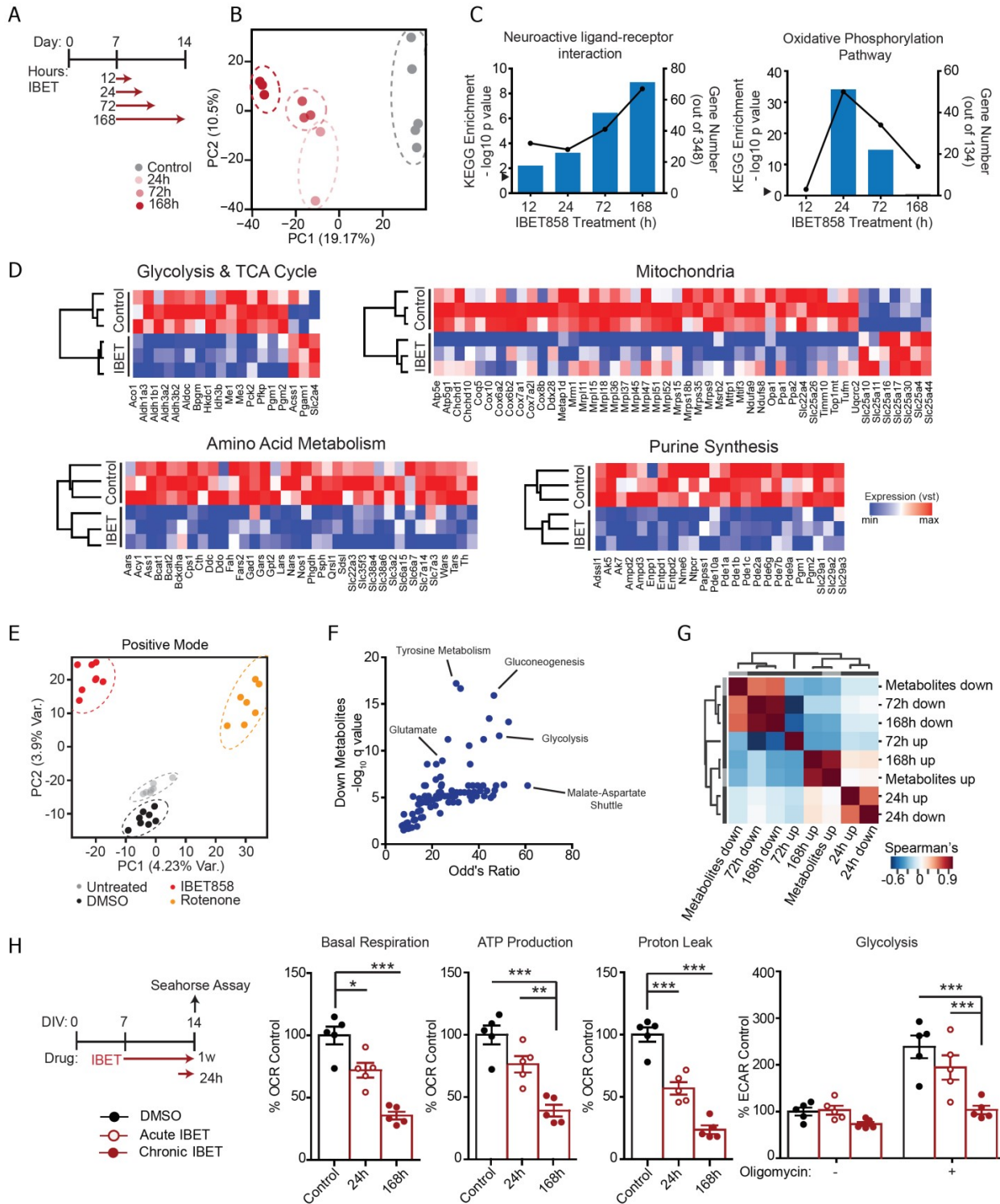
Figure 3. Impact of neuronal deletion of Brd2 on glutamate toxicity in vitro. (A,C) Brd2$^{fl/fl}$ neuronal cultures were infected with AAV(Php.EB)-SynGFP or AAV(Php.EB)-SynCre on day 1. Immunofluorescence for BRD2 (A) at day 14. Scale bar is 10 μm. (B) Infected cultures were treated with I-BET858 (1 μM) or vehicle on day 7 in vitro. At day 14, neurons were exposed to glutamate (1 mM) for 6, 24, and 72 hours before measuring LDH release. (Statistics: Two-way Repeated measures ANOVA with Bonferroni post-tests, ***p<0.001, n =3-4 per group, experiments independently repeated three times).

glutamate toxicity to the same magnitude as I-BET858 (data not shown). These data

suggest that Brd4 may mediate the neuroprotective effect of I-BET858 in primary

cortical neurons, however more experiments are required to confirm this.

BET inhibition initiates a progressive metabolic switch in neurons

The neuroprotective state induced by I-BET858 was associated with a gradual

reprogramming of neuronal gene networks such that genes supporting cell metabolism

and protein synthesis were suppressed and longevity-associated genes were increased.

Short-term BET inhibition (24 hours) suppressed 821 genes, whereas chronic BET

inhibition suppressed 1001 genes after 72 hours and 1786 after 1 week (Fig. 4A, B).

While neuronal and synaptic genes were consistently repressed, numerous metabolic

pathways were down-regulated, starting 12 hours after BET inhibition in neurons (Fig.

4C, left). Initially, oxidative phosphorylation was the top pathway inhibited by I-

BET858, with a reduction in one-third of the pathway (37%, 50/134 genes, q = 2.5 E -

32) including *Atp5e, Cox7a1,* and *Ndufb4* (Fig. 4C, right). As BET inhibition continued, a

broader range of metabolic pathways were suppressed including amino acid synthesis

(*Ass1*, *Cth*, *Slc7a3, Slc6a15,* and *Slc38a4*), glycolysis/TCA cycle (*Hkdc1*, *Pfkp, Idh3b,*

and *Me1/3*), purine metabolism (*Ampd2/3, Ak5/7, Nme6, and Slc29a1/2/3*), and

mitochondria function and biogenesis (*Atp5e, Cox6a2, Mrpl11, Mrps9*, and *Mtfp1*)

Figure 4. Metabolic adaptations after I-BET858 in neurons. (A) Primary cortical neurons were treated with either I-BET858 (1 μM) or control for 24, 72 or 168 hours before RNA sequencing (n=3 per group). Datasets were compared to 12 h I-BET858 microarray published in Sullivan et al. JEM 2015. (B) Principal component analysis of 24, 72 and 168h transcriptomes. Continued on page 90.

(Fig. 4D). Notably, alterations in metabolic gene networks were accompanied by metabolic adaptations after chronic BET inhibition in neurons (1 μM, Fig. 4E-H).

Metabolomic changes as measured by mass spectrometry after one week of I-BET858 exposure were modest in comparison to an acute exposure of rotenone (24 h, 50nM) which abolishes mitochondrial respiration leading to rapid cell death (Fig. 4E, data not shown) [258]. Decreased expression of amino acid synthesis and import genes resulted in a significant decrease in the intracellular levels of 13 amino acids, including methionine, glutamine, and glutamate (Fig. 4D, F). Parallel to the suppression of amino acid supply, treatment with I-BET858 significantly reduced levels of metabolites associated with glycolysis (p = 1.22e-15, OR: 48.8), the pentose phosphate pathway (p=5e-15, OR: 42), and purine metabolism (p =4.23e-12, OR: 17.9) (Fig. 4F). Furthermore, there was a strong concordance between transcriptomic and metabolomic alterations in neurons after BET inhibition. Down-regulated genes were increasingly correlated with decreased metabolites over time (Spearman coefficient, 24h: -0.07; 72h: r=0.59, 1week: r=0.62) (Fig. 4G) which strongly suggests that the metabolic

Figure 4. Continued. (C) Bar plots indicate selected KEGG pathway enrichment over time. Arrow indicates significance cutoff of p=0.05. Line indicates number of genes within the pathway suppressed at each time point. (D) Heatmaps display normalized gene expression of metabolic pathways after 168h of BET inhibition. (E) Principal component analysis of polar metabolite mass spectrometry data from primary cortical neurons treated with I-BET858 (1 μM) or control for 168h or Rotenone (50 nM) for 24h (n = 7-8 per condition). (F) Scatter plot showing metabolic pathway enrichment and Odd's ratios of decreased metabolites. (G) Heatmap of spearman correlation between metabolomics data and differential gene expression after I-BET858. (H) Oxygen consumption and extracellular acidification rates were measured in neuronal cultures after 24 or 168 h of I-BET858. One-Way ANOVA with Tukey posttest, *p<0.05, **p<0.01, ***p<0.0001, n=5 per group, Experiment independently replicated three times.
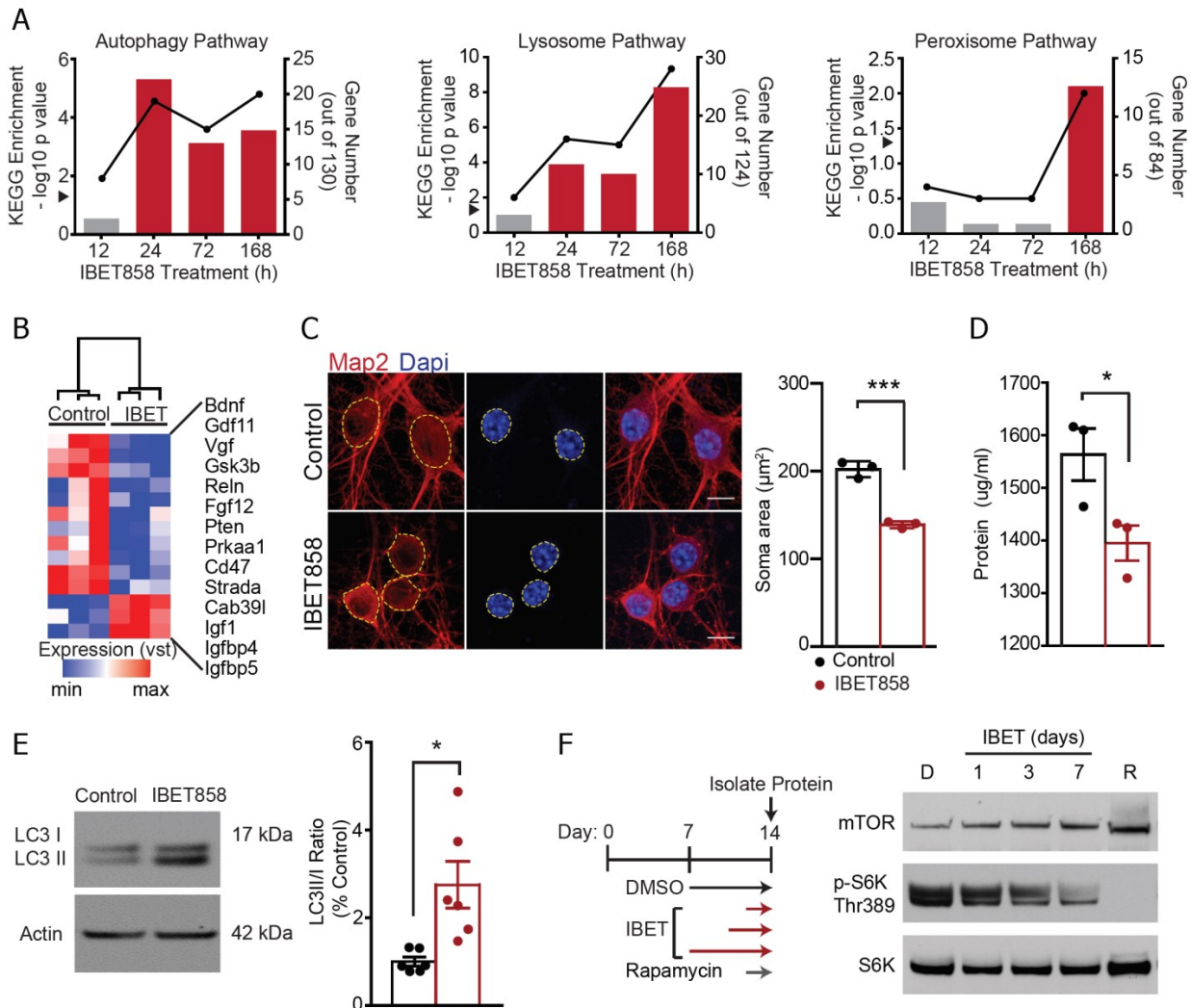
profile of neurons depends on BET activity.

Further emphasizing the impact of BET-dependent transcription on the neuronal metabolism, I-BET858 led to a gradual suppression of oxidative phosphorylation as indicated by decreased basal mitochondrial respiration (%Control, 24h: 72 ± 5.9%, 1week: 35.7 ± 3.2%) and ATP production rates (%Control, 24h: 76.4 ± 6.6%, 1week: 39.1 ± 4.7%) (Fig. 4H). The maximum mitochondrial activity of I-BET858-treated neurons was also decreased, indicating the total metabolic capacity of neurons was suppressed after BET inhibition (data not shown). In addition to lower mitochondrial activity, proton leak ,which contributes to the production of reactive oxygen species (ROS), was lower after BET inhibition (%Control, 24h: 56.8 ± 3.5%, 1week: 23.6 ± 5.0%) (Fig. 4H). The maximum glycolytic rate was also significantly attenuated after BET inhibition as measured by the extracellular acidification rate in neuronal cultures after the addition of oligomycin (2 mM, %Control Pre-Oligomycin, Control: 238.6 ± 24.3%, 24h: 194.5 ± 26.2%, 1 week: 103.4 ± 9.0%) (Fig. 4H). These results confirm that BET inhibition decreased oxidative phosphorylation and glycolysis in neuronal cultures, which could contribute to the increased lifespan caused by I-BET858. However, not all energy-producing pathways were suppressed after I-BET858. Peroxisome genes (*Pex7, Pex10,* and *Pex13*) were induced, suggesting neurons may switch to fatty acid oxidation as an alternative energy production pathway (Fig. 5A, right).

The I-BET858-mediated alterations in neuronal metabolism coincided with an induction of genes that support autophagy and protein degradation including *Acss2, Hspa8, Lamp1/2, Map1lc3b,* and *Ulk1/2,* as well as several ubiquitin ligases (Fig. 5A). In addition, numerous growth factors (*Bdnf, Gdf11, Gsk3b*) and negative regulators of mTOR signaling (*Prkaa1:* the AMPK catalytic subunit, *Pten, Strada, Ulk2*) were among the up-regulated genes (Fig. 5B) [259,260]. These gene networks suggest an increase in protein degradation in I-BET858-treated neurons after 1 week. Accordingly, I-BET858-treated neurons were 25% smaller (Soma Area: μm^2, Control: 202.3 ± 5.4, I-BET858: 139.1 ± 2.2) and contained 13% less total protein (Protein µg/mL, Control: 1563 ± 49.6, I-BET858: 1395 ± 33.3). (Fig. 5C, D). Furthermore, there was a three-fold increase in the ratio of LC3-I versus LC3-II, a common autophagy marker which indicates that the transcriptional increase in *Map1lc3b* corresponds to an increase in functional autophagy (Fig. 5E).

The metabolic adaptations initiated by decoupling BET-dependent transcription in neurons are reminiscent of those observed during mTOR-low cell states where cellular survival is maintained by depressing glycolysis, oxidative phosphorylation, lipogenesis, and purine synthesis while inducing autophagy and fatty acid degradation mechanisms [261]. This suggests that suppression of separate anabolic pathways (transcription vs translation) may converge onto the same neuroprotective state. Accordingly, mTOR signaling may be impaired after chronic BET inhibition. Although mTOR mRNA and protein expression were unaffected, there was a time-dependent decrease in mTOR
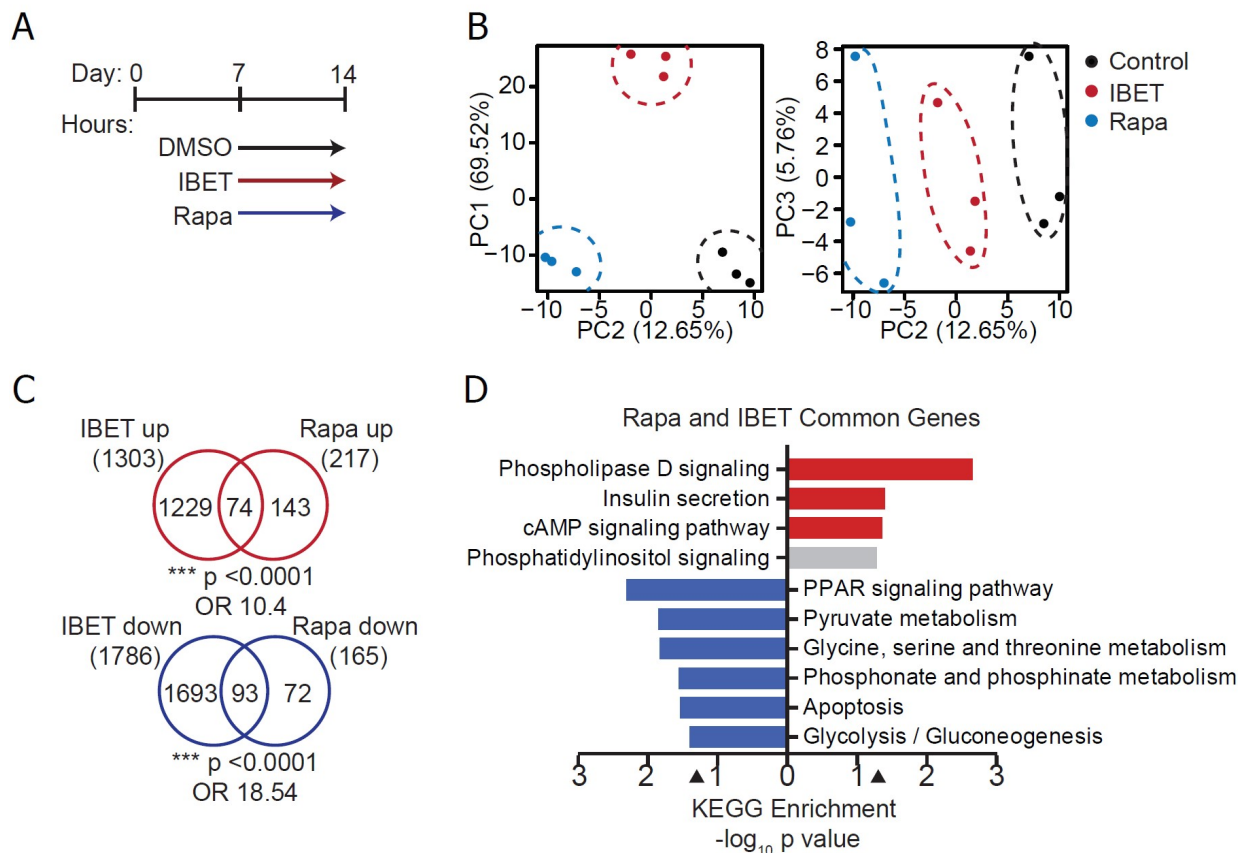
activity as indicated by phosphorylation of p70-S6k at Thr389 after BET inhibition in primary cortical neurons (Fig. 5F).

Figure 5. Increased protein degradation after chronic BET inhibition. (A) Bar plots indicate selected KEGG pathway enrichment of genes induced by I-BET858 in primary cortical neurons over time. Arrow indicates significance cutoff of $p=0.05$. Line indicates number of genes within the pathway suppressed at each time point. (B) Heatmaps display normalized gene expression of longevity-regulating genes after 1 week of BET inhibition. (C) Immunofluorescence and quantification of MAP2+ somatic area in cortical neurons after BET inhibition. (Scale bar = 10 μM, Statistics: two-tailed Student's t-test ***$p<0.001$, 3 images averaged for each biological replicate, n= 3) (D) Total protein content of neuronal cultures after 1 week of I-BET858 or vehicle treatment. (Statistics: two-tailed Student's t-test *$p<0.05$, n= 3 per group, experiment replicated independently three times) (E) Western blot analysis of LC3 after 1 week of I-BET858 or vehicle treatment. (Statistics: two-tailed Student's t-test ***$p<0.05$, n= 6 per group) (F) Time course western blot analysis of mTOR, phosphorylated S6K, and total S6K proteins levels. (n=3 per group).

Further supporting the commonality between the two neuroprotective states, there was significant agreement between genes sensitive to BET inhibition and mTOR inhibition (Fig. 6A, B). The majority of genes down-regulated after chronic mTOR inhibition (56%, 93/165 genes, $p < 0.0001$, OR: 18.54) in cortical neurons were also suppressed by I-BET858 (Fig. 6C). Moreover, the commonly repressed genes were enriched in Brd target genes encoding regulators of glycolysis and TCA cycle (Fig. 6D). Analysis of transcription factor networks of BET- and mTOR-dependent genes revealed

Figure 6. Comparison between BET and mTOR inhibition on neuronal gene expression. (A) Primary cortical neurons were treated with either I-BET858 (1 μM, red) or Rapamycin (20 nM, Rapa, blue) for 1 week before RNA sequencing (n=3 per group) (B) Principal component analysis of differential gene expression. (C) Venn overlaps of significantly induced (red) or suppressed (blue) genes after I-BET858 or Rapamycin (Deseq2 analysis with significance cutoff of q < 0.05). (D) Bar plot indicates KEGG pathway enrichment of shared genes. Arrow indicates significance cutoff of p=0.05.

a strong correlation between down-regulated genes sets (Spearman coefficient, Down: r= 0.41) suggesting that long-term rapamycin treatment and chronic BET inhibition yield a common neuroprotective transcriptional network. These data strongly indicate that BET inhibition converges on the same protective phenotype induced by mTOR inhibition.
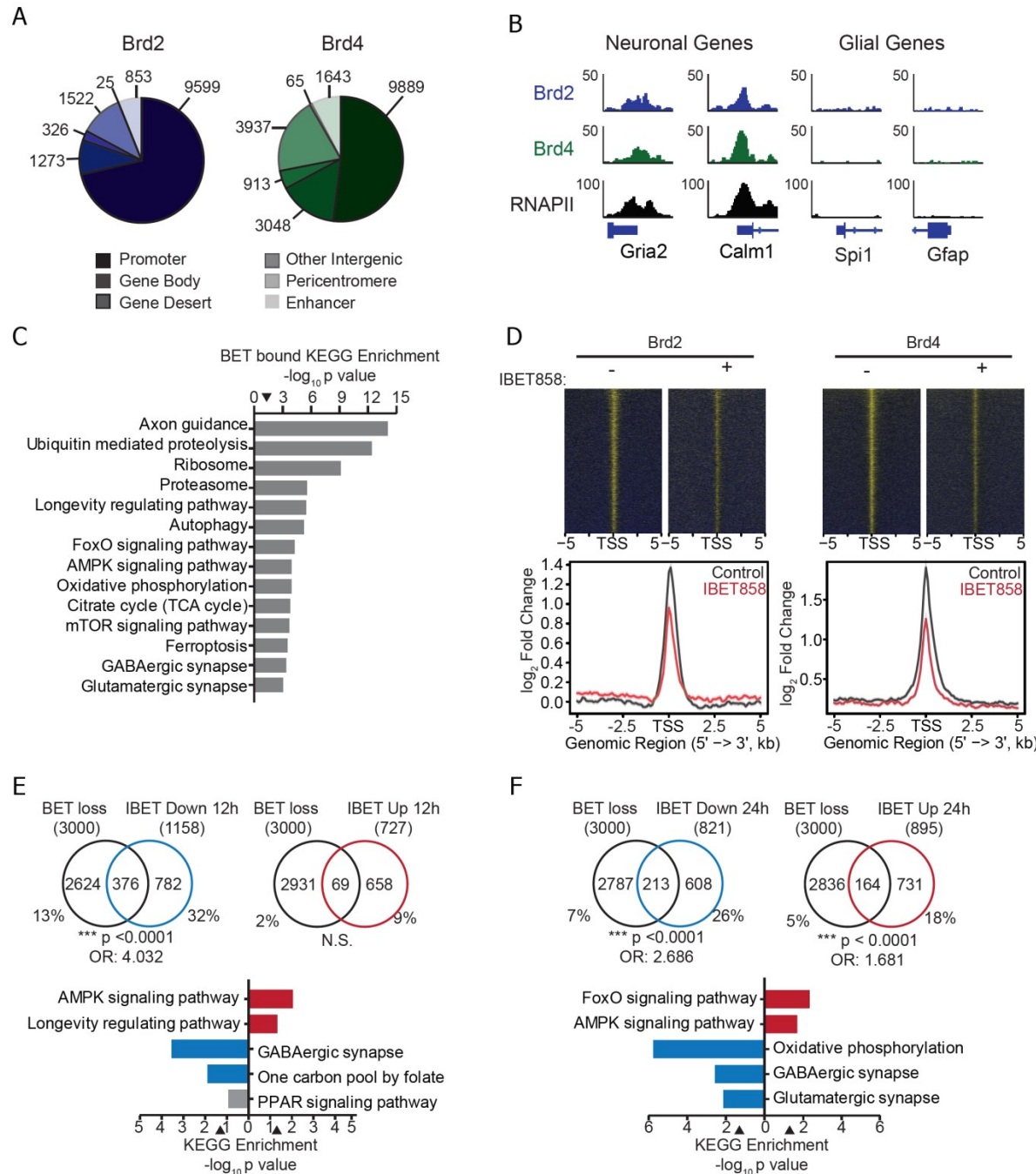
BETs directly regulate anabolic and catabolic gene expression

While the defined transcriptional changes after BET inhibition strongly correlated with observed changes in cellular phenotype, it is possible that these are secondary to the loss of BET binding, particularly because of the extended treatment duration. To understand if these changes were primarily caused by the loss of BET activity, chromatin immunoprecipitation coupled with sequencing was used to determine which genes 1) are directly bound by BET proteins in neurons and 2) lose BET binding after I-BET858.

Similar to other cell types, Brd2 and Brd4 were primarily bound to promoters in wild-type neurons (Brd2: 9599/13598 peaks, 71%, Brd4: 9889/19495 peaks, 51%)(Fig. 7A), and approximately half of these loci (56%, 4748) were co-bound by Brd2 and Brd4. BETs were bound to RNAPII-associated promoters in neurons in contrast to non-expressed glial genes such as *Spi1* and *Gfap* (Fig. 7B). Additionally, BET proteins displayed modest, intermittent binding along gene bodies (10-20% of loci) and were

present at numerous intergenic sites including enhancers, 853 and 1643 respectively (Fig. 7A). In terms of function, BET-bound genes encode proteins that regulate synapse development but also metabolic pathways, such as mTOR signaling and oxidative phosphorylation, and longevity regulating pathways including autophagy, FOXO and AMPK signaling (Fig. 7C).

Because BET proteins have been reported to both activate [59,60] and repress [254,262,263] transcription, it is possible the observed transcriptomic changes are due to direct inhibition/loss of BET proteins from the chromatin. In support of this notion, a significant number of the genes either up- or down-regulated (Up: 48%, 351/727, Down: 57%, 665/1158) after 12h I-BET858 were bound by Brd2 or Brd4. This pattern of BET binding, therefore, supports a role for BET-dependent transcription in both anabolic and catabolic cellular processes. Moreover, acute BET inhibition (6h, 1 μM) in primary cortical neurons at day 7 decreased Brd2 and Brd4 occupancy at 3000 individual promoters (Fig. 7D). A significant fraction of genes suppressed by I-BET858 at 12 (Fig. 6E, 32%, 376/1158) and 24 h (Fig. 6F, 26%, 213/821) lost BET binding after I-BET858 confirming direct control of synaptic and metabolic gene expression by the BET protein family (Fig. 7E, F). Additionally, BETs were displaced from 18% of I-BET858 induced genes at 24 h including *Sirt1, Hspa4,* and *Ulk2.* Together, this confirms the transcriptional and subsequent metabolic reprogramming initiated by BET inhibition in neurons is a direct result of BET displacement from selected gene loci.

Figure 7. Genome-wide distribution of Brd2 and Brd4 before and after I-BET858. (A) Chromatin immunoprecipitation coupled with sequencing (ChIP-Seq) reveals the genomic distribution of Brd2 and Brd4 in primary cortical neurons at day 7 *in vitro*. (B) Representative traces of ChIP-Seq counts for Brd2, Brd4, and RNAPII at neuronal (*Gria2, Calm1*) and glial (*Spi1, Gfap*) promoters. (C) KEGG pathway enrichment for Brd2 or Brd4 bound promoters. (D) Chip-Seq for Brd2 and Brd4 after 6h of vehicle or I-BET858 (1 µM) at day 7 *in vitro.* Heatmaps (top) and NGS plots (bottom) of gene promoters that decrease Brd2 or Brd4 binding. (E-F) Venn overlaps of differential gene expression after 12 (E) and 24h (F) of I-BET858 with genes that lose BET binding. Bar graphs indicate pathway enrichment of genes shared between differential transcriptome and Chip-Seq analyses. Arrows indicate significance cutoff of p=0.05.

97

BET proteins, therefore, control the metabolic state of neurons and inhibition of these proteins significantly improves neuronal survival.

Discussion

Currently, there are no therapies to prevent, reverse, or even halt cognitive decline in neurodegeneration. Understanding the factors that regulate neuronal survival is therefore essential both biologically and clinically as our population ages and the incidence of neurodegenerative disease increases. Here we identify a novel role for the BET proteins in the negative regulation of neuronal survival. We show that pharmacological BET inhibition progressively alters neuronal gene networks, leading to a decline in glycolysis and mitochondrial respiration and concomitant induction of pro-longevity and protein degradation pathways. Furthermore, BET inhibition dramatically increases neuronal longevity and resistance to toxic substances *in vitro* and *in vivo*. We propose the protective effect of I-BET858 arises from a multifactorial process that causes a metabolic switch in neuronal cell state similar to that observed after mTOR inhibition.

Previous findings support a role for BET proteins in metabolic control. Brd4 directly interacts with metabolic enzymes within the purine and folate synthesis pathways [264,265], both of which are suppressed in neurons after I-BET858. Notably, BET inhibition decreases mitochondrial respiration in cardiac tissue [266] and increases fatty acid oxidation in pancreatic cells [263]. This reflects our findings in neurons that suggest a

switch in ATP production from glycolysis and oxidative phosphorylation to fatty acid oxidation. This transition may be driven by the decreased expression of *Pparg*, which can itself reprogram cellular metabolism [267] and is a BET target gene [268,269]. In contrast to our findings, BET inhibition increased mitochondrial gene expression in cybrids deficient for Complex 1 which is a more artificial system than primary cells [270]. Nevertheless, this unbiased screen identified the potential of BET inhibition to rewire cellular metabolism, supporting the data presented here. At the same time, autophagy and catabolic processes were increased after I-BET858. BETs bind to catabolic genes in neurons and in other cell types [254,271] and can both activate [59,60] and repress [254,263,270] transcription. Notably, while mTOR inhibition increases autophagy via signaling mechanisms, BET inhibition increases autophagy and protein degradation pathways via gene network induction. Accordingly, the observed BET displacement from both induced and suppressed genes in neurons confirmed a direct role for BET proteins in the transcriptional control of metabolic and proteostatic pathways.

The neuroprotective effect of I-BET858 is similar to, and in some cases even exceeds, that of well-known protective treatments including the mTOR inhibitor, rapamycin, and caloric restriction. In contrast to glutamate antagonism which is immediately protective [272], mTOR and BET inhibition require days to initiate a neuroprotective state. Therefore, while short-term glutamate receptor inhibition can prevent neuronal death, BET-dependent expression of glutamatergic receptors [111,139] is unlikely to be the sole mechanism underlying I-BET858-mediated survival.

Instead, we propose that suppression of distinct anabolic processes, translation and transcription, results in a common metabolic state that affords significant neuroprotection. The convergence onto a shared neuroprotective state is evidenced by the correlation of transcriptional signatures in neurons after BET or mTOR inhibition as well as the magnitude and kinetics of protection conferred by the two inhibitors. Indeed, the majority of rapamycin-sensitive genes are BET-dependent, suggesting BETs may even act downstream of mTOR signaling.

Moreover, I-BET858 also increased the expression of genes encoding negative regulators of the mTOR pathway, including *Sirt1*, *Pten*, and *Prkaa1*, an AMPK subunit. Accordingly, mTOR signaling is decreased after chronic BET inhibition in neurons. In summary, our data suggest that BET inhibition in neurons triggers a metabolic state that mimics that caused by mTOR inhibition. As such, BET inhibition represents a novel and powerful strategy for neuroprotection.

Chapter Six

Overarching Discussion and Future Perspectives

Here we present the role of BET-dependent gene networks in diverse cellular and developmental contexts within the central nervous system. In Chapter 3, we describe BET-mediated transcriptional control of long, synaptic genes implicated in Autism Spectrum disorder. Dysregulation of these networks during development causes an autism-like phenotype in young mice providing support to the proposed epigenetic mechanism underlying ASD. In Chapter 4, we show that BET proteins are required for microglia-mediated inflammation. Pharmacological inhibition of the BET proteins prevents neurodegeneration in various mouse models which is at least partly due to blunted pro-inflammatory microglia activity. Lastly, in Chapter 5, we elucidate a novel role for the BET proteins as negative regulators of neuronal survival. While these roles may appear disparate, these data highlight the central function of BET proteins in the definition and regulation of transcriptional networks in response to cellular stimuli. This is in accordance with other data that show BETs regulate the induction of cell-type and stimulus-specific gene expression in peripheral cells [1,273]. These diverse roles for BETs in neurodevelopment, inflammation, and neurodegeneration can be unified by applying the attractor state model of gene network regulation, which has been widely discussed in the context of differentiation.

Autism spectrum disorder as a novel cellular attractor states
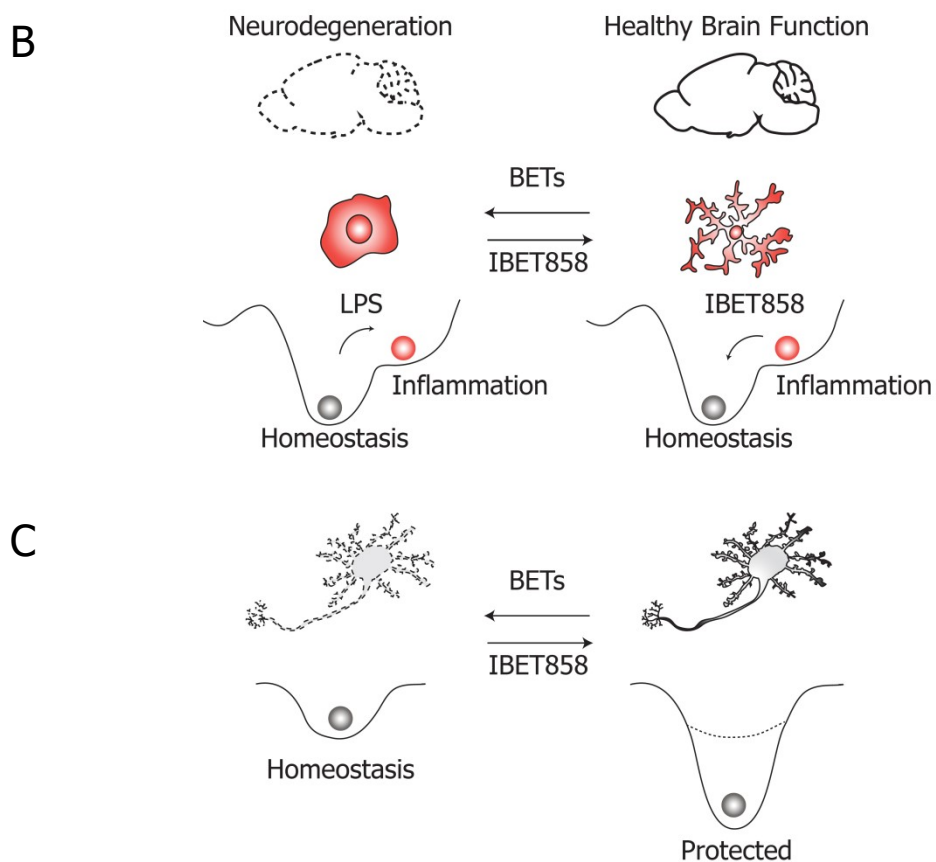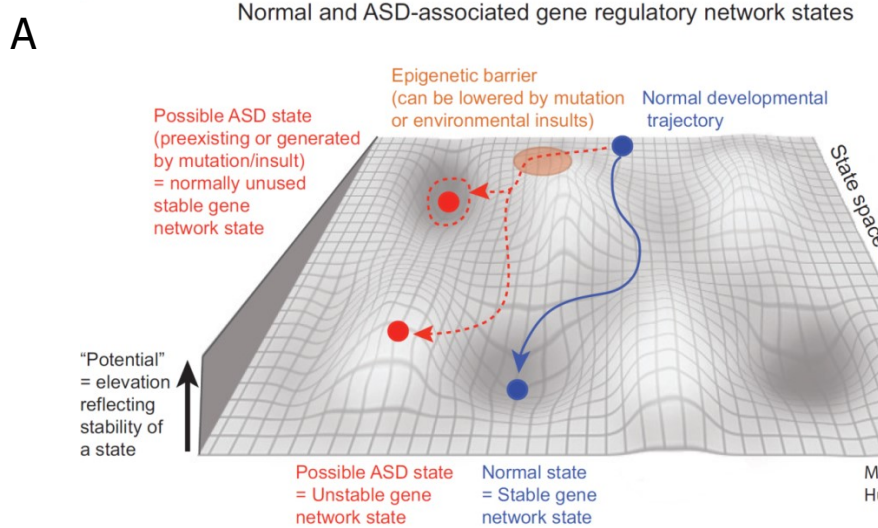
In ASD it is unclear how the many diverse mutations in genes that encode synaptic and transcriptional regulators converge onto the same phenotypes [9,13]. Here we show that altering transcriptional efficiency in developing neurons disrupts synaptic gene networks and leads to an autism-like phenotype [139] similar to that induced by direct loss of synaptic proteins like Shank3 [133]. If we consider the idea of attractor states, which, in physics, would be defined by low potential energy, we can begin to understand how diverse mutations act as different signals that drive neuronal development towards a common disease state [15].

Gene expression is a complex, dynamic system where the coordinated transcription of thousands of individual genes gives rise to a particular cell state or function [274]. While a cell can theoretically express any combination of the 20,000 genes in the genome, not all of these gene networks lead to a viable or stable cell state [16]. Thinking of gene networks and their associated stability, we can imagine a landscape with hills, which have high potential energy, and valleys with low potential energy, representing unstable and stable states respectively.

Perhaps the best-known example of this notion is Waddington's epigenetic landscape, where the metaphor of a ball rolling down a hill into deep valleys is used to explain the cellular differentiation process. A multipotent stem cell, beginning at the top of the metaphorical hill, follows a "canalization" process towards a specific outcome

which is guided by exposure to both external and internal signals [275]. As differentiation proceeds, the now progenitor cell is drawn towards terminal differentiation as a mature cell type such as a medium spiny neuron. This process is defined by the precise coordination of specific transcription factors [6], gene regulatory networks [2,4], and epigenetic modifiers [16,17] that maintain and enforce the cell state.

These attractor states are the defined, common outcome of numerous interactions within any given network [276]. For example, progenitor cells in culture stimulated with different signals will reach the same differentiation state because the gene expression networks, despite being initiated by distinct signaling pathways, eventually converge onto the same attractor state or transcriptional profile [277]. However, these attractor states can be hijacked during disease like the case of malignancy, where mutations in various, discrete genes cause the same immortal and invasive cell state similar that observed in cancer [278–280]. In this model, mutations or environmental factors contributing to ASD risk could lower the barriers defining cell states and divert the neuron from its typical developmental trajectory towards a new neuronal attractor state that induces the formation of a unique phenotype (Figure 1A) [280,281]. This model switches the focus from the impact of individual genes to ASD pathology towards that of impaired gene regulatory networks. Importantly, these ASD attractor states could be stable or unstable and, if so, the induced phenotype may be reversible.

Figure 1. BET-dependent control of neuronal attractor states. (A) Complex gene networks projected onto a two-dimensional state space where the y axis represents relative stability. Typical neuronal developmental follows a defined trajectory (blue) to a stable state. BET inhibition (orange area) alters neuronal gene networks such that the developmental trajectory is shifted to an abnormal ASD attractor state (red dashed arrow). (B) Upon an inflammatory stimulus, microglial gene networks shift homeostatic state to a new state space which is prevented by I-BET858. (C) BET inhibition suppresses metabolic gene networks, revealing a latent, protected attractor state.

This is supported by recent studies including the data presented here that report reversal of transcriptional and behavioral changes after reinstating ASD risk gene function in the adult brain [139,282–285]. Given this model, it would be interesting to understand how BET inhibition alters gene expression on a single cell level because cortical cultures contain heterogeneous neuron subtypes similar to that observed in the cortex *in vivo* [286]. If BET inhibition induces a new attractor state, these neuron subtype-specific gene expression profiles may be replaced or superseded by a common transcriptional profile.

In accordance with the BET-dependent regulation of synaptic gene expression presented in Chapter 3, BET inhibition delays the development of neuronal firing *in vitro* that eventually normalizes in Chapter 5. Others have also shown the requirement of BET activity for proper dendritic and spine development [107,146]. These data provide a crucial functional link between the observed transcriptional and behavioral changes discussed previously and highlight the need for more investigation. Remarkably, despite the significant down-regulation of solute-carriers, ion channels and neurotransmitter receptors, I-BET858 treated neurons exhibit wild-type levels of electrical activity after recovering from this initial developmental delay. As such, there must be robust mechanisms of homeostatic plasticity that compensate for the loss of these channels and receptors and it would be interesting to investigate the mechanism underlying this phenomenon. This highlights the critical importance of neuronal activity such that even in a starvation-like state, appropriate electrical activity is maintained.

Inflammation as an attractor state

The attractor state framework is useful because it can apply to any cell state that is defined by transcriptional networks. For instance, during homeostasis microglia, the brain's immune cells, survey neuronal tissues in a quiescent state which is directed by a unique transcriptional profile [172]. When an injury is sensed, microglia completely switch morphology, function and gene expression profiles [171,274]. Instead of expressing actin polymerization genes, microglia now induce the expression of a wide array of cytokines and chemokines which would be expressed only modestly in a homeostatic state. The state space of the microglia completely changed in response to an external stimulus. Within this context, we show in Chapter 4 that BET inhibition, rather than inducing a pathological attractor state, restrains inflammation and promotes a homeostatic state in microglia (Fig. 1B).

While several mechanisms including the recruitment of super-enhancers have been proposed for the BET-dependent regulation of cytokine gene expression in peripheral immune cells [1,155,273], the present study does not offer much insight into how BET proteins specifically regulate the expression of inflammatory genes in microglia. Unlike BET-dependent genes in neurons, the genes sensitive to BET inhibition in microglia are not of extended length (data not shown). As in peripheral macrophages [1], interferon- and TNF-inducible genes are especially susceptible to BET inhibition in microglia while NFkB genes are largely IBET-insensitive. Going forward, it will be

essential to understand how BET proteins are recruited to the chromatin during inflammation and why selective loci preferentially lose BET binding after I-BET858.

Neuronal survival as an attractor state

In Chapter 5, we show that BET proteins negatively regulate neuronal survival. BET inhibition induces a protected neuronal state defined by low metabolic activity and high protein degradation remarkably similar to that caused by caloric restriction or mTOR inhibition (Fig. 1C). It is important to note that there are numerous examples of I-BET858-mediated alterations that may increase neuronal survival on their own such as increased *Sirt1* [287], *Gdf11* [288], or aspartate [289,290] or decreased *CCR5* [291]. For the sake of brevity, we described a few of these changes to illustrate the depth/breadth of the pro-survival phenotype induced by I-BET858 but did not provide an exhaustive list. Any one of these impacts is worthy of study in its own right; however, we propose that these changes are properties of an emergent, neuroprotective attractor state. Similar to the ASD attractor state, we hope to focus on the totality of the cellular state rather than one particular gene or pathway. As such, this neuroprotective attractor state may explain how CR and rapamycin lead to the same cellular phenotype as I-BET858 despite entirely different mechanisms of action.

The commonality of these states suggests that existing natural systems may employ mechanisms to alter BET activity as an endogenous strategy to promote

survival. Supporting this, Brd2 is shuttled out of the nucleus in response to serum

withdrawal in drosophila [292]. Additionally, a naturally-occurring inhibitor of the BET

proteins was recently identified [293]. Our data suggest that high BET protein activity may

contribute to the vulnerability of distinct neuronal populations by regulating metabolic

gene expression. This indicates that there may, in turn, be protected neuron subtypes

which we would predict to be low in BET expression. For example, pacemaker cells that

regulate breathing may be metabolically less active and show little to no BET

expression. While more work is necessary to elucidate these mechanisms, it is highly

possible that natural mechanisms exist to inhibit BET-dependent transcription in times

of stress.

The neuroprotective effect of BET inhibition *in vitro* is likely neuron-intrinsic

because pharmacological depletion of microglia from neuronal cultures did not alter

neuronal survival after I-BET858 (data not shown). However, it is unclear how I-BET858

increases neuronal survival in the P25 mouse model of neurodegeneration described in

Chapter 4. It is possible that the two I-BET858-initiated states (e.g. decreased

inflammation and increased neuronal resilience) synergize to afford protection *in vivo.*

Interestingly, BET inhibition in microglia also suppresses metabolic gene expression

(*Bcat1, Igf1, Me3, and Lpl*) and induces protein degradation pathways (*Ulk2, Atg12/14,*

and Hspa1a/1b) in addition to preventing inflammatory gene expression. This suggests

that BET control of metabolic gene expression is not neuron-specific and that any cell

type could be metabolic reprogrammed by I-BET858. The exact outcome of this

rewiring may then depend on the cell type rather than BET activity, perhaps leading to blunted inflammation in microglia but increased lifespan in neurons.

It is also possible that, given the cognate interactions between neurons and glial cells, that the neuroprotective state caused by I-BET858 may increase neurotrophic support by glia, independent of BET activity. Specifically, the pro-longevity factor *Gdf11,* which is mainly produced by astrocytes [288], is increased in neuronal cultures after I-BET858. Although astrocytes are fewer than 5% of all cells in our culture, it would interesting to determine which cell type, neurons or astrocytes, stimulates *Gdf11* expression after BET inhibition.

In Conclusion

In conclusion, our data elucidate previously unknown roles for BET proteins in the central nervous system and provide critical support to the idea that Autism Spectrum Disorders may arise from an epigenetic rather than synaptic mechanism. We identify for the first time in neurons, the direct gene targets of Brd2 and Brd4 which likely have unique functions. Lastly, this work identifies BET inhibition as a promising and multifunctional therapeutic strategy for neurodegenerative disease.

References

1. Nicodeme, E. *et al.* Suppression of inflammation by a synthetic histone mimic. *Nature* **468**, 1119–1123 (2010).

2. Heiman, M. *et al.* A Translational Profiling Approach for the Molecular Characterization of CNS Cell Types. *Cell* **135**, 738–748 (2008).

3. Zeisel, A. *et al.* Molecular Architecture of the Mouse Nervous System Resource Molecular Architecture of the Mouse Nervous System. *Cell* **174**, 999-1014.e22 (2018).

4. Doyle, J. P. *et al.* Application of a Translational Profiling Approach for the Comparative Analysis of CNS Cell Types. *Cell* **135**, 749–762 (2008).

5. Gokce, O. *et al.* Cellular Taxonomy of the Mouse Striatum as Revealed by Single-Cell RNA-Seq. *Cell Rep.* **16**, 1126–1137 (2016).

6. Hobert, O. Regulatory logic of neuronal diversity: Terminal selector genes and selector motifs. *Proc. Natl. Acad. Sci.* **105**, 20067–20071 (2008).

7. Hobert, O. Terminal Selectors of Neuronal Identity. in 455–475 (2016). doi:10.1016/bs.ctdb.2015.12.007

8. Hobert, O. Regulation of Terminal Differentiation Programs in the Nervous System. *Annu. Rev. Cell Dev. Biol.* **27**, 681–696 (2011).

9. De Rubeis, S. *et al.* Synaptic, transcriptional and chromatin genes disrupted in autism. *Nature* **515**, 209–215 (2014).

10. An, J.-Y. *et al.* Genome-wide de novo risk score implicates promoter variation in autism spectrum disorder. *Science (80-.).* **362**, eaat6576 (2018).

11. Satterstrom, F. K. *et al.* Large-scale exome sequencing study implicates both developmental and functional changes in the neurobiology of autism. *bioRxiv* 484113 (2018). doi:10.1101/484113

12. Iossifov, I. *et al.* De Novo Gene Disruptions in Children on the Autistic Spectrum. *Neuron* **74**, 285–299 (2012).

13. Zoghbi, H. Y. Postnatal Neurodevelopmental Disorders: Meeting at the Synapse? *Science* **302**, 826–830 (2003).

14. King, I. F. *et al.* Topoisomerases facilitate transcription of long genes linked to autism. *Nature* **501**, 58–62 (2013).

15. Sullivan, J. M., De Rubeis, S. & Schaefer, A. Convergence of spectrums: neuronal gene network states in autism spectrum disorder. *Curr. Opin. Neurobiol.* **59**, 102–111 (2019).

16. von Schimmelmann, M. *et al.* Polycomb repressive complex 2 (PRC2) silences genes responsible for neurodegeneration. *Nat. Neurosci.* **19**, 1321–1330 (2016).

17. Ayata, P. *et al.* Epigenetic regulation of brain region-specific microglia clearance activity. *Nat. Neurosci.* **21**, 1049–1060 (2018).

18. Serrano-Saiz, E., Leyva-Díaz, E., De La Cruz, E. & Hobert, O. BRN3-type POU Homeobox Genes Maintain the Identity of Mature Postmitotic Neurons in Nematodes and Mice. *Curr. Biol.* **28**, 2813-2823.e2 (2018).

19. Wever, I., von Oerthel, L., Wagemans, C. M. R. J. & Smidt, M. P. EZH2 Influences mdDA Neuronal Differentiation, Maintenance and Survival. *Front. Mol. Neurosci.* **11**, 491 (2019).

20. Hervás-Corpión, I. *et al.* Early alteration of epigenetic-related transcription in Huntington's disease mouse models. *Sci. Rep.* **8**, 9925 (2018).

21. CRICK, F. H. On protein synthesis. *Symp. Soc. Exp. Biol.* **12**, 138–63 (1958).

22. Crick, F. Central dogma of molecular biology. *Nature* **227**, 561–3 (1970).

23. Richmond, T. J., Finch, J. T., Rushton, B., Rhodes, D. & Klug, A. Structure of the nucleosome core particle at 7 Å resolution. *Nature* **311**, 532–537 (1984).

24. Olins, A. L. & Olins, D. E. Spheroid chromatin units (v bodies). *Science* **183**, 330–2 (1974).

25. Kornberg, R. D. Chromatin Structure : A Repeating Unit of Histones and DNA Chromatin structure is based on a repeating unit of eight histone molecules and about 200 DNA base pairs. *Science* **184**, 3–6 (1974).

26. Finch, J. T. & Klug, A. Solenoidal model for superstructure in chromatin. *Proc. Natl. Acad. Sci. U. S. A.* **73**, 1897–901 (1976).

27. Hansen, J. C., Lu, X., Ross, E. D. & Woody, R. W. Intrinsic Protein Disorder, Amino Acid Composition, and Histone Terminal Domains. *J. Biol. Chem.* **281**, 1853–1856 (2006).

28. Bannister, A. J. & Kouzarides, T. Regulation of chromatin by histone modifications. *Cell Res.* **21**, 381–395 (2011).

29. Chen, Y. *et al.* Lysine propionylation and butyrylation are novel post-translational modifications in histones. *Mol. Cell. Proteomics* **6**, 812–9 (2007).

30. Farrelly, L. A. *et al.* Histone serotonylation is a permissive modification that enhances TFIID binding to H3K4me3. *Nature* **567**, 535–539 (2019).

31. PHILLIPS, D. M. The presence of acetyl groups of histones. *Biochem. J.* **87**, 258–63 (1963).

32. ALLFREY, V. G., FAULKNER, R. & MIRSKY, A. E. Acetylation and Methylation of Histones and Their Possible Role in the Regulation of Rna Synthesis. *Proc. Natl. Acad. Sci. U. S. A.* **51**, 786–94 (1964).

33. Jenuwein, T. & Allis, C. D. Translating the histone code. *Science* **293**, 1074–80 (2001).

34. Taunton, J., Hassig, C. A. & Schreiber, S. L. A mammalian histone deacetylase related to the yeast transcriptional regulator Rpd3p. *Science* **272**, 408–11 (1996).

35. Brownell, J. E. *et al.* Tetrahymena histone acetyltransferase A: a homolog to yeast Gcn5p linking histone acetylation to gene activation. *Cell* **84**, 843–51 (1996).

36. Tamkun, J. W. *et al.* brahma: A regulator of Drosophila homeotic genes structurally related to the yeast transcriptional activator SNF2SWI2. *Cell* **68**, 561–572 (1992).

37. Dhalluin, C. *et al.* Structure and ligand of a histone acetyltransferase bromodomain. *Nature* **399**, 491–496 (1999).

38. Kim, T. K., Ebright, R. H. & Reinberg, D. Mechanism of ATP-dependent promoter melting by transcription factor IIH. *Science* **288**, 1418–22 (2000).

39. Rasmussen, E. B. & Lis, J. T. In vivo transcriptional pausing and cap formation on three Drosophila heat shock genes. *Proc. Natl. Acad. Sci. U. S. A.* **90**, 7923–7 (1993).

40. Core, L. J., Waterfall, J. J. & Lis, J. T. Nascent RNA sequencing reveals widespread pausing and divergent initiation at human promoters. *Science (80-.).* **322**, 1845–1848 (2008).

41. Kwak, H., Fuda, N. J., Core, L. J. & Lis, J. T. Precise Maps of RNA Polymerase Reveal How Promoters Direct Initiation and Pausing. *Science (80-.).* **339**, 950–953 (2013).

42. Nechaev, S. *et al.* Global Analysis of Short RNAs Reveals Widespread Promoter-Proximal Stalling and Arrest of Pol II in Drosophila. *Science (80-.).* **327**, 335–338 (2010).

43. Komarnitsky, P., Cho, E. J. & Buratowski, S. Different phosphorylated forms of

RNA polymerase II and associated mRNA processing factors during transcription. *Genes Dev.* **14**, 2452–60 (2000).

44. Glover-Cutter, K. *et al.* TFIIH-Associated Cdk7 Kinase Functions in Phosphorylation of C-Terminal Domain Ser7 Residues, Promoter-Proximal Pausing, and Termination by RNA Polymerase II. *Mol. Cell. Biol.* **29**, 5455–5464 (2009).

45. Akhtar, M. S. *et al.* TFIIH Kinase Places Bivalent Marks on the Carboxy-Terminal Domain of RNA Polymerase II. *Mol. Cell* **34**, 387–393 (2009).

46. Wada, T. *et al.* DSIF, a novel transcription elongation factor that regulates RNA polymerase II processivity, is composed of human Spt4 and Spt5 homologs. *Genes Dev.* **12**, 343–56 (1998).

47. Yamaguchi, Y. *et al.* NELF, a multisubunit complex containing RD, cooperates with DSIF to repress RNA polymerase II elongation. *Cell* **97**, 41–51 (1999).

48. Lee, C. *et al.* NELF and GAGA Factor Are Linked to Promoter-Proximal Pausing at Many Genes in Drosophila. *Mol. Cell. Biol.* **28**, 3290–3300 (2008).

49. Muse, G. W. *et al.* RNA polymerase is poised for activation across the genome. *Nat. Genet.* **39**, 1507–1511 (2007).

50. Rougvie, A. E. & Lis, J. T. The RNA polymerase II molecule at the 5' end of the uninduced hsp70 gene of D. melanogaster is transcriptionally engaged. *Cell* **54**, 795–804 (1988).

51. Ahn, S. H., Kim, M. & Buratowski, S. Phosphorylation of serine 2 within the RNA polymerase II C-terminal domain couples transcription and 3' end processing. *Mol. Cell* **13**, 67–76 (2004).

52. Renner, D. B., Yamaguchi, Y., Wada, T., Handa, H. & Price, D. H. A Highly Purified RNA Polymerase II Elongation Control System. *J. Biol. Chem.* **276**, 42601–42609 (2001).

53. Wu, C.-H. *et al.* NELF and DSIF cause promoter proximal pausing on the hsp70 promoter in Drosophila. *Genes Dev.* **17**, 1402–1414 (2003).

54. Peterlin, B. M. & Price, D. H. Controlling the elongation phase of transcription with P-TEFb. *Mol. Cell* **23**, 297–305 (2006).

55. Nguyen, V. T., Kiss, T., Michels, A. A. & Bensaude, O. 7SK small nuclear RNA binds to and inhibits the activity of CDK9/cyclin T complexes. *Nature* **414**, 322–325 (2001).

56. Yang, Z., Zhu, Q., Luo, K. & Zhou, Q. The 7SK small nuclear RNA inhibits the

CDK9/cyclin T1 kinase to control transcription. *Nature* **414**, 317–322 (2001).

57. Michels, A. A. *et al.* MAQ1 and 7SK RNA interact with CDK9/cyclin T complexes in a transcription-dependent manner. *Mol. Cell. Biol.* **23**, 4859–69 (2003).

58. Zhou, Q., Li, T. & Price, D. H. RNA Polymerase II Elongation Control. *Annu. Rev. Biochem.* **81**, 119–143 (2012).

59. Jang, M. K. *et al.* The bromodomain protein Brd4 is a positive regulatory component of P-TEFb and stimulates RNA polymerase II-dependent transcription. *Mol. Cell* **19**, 523–34 (2005).

60. Yang, Z. *et al.* Recruitment of P-TEFb for stimulation of transcriptional elongation by the bromodomain protein Brd4. *Mol. Cell* **19**, 535–45 (2005).

61. Luo, Z. *et al.* The Super Elongation Complex Family of RNA Polymerase II Elongation Factors: Gene Target Specificity and Transcriptional Output. *Mol. Cell. Biol.* **32**, 2608–2617 (2012).

62. Uhlen, M. *et al.* Tissue-based map of the human proteome. *Science (80-.).* **347**, 1260419–1260419 (2015).

63. Filippakopoulos, P. *et al.* Histone Recognition and Large-Scale Structural Analysis of the Human Bromodomain Family. *Cell* **149**, 214–231 (2012).

64. Bisgrove, D. A., Mahmoudi, T., Henklein, P. & Verdin, E. Conserved P-TEFb-interacting domain of BRD4 inhibits HIV transcription. *Proc. Natl. Acad. Sci. U. S. A.* **104**, 13690–5 (2007).

65. Filippakopoulos, P. & Knapp, S. The bromodomain interaction module. *FEBS Lett.* **586**, 2692–704 (2012).

66. Dey, A., Chitsaz, F., Abbasi, A., Misteli, T. & Ozato, K. The double bromodomain protein Brd4 binds to acetylated chromatin during interphase and mitosis. *Proc. Natl. Acad. Sci. U. S. A.* **100**, 8758–63 (2003).

67. LeRoy, G., Rickards, B. & Flint, S. J. The double bromodomain proteins Brd2 and Brd3 couple histone acetylation to transcription. *Mol. Cell* **30**, 51–60 (2008).

68. Morinière, J. *et al.* Cooperative binding of two acetylation marks on a histone tail by a single bromodomain. *Nature* **461**, 664–668 (2009).

69. Vollmuth, F., Blankenfeldt, W. & Geyer, M. Structures of the dual bromodomains of the P-TEFb-activating protein Brd4 at atomic resolution. *J. Biol. Chem.* **284**, 36547–56 (2009).

70. Goudarzi, A. *et al.* Dynamic Competing Histone H4 K5K8 Acetylation and

Butyrylation Are Hallmarks of Highly Active Gene Promoters. *Mol. Cell* **62**, 169–180 (2016).

71.   Shi, J. *et al.* Disrupting the Interaction of BRD4 with Diacetylated Twist Suppresses Tumorigenesis in Basal-like Breast Cancer. *Cancer Cell* **25**, 210–225 (2014).

72.   Gamsjaeger, R. *et al.* Structural basis and specificity of acetylated transcription factor GATA1 recognition by BET family bromodomain protein Brd3. *Mol. Cell. Biol.* **31**, 2632–40 (2011).

73.   Lamonica, J. M. *et al.* Bromodomain protein Brd3 associates with acetylated GATA1 to promote its chromatin occupancy at erythroid target genes. *Proc. Natl. Acad. Sci. U. S. A.* **108**, E159-68 (2011).

74.   Huang, B., Yang, X.-D., Zhou, M.-M., Ozato, K. & Chen, L.-F. Brd4 Coactivates Transcriptional Activation of NF- B via Specific Binding to Acetylated RelA. *Mol. Cell. Biol.* **29**, 1375–1387 (2009).

75.   Houzelstein, D. *et al.* Growth and Early Postimplantation Defects in Mice Deficient for the Bromodomain-Containing Protein Brd4 . *Mol. Cell. Biol.* **22**, 3794–3802 (2002).

76.   Shang, E., Wang, X., Wen, D., Greenberg, D. A. & Wolgemuth, D. J. Double bromodomain-containing gene Brd2 is essential for embryonic development in mouse. *Dev. Dyn.* **238**, 908–17 (2009).

77.   Filippakopoulos, P. *et al.* Selective inhibition of BET bromodomains. *Nature* **468**, 1067–1073 (2010).

78.   Zhan, Y. *et al.* Development of novel cellular histone-binding and chromatin-displacement assays for bromodomain drug discovery. *Epigenetics and Chromatin* **8**, 1–19 (2015).

79.   Picaud, S. *et al.* RVX-208, an inhibitor of BET transcriptional regulators with selectivity for the second bromodomain. *Proc. Natl. Acad. Sci.* **110**, 19754–19759 (2013).

80.   Gacias, M. *et al.* Selective chemical modulation of gene transcription favors oligodendrocyte lineage progression. *Chem. Biol.* **21**, 841–854 (2014).

81.   Sakamoto, K. M. *et al.* Protacs: Chimeric molecules that target proteins to the Skp1-Cullin-F box complex for ubiquitination and degradation. *Proc. Natl. Acad. Sci.* **98**, 8554–8559 (2001).

82.   Lu, J. *et al.* Hijacking the E3 Ubiquitin Ligase Cereblon to Efficiently Target BRD4. *Chem. Biol.* **22**, 755–763 (2015).

83. Winter, G. E. *et al.* Phthalimide conjugation as a strategy for in vivo target protein degradation. *Science (80-.).* **348**, 1376–1381 (2015).

84. Wu, S.-Y., Lee, A.-Y., Lai, H.-T., Zhang, H. & Chiang, C.-M. Phospho switch triggers Brd4 chromatin binding and activator recruitment for gene-specific targeting. *Mol. Cell* **49**, 843–857 (2013).

85. Rahman, S. *et al.* The Brd4 extraterminal domain confers transcription activation independent of pTEFb by recruiting multiple proteins, including NSD3. *Mol. Cell. Biol.* **31**, 2641–52 (2011).

86. Liu, W. *et al.* Brd4 and JMJD6-associated anti-pause enhancers in regulation of transcriptional pause release. *Cell* **155**, 1581–95 (2013).

87. Jiang, Y. W. *et al.* Mammalian mediator of transcriptional regulation and its possible role as an end-point of signal transduction pathways. *Proc. Natl. Acad. Sci.* **95**, 8538–8543 (1998).

88. Lovén, J. *et al.* Selective inhibition of tumor oncogenes by disruption of super-enhancers. *Cell* **153**, 320–334 (2013).

89. Delmore, J. E. *et al.* BET bromodomain inhibition as a therapeutic strategy to target c-Myc. *Cell* **146**, 904–917 (2011).

90. Zhang, W. *et al.* Bromodomain-containing protein 4 (BRD4) regulates RNA polymerase II serine 2 phosphorylation in human CD4+ T cells. *J. Biol. Chem.* **287**, 43137–55 (2012).

91. Anand, P. *et al.* BET Bromodomains Mediate Transcriptional Pause Release in Heart Failure. *Cell* **154**, 569–582 (2013).

92. Di Micco, R. *et al.* Control of Embryonic Stem Cell Identity by BRD4-Dependent Transcriptional Elongation of Super-Enhancer-Associated Pluripotency Genes. *Cell Rep.* **9**, 234–247 (2014).

93. Hsu, S. C. *et al.* The BET Protein BRD2 Cooperates with CTCF to Enforce Transcriptional and Architectural Boundaries. *Mol. Cell* **66**, 102-116.e7 (2017).

94. LeRoy, G. *et al.* Proteogenomic characterization and mapping of nucleosomes decoded by Brd and HP1 proteins. *Genome Biol.* **13**, R68 (2012).

95. Devaiah, B. N. *et al.* BRD4 is a histone acetyltransferase that evicts nucleosomes from chromatin. *Nat. Struct. Mol. Biol.* **23**, 540–548 (2016).

96. Kanno, T. *et al.* BRD4 assists elongation of both coding and enhancer RNAs by interacting with acetylated histones. *Nat. Struct. Mol. Biol.* **21**, 1047–1057 (2014).

97.   Cheung, K. L. *et al.* Distinct Roles of Brd2 and Brd4 in Potentiating the Transcriptional Program for Th17 Cell Differentiation. *Mol. Cell* **65**, 1068-1080.e5 (2017).

98.   Tyler, D. S. *et al.* Click chemistry enables preclinical evaluation of targeted epigenetic therapies. *Science (80-.).* **356**, 1397–1401 (2017).

99.   Dawson, M. A. *et al.* Inhibition of BET recruitment to chromatin as an effective treatment for MLL-fusion leukaemia. *Nature* **478**, 529–533 (2011).

100.   Krumm, N. *et al.* Excess of rare, inherited truncating mutations in autism. *Nat. Genet.* **47**, 582–588 (2015).

101.   Greenberg, D. A. *et al.* Reproducibility and Complications in Gene Searches: Linkage on Chromosome 6, Heterogeneity, Association, and Maternal Inheritance in Juvenile Myoclonic Epilepsy. *Am. J. Hum. Genet.* **66**, 508–516 (2000).

102.   Pal, D. K. *et al.* BRD2 (RING3) Is a Probable Major Susceptibility Gene for Common Juvenile Myoclonic Epilepsy. *Am. J. Hum. Genet.* **73**, 261–270 (2003).

103.   Cavalleri, G. L. *et al.* A Multicenter Study of BRD2 as a Risk Factor for Juvenile Myoclonic Epilepsy. *Epilepsia* **48**, 706–712 (2007).

104.   Lorenz, S. *et al.* Association of BRD2 polymorphisms with photoparoxysmal response. *Neurosci. Lett.* **400**, 135–139 (2006).

105.   Pathak, S., Miller, J., Morris, E. C., Stewart, W. C. L. & Greenberg, D. A. DNA methylation of the *BRD 2* promoter is associated with juvenile myoclonic epilepsy in Caucasians. *Epilepsia* **59**, 1011–1019 (2018).

106.   Schulz, H. *et al.* No evidence for a BRD2 promoter hypermethylation in blood leukocytes of Europeans with juvenile myoclonic epilepsy. *Epilepsia* epi.14657 (2019). doi:10.1111/epi.14657

107.   Bagley, J. A. *et al.* Double-bromo and extraterminal (BET) domain proteins regulate dendrite morphology and mechanosensory function. *Genes Dev.* **28**, 1940–1956 (2014).

108.   Velíšek, L. *et al.* GABAergic Neuron Deficit As An Idiopathic Generalized Epilepsy Mechanism: The Role Of BRD2 Haploinsufficiency In Juvenile Myoclonic Epilepsy. *PLoS One* **6**, e23656 (2011).

109.   Chachua, T. *et al.* Sex-specific behavioral traits in the Brd2 mouse model of juvenile myoclonic epilepsy. *Genes. Brain. Behav.* **13**, 702–12 (2014).

110.   Sartor, G. C., Powell, S. K., Brothers, S. P. & Wahlestedt, C. Epigenetic Readers of Lysine Acetylation Regulate Cocaine-Induced Plasticity. *J. Neurosci.* **35**, 15062–72

(2015).

111. Korb, E., Herre, M., Zucker-Scharff, I., Darnell, R. B. & Allis, C. D. BET protein Brd4 activates transcription in neurons and BET inhibitor Jq1 blocks memory in mice. *Nat. Neurosci.* **18**, 1464–1473 (2015).

112. Sartor, G. C. *et al.* Enhancement of BDNF Expression and Memory by HDAC Inhibition Requires BET Bromodomain Reader Proteins. *J. Neurosci.* **39**, 612–626 (2019).

113. Benito, E. *et al.* The BET/BRD inhibitor JQ1 improves brain plasticity in WT and APP mice. *Transl. Psychiatry* **7**, e1239 (2017).

114. Li, J. *et al.* BET bromodomain inhibition promotes neurogenesis while inhibiting gliogenesis in neural progenitor cells. *Stem Cell Res.* **17**, 212–221 (2016).

115. Jung, K. *et al.* RNA sequencing reveals distinct mechanisms underlying BET inhibitor JQ1-mediated modulation of the LPS-induced activation of BV-2 microglial cells. *J. Neuroinflammation* **12**, 36 (2015).

116. DeMars, K. M., Yang, C., Castro-Rivera, C. I. & Candelario-Jalil, E. Selective degradation of BET proteins with dBET1, a proteolysis-targeting chimera, potently reduces pro-inflammatory responses in lipopolysaccharide-activated microglia. *Biochem. Biophys. Res. Commun.* **497**, 410–415 (2018).

117. Schaefer, A. *et al.* Control of Cognition and Adaptive Behavior by the GLP/G9a Epigenetic Suppressor Complex. *Neuron* **64**, 678–691 (2009).

118. Chen, J. A., Peñagarikano, O., Belgard, T. G., Swarup, V. & Geschwind, D. H. The Emerging Picture of Autism Spectrum Disorder: Genetics and Pathology. *Annu. Rev. Pathol. Mech. Dis.* **10**, 111–144 (2015).

119. Sanchez, R., Meslamani, J. & Zhou, M.-M. The bromodomain: from epigenome reader to druggable target. *Biochim. Biophys. Acta* **1839**, 676–85 (2014).

120. Brès, V., Yoh, S. M. & Jones, K. a. The multi-tasking P-TEFb complex. *Curr. Opin. Cell Biol.* **20**, 334–40 (2008).

121. Barbieri, I., Cannizzaro, E. & Dawson, M. A. Bromodomains as therapeutic targets in cancer. *Brief. Funct. Genomics* **12**, 219–230 (2013).

122. Basu, S. N., Kollu, R. & Banerjee-Basu, S. AutDB: a gene reference resource for autism research. *Nucleic Acids Res.* **37**, D832-6 (2009).

123. Gosmini, R. *et al.* The Discovery of I-BET726 (GSK1324726A), a Potent Tetrahydroquinoline ApoA1 Up-Regulator and Selective BET Bromodomain Inhibitor. *J. Med. Chem.* **57**, 8111–8131 (2014).

124. Theodoulou, N. H. *et al.* Discovery of I-BRD9, a Selective Cell Active Chemical Probe for Bromodomain Containing Protein 9 Inhibition. *J. Med. Chem.* **59**, 1425–1439 (2016).

125. Bacon, C. *et al.* Brain-specific Foxp1 deletion impairs neuronal development and causes autistic-like behaviour. *Mol. Psychiatry* **20**, 632–639 (2015).

126. Ozburn, A. R. *et al.* Direct regulation of diurnal Drd3 expression and cocaine reward by NPAS2. *Biol. Psychiatry* **77**, 425–433 (2015).

127. Qiu, S., Lu, Z. & Levitt, P. MET Receptor Tyrosine Kinase Controls Dendritic Complexity, Spine Morphogenesis, and Glutamatergic Synapse Maturation in the Hippocampus. *J. Neurosci.* **34**, 16166–16179 (2014).

128. Zhou, Y. D. *et al.* Molecular characterization of two mammalian bHLH-PAS domain proteins selectively expressed in the central nervous system. *Proc. Natl. Acad. Sci. U. S. A.* **94**, 713–8 (1997).

129. Park, H. & Poo, M. Neurotrophin regulation of neural circuit development and function. *Nat. Rev. Neurosci.* **14**, 7–23 (2013).

130. Alder, J. *et al.* Brain-Derived Neurotrophic Factor-Induced Gene Expression Reveals Novel Actions of VGF in Hippocampal Synaptic Plasticity. *J. Neurosci.* **23**, 10800–10808 (2003).

131. Calella, A. M. *et al.* Neurotrophin/Trk receptor signaling mediates C/EBPalpha, -beta and NeuroD recruitment to immediate-early gene promoters in neuronal cells and requires C/EBPs to induce immediate-early gene transcription. *Neural Dev.* **2**, 4 (2007).

132. Di Martino, A. *et al.* Aberrant striatal functional connectivity in children with autism. *Biol. Psychiatry* **69**, 847–56 (2011).

133. Peça, J. *et al.* Shank3 mutant mice display autistic-like behaviours and striatal dysfunction. *Nature* **472**, 437–442 (2011).

134. Rothwell, P. E. *et al.* Autism-Associated Neuroligin-3 Mutations Commonly Impair Striatal Circuits to Boost Repetitive Behaviors. *Cell* **158**, 198–212 (2014).

135. Gabel, H. W. *et al.* Disruption of DNA-methylation-dependent long gene repression in Rett syndrome. *Nature* **522**, 89–93 (2015).

136. Patel, M. C. *et al.* BRD4 coordinates recruitment of pause release factor P-TEFb and the pausing complex NELF/DSIF to regulate transcription elongation of interferon-stimulated genes. *Mol. Cell. Biol.* **33**, 2497–507 (2013).

137. Jonkers, I. & Lis, J. T. Getting up to speed with transcription elongation by RNA

polymerase II. *Nat. Rev. Mol. Cell Biol.* **16**, 167–177 (2015).

138. Ellegood, J. & Crawley, J. N. Behavioral and Neuroanatomical Phenotypes in Mouse Models of Autism. *Neurotherapeutics* **12**, 521–533 (2015).

139. Sullivan, J. M. *et al.* Autism-like syndrome is induced by pharmacological suppression of BET proteins in young mice. *J. Exp. Med.* **212**, 1771–1781 (2015).

140. Iossifov, I. *et al.* The contribution of de novo coding mutations to autism spectrum disorder. *Nature* **515**, 216–221 (2014).

141. Sanders, S. J. *et al.* Insights into Autism Spectrum Disorder Genomic Architecture and Biology from 71 Risk Loci. *Neuron* **87**, 1215–1233 (2015).

142. Katayama, Y. *et al.* CHD8 haploinsufficiency results in autistic-like phenotypes in mice. *Nature* **537**, 675–679 (2016).

143. Jung, E.-M. *et al.* Arid1b haploinsufficiency disrupts cortical interneuron development and mouse behavior. *Nat. Neurosci.* **20**, 1694–1707 (2017).

144. Zylka, M. J., Simon, J. M. & Philpot, B. D. Gene Length Matters in Neurons. *Neuron* **86**, 353–355 (2015).

145. Zhao, Y.-T. *et al.* Long genes linked to autism spectrum disorders harbor broad enhancer-like chromatin domains. *Genome Res.* **28**, 933–942 (2018).

146. Korb, E. *et al.* Excess Translation of Epigenetic Regulators Contributes to Fragile X Syndrome and Is Alleviated by Brd4 Inhibition. *Cell* **170**, 1209-1223.e20 (2017).

147. Bartholomeeusen, K., Xiang, Y., Fujinaga, K. & Peterlin, B. M. Bromodomain and extra-terminal (BET) bromodomain inhibition activate transcription via transient release of positive transcription elongation factor b (P-TEFb) from 7SK small nuclear ribonucleoprotein. *J. Biol. Chem.* **287**, 36609–16 (2012).

148. Liu, P. *et al.* Release of Positive Transcription Elongation Factor b (P-TEFb) from 7SK Small Nuclear Ribonucleoprotein (snRNP) Activates Hexamethylene Bisacetamide-inducible Protein (HEXIM1) Transcription. *J. Biol. Chem.* **289**, 9918–9925 (2014).

149. Bayer, S. A., Yackel, J. W. & Puri, P. S. Neurons in the rat dentate gyrus granular layer substantially increase during juvenile and adult life. *Science* **216**, 890–2 (1982).

150. Cameron, H. A., Woolley, C. S., McEwen, B. S. & Gould, E. Differentiation of newly born neurons and glia in the dentate gyrus of the adult rat. *Neuroscience* **56**, 337–44 (1993).

151. Guerreiro, R. *et al.* TREM2 Variants in Alzheimer's Disease. *N. Engl. J. Med.* **368**, 117–27 (2013).

152. Jonsson, T. *et al.* Variant of TREM2 associated with the risk of Alzheimer's disease. *N. Engl. J. Med.* **368**, 107–16 (2013).

153. Naj, A. C. *et al.* Common variants at MS4A4/MS4A6E, CD2AP, CD33 and EPHA1 are associated with late-onset Alzheimer's disease. *Nat. Genet.* **43**, 436–41 (2011).

154. Hollingworth, P. *et al.* Common variants at ABCA7, MS4A6A/MS4A4E, EPHA1, CD33 and CD2AP are associated with Alzheimer's disease. *Nat. Genet.* **43**, 429–35 (2011).

155. Tasdemir, N. *et al.* BRD4 connects enhancer remodeling to senescence immune surveillance. *Cancer Discov.* **6**, 613–629 (2016).

156. Ginhoux, F. *et al.* Fate Mapping Analysis Reveals That Adult Microglia Derive from Primitive Macrophages. *Science (80-.).* **330**, 841–845 (2010).

157. Schulz, C. *et al.* A lineage of myeloid cells independent of Myb and hematopoietic stem cells. *Science* **336**, 86–90 (2012).

158. Kierdorf, K. *et al.* Microglia emerge from erythromyeloid precursors via Pu.1- and Irf8-dependent pathways. *Nat. Neurosci.* **16**, 273–80 (2013).

159. Gomez Perdiguero, E. *et al.* Tissue-resident macrophages originate from yolk-sac-derived erythro-myeloid progenitors. *Nature* **518**, 547–551 (2015).

160. Nimmerjahn, A., Kirchhoff, F. & Helmchen, F. Resting microglial cells are highly dynamic surveillants of brain parenchyma in vivo. *Science* **308**, 1314–8 (2005).

161. Haynes, S. E. *et al.* The P2Y12 receptor regulates microglial activation by extracellular nucleotides. *Nat. Neurosci.* **9**, 1512–1519 (2006).

162. Hickman, S. E. *et al.* The microglial sensome revealed by direct RNA sequencing. *Nat. Neurosci.* **16**, 1896–1905 (2013).

163. Fourgeaud, L. *et al.* TAM receptors regulate multiple features of microglial physiology. *Nature* **532**, 240–244 (2016).

164. Chu, Y. *et al.* Enhanced synaptic connectivity and epilepsy in C1q knockout mice. *Proc. Natl. Acad. Sci. U. S. A.* **107**, 7975–80 (2010).

165. Schafer, D. P. *et al.* Microglia Sculpt Postnatal Neural Circuits in an Activity and Complement-Dependent Manner. *Neuron* **74**, 691–705 (2012).

166. Trang, T., Beggs, S. & Salter, M. W. Brain-derived neurotrophic factor from

microglia: a molecular substrate for neuropathic pain. *Neuron Glia Biol.* **7**, 99–108 (2011).

167. Ueno, M. *et al.* Layer V cortical neurons require microglial support for survival during postnatal development. *Nat. Neurosci.* **16**, (2013).

168. Parkhurst, C. N. *et al.* Microglia Promote Learning-Dependent Synapse Formation through Brain-Derived Neurotrophic Factor. *Cell* **155**, 1596–1609 (2013).

169. Marín-Teva, J. L. *et al.* Microglia promote the death of developing Purkinje cells. *Neuron* **41**, 535–47 (2004).

170. Sierra, A. *et al.* Microglia Shape Adult Hippocampal Neurogenesis through Apoptosis-Coupled Phagocytosis. *Cell Stem Cell* **7**, 483–495 (2010).

171. Keren-Shaul, H. *et al.* A Unique Microglia Type Associated with Restricting Development of Alzheimer's Disease. *Cell* **169**, 1276-1290.e17 (2017).

172. Gosselin, D. *et al.* An environment-dependent transcriptional network specifies human microglia identity. *Science* **356**, eaal3222 (2017).

173. Piani, D., Frei, K., Do, K. Q., Cuénod, M. & Fontana, A. Murine brain macrophages induced NMDA receptor mediated neurotoxicity in vitro by secreting glutamate. *Neurosci. Lett.* **133**, 159–62 (1991).

174. Frakes, A. E. *et al.* Microglia induce motor neuron death via the classical NF-κB pathway in amyotrophic lateral sclerosis. *Neuron* **81**, 1009–1023 (2014).

175. Tansey, M. G. & Goldberg, M. S. Neuroinflammation in Parkinson's disease: Its role in neuronal death and implications for therapeutic intervention. *Neurobiol. Dis.* **37**, 510–518 (2010).

176. Heneka, M. T. *et al.* Neuroinflammation in Alzheimer's disease. *Lancet Neurol.* **14**, 388–405 (2015).

177. Eikelenboom, P. & Stam, F. C. Immunoglobulins and complement factors in senile plaques. An immunoperoxidase study. *Acta Neuropathol.* **57**, 239–42 (1982).

178. Frautschy, S. A. *et al.* Microglial response to amyloid plaques in APPsw transgenic mice. *Am. J. Pathol.* **152**, 307–17 (1998).

179. Akiyama, H. *et al.* Inflammation and Alzheimer's disease. *Neurobiol. Aging* **21**, 383–421

180. McGeer, P. L., Itagaki, S., Tago, H. & McGeer, E. G. Reactive microglia in patients with senile dementia of the Alzheimer type are positive for the histocompatibility glycoprotein HLA-DR. *Neurosci. Lett.* **79**, 195–200 (1987).

181. Rogers, J., Luber-Narod, J., Styren, S. D. & Civin, W. H. Expression of immune system-associated antigens by cells of the human central nervous system: Relationship to the pathology of Alzheimer's disease. *Neurobiol. Aging* **9**, 339–349 (1988).

182. Itagaki, S., McGeer, P. L., Akiyama, H., Zhu, S. & Selkoe, D. Relationship of microglia and astrocytes to amyloid deposits of Alzheimer disease. *J. Neuroimmunol.* **24**, 173–82 (1989).

183. McGeer, E. G. & McGeer, P. L. The role of the immune system in neurodegenerative disorders. *Mov. Disord.* **12**, 855–858 (1997).

184. Itagaki, S. & Mcgeer, P.L. Akiyama, S. Relationship of microglia and astrocytes to amyloid deposits Heb. *J. Chem. Inf. Model.* **53**, 1689–1699 (2013).

185. Barger, S. W. & Harmon, A. D. Microglial activation by Alzheimer amyloid precursor protein and modulation by apolipoprotein E. *Nature* **388**, 878–81 (1997).

186. Lambert, J.-C. *et al.* Genome-wide association study identifies variants at CLU and CR1 associated with Alzheimer's disease. *Nat. Genet.* **41**, 1094–1099 (2009).

187. Li, J., Zhao, L., Urabe, G., Fu, Y. & Guo, L.-W. Epigenetic intervention with a BET inhibitor ameliorates acute retinal ganglion cell death in mice. *Mol. Vis.* **23**, 149–159 (2017).

188. Dey, A. *et al.* BRD4 directs hematopoietic stem cell development and modulates macrophage inflammatory responses. *EMBO J.* **38**, e100293 (2019).

189. Fischer, A., Sananbenesi, F., Pang, P. T., Lu, B. & Tsai, L.-H. Opposing Roles of Transient and Prolonged Expression of p25 in Synaptic Plasticity and Hippocampus-Dependent Memory. *Neuron* **48**, 825–838 (2005).

190. Patrick, G. N. *et al.* Conversion of p35 to p25 deregulates Cdk5 activity and promotes neurodegeneration. *Nature* **402**, 615–622 (1999).

191. Lee, K. Y. *et al.* Elevated neuronal Cdc2-like kinase activity in the Alzheimer disease brain. *Neurosci. Res.* **34**, 21–9 (1999).

192. Swatton, J. E. *et al.* Increased MAP kinase activity in Alzheimer's and Down syndrome but not in schizophrenia human brain. *Eur. J. Neurosci.* **19**, 2711–2719 (2004).

193. Gjoneska, E. *et al.* Conserved epigenomic signals in mice and humans reveal immune basis of Alzheimer's disease. *Nature* **518**, 365–369 (2015).

194. Fischer, A., Sananbenesi, F., Wang, X., Dobbin, M. & Tsai, L.-H. Recovery of

learning and memory is associated with chromatin remodelling. *Nature* **447**, 178–82 (2007).

195. Giusti-Rodríguez, P. *et al.* Synaptic deficits are rescued in the p25/Cdk5 model of neurodegeneration by the reduction of β-secretase (BACE1). *J. Neurosci.* **31**, 15751–6 (2011).

196. Gräff, J. *et al.* An epigenetic blockade of cognitive functions in the neurodegenerating brain. *Nature* **483**, 222–226 (2012).

197. Elmore, M. R. P. *et al.* Colony-Stimulating Factor 1 Receptor Signaling Is Necessary for Microglia Viability, Unmasking a Microglia Progenitor Cell in the Adult Brain. *Neuron* **82**, 380–397 (2014).

198. Liddelow, S. A. *et al.* Neurotoxic reactive astrocytes are induced by activated microglia. *Nature* **541**, 481–487 (2017).

199. Gibson, E. M. *et al.* Methotrexate Chemotherapy Induces Persistent Tri-glial Dysregulation that Underlies Chemotherapy-Related Cognitive Impairment. *Cell* **176**, 43-55.e13 (2019).

200. Matzuk, M. M. *et al.* Small-molecule inhibition of BRDT for male contraception. *Cell* **150**, 673–84 (2012).

201. Magistri, M. *et al.* The BET-Bromodomain Inhibitor JQ1 Reduces Inflammation and Tau Phosphorylation at Ser396 in the Brain of the 3xTg Model of Alzheimer's Disease. *Curr. Alzheimer Res.* **13**, 985–995 (2016).

202. Wang, J. *et al.* BRD4 inhibition attenuates inflammatory response in microglia and facilitates recovery after spinal cord injury in rats. *J. Cell. Mol. Med.* (2019). doi:10.1111/jcmm.14196

203. DeMars, K. M., Yang, C. & Candelario-Jalil, E. Neuroprotective effects of targeting BET proteins for degradation with dBET1 in aged mice subjected to ischemic stroke. *Neurochem. Int.* (2019). doi:10.1016/J.NEUINT.2019.03.004

204. Barrett, E., Brothers, S., Wahlestedt, C. & Beurel, E. I-BET151 selectively regulates IL-6 production. *Biochim. Biophys. Acta - Mol. Basis Dis.* **1842**, 1549–1555 (2014).

205. Sokoloff, L. Energetics of functional activation in neural tissues. *Neurochem. Res.* **24**, 321–9 (1999).

206. Harris, J. J., Jolivet, R. & Attwell, D. Synaptic Energy Use and Supply. *Neuron* **75**, 762–777 (2012).

207. Bruce-Keller, A. J., Umberger, G., McFall, R. & Mattson, M. P. Food restriction

reduces brain damage and improves behavioral outcome following excitotoxic and metabolic insults. *Ann. Neurol.* **45**, 8–15 (1999).

208. Duan, W. & Mattson, M. P. Dietary restriction and 2-deoxyglucose administration improve behavioral outcome and reduce degeneration of dopaminergic neurons in models of Parkinson's disease. *J. Neurosci. Res.* **57**, 195–206 (1999).

209. Yu, Z. F. & Mattson, M. P. Dietary restriction and 2-deoxyglucose administration reduce focal ischemic brain damage and improve behavioral outcome: evidence for a preconditioning mechanism. *J. Neurosci. Res.* **57**, 830–9 (1999).

210. Caccamo, A., Majumder, S., Richardson, A., Strong, R. & Oddo, S. Molecular interplay between mammalian target of rapamycin (mTOR), amyloid-beta, and Tau: effects on cognitive impairments. *J. Biol. Chem.* **285**, 13107–20 (2010).

211. Cole, S. L. & Corday, E. FOUR-MINUTE LIMIT FOR CARDIAC RESUSCITATION. *J. Am. Med. Assoc.* **161**, 1454 (1956).

212. Safar, P. Cerebral resuscitation after cardiac arrest: a review. *Circulation* **74**, IV138-53 (1986).

213. Safar, P. Resuscitation from clinical death: pathophysiologic limits and therapeutic potentials. *Crit. Care Med.* **16**, 923–41 (1988).

214. Latil, M. *et al.* Skeletal muscle stem cells adopt a dormant cell state post mortem and retain regenerative capacity. *Nat. Commun.* **3**, 903 (2012).

215. Pulsinelli, W. A., Brierley, J. B. & Plum, F. Temporal profile of neuronal damage in a model of transient forebrain ischemia. *Ann. Neurol.* **11**, 491–498 (1982).

216. Sims, N. R. Energy metabolism and selective neuronal vulnerability following global cerebral ischemia. *Neurochem. Res.* **17**, 923–931 (1992).

217. Sieber, F. E., Palmon, S. C., Traystman, R. J. & Martin, L. J. Global Incomplete Cerebral Ischemia Produces Predominantly Cortical Neuronal Injury. *Stroke* **26**, 2091–2096 (1995).

218. Wang, X. & Michaelis, E. K. Selective neuronal vulnerability to oxidative stress in the brain. *Front. Aging Neurosci.* **2**, 12 (2010).

219. Frumkin, I. *et al.* Gene Architectures that Minimize Cost of Gene Expression. *Mol. Cell* **65**, 142–153 (2017).

220. Kafri, M., Metzl-Raz, E., Jona, G. & Barkai, N. The Cost of Protein Production. *Cell Rep.* **14**, 22–31 (2016).

221. Pissadaki, E. K. & Bolam, J. P. The energy cost of action potential propagation in

dopamine neurons: clues to susceptibility in Parkinson's disease. *Front. Comput. Neurosci.* **7**, 13 (2013).

222. Pacelli, C. *et al.* Elevated Mitochondrial Bioenergetics and Axonal Arborization Size Are Key Contributors to the Vulnerability of Dopamine Neurons. *Curr. Biol.* **25**, 2349–2360 (2015).

223. Munns, S. E., Meloni, B. P., Knuckeyà, N. W. & Arthur, P. G. Primary cortical neuronal cultures reduce cellular energy utilization during anoxic energy deprivation. *J. Neurochem.* **87**, 764–772 (2003).

224. Giguère, N. *et al.* Increased vulnerability of nigral dopamine neurons after expansion of their axonal arborization size through D2 dopamine receptor conditional knockout. *PLOS Genet.* **15**, e1008352 (2019).

225. Herrero-Mendez, A. *et al.* The bioenergetic and antioxidant status of neurons is controlled by continuous degradation of a key glycolytic enzyme by APC/C–Cdh1. *Nat. Cell Biol.* **11**, 747–752 (2009).

226. Ingram, D. K., Weindruch, R., Spangler, E. L., Freeman, J. R. & Walford, R. L. Dietary Restriction Benefits Learning and Motor Performance of Aged Mice. *J. Gerontol.* **42**, 78–81 (1987).

227. Means, L. W., Higgins, J. L. & Fernandez, T. J. *Mid-Life Onset of Dietary Restriction Extends Life and Prolongs Cognitive Functioning*. *Physiology & Behavior* **54**, (1993).

228. Parikh, I. *et al.* Caloric restriction preserves memory and reduces anxiety of aging mice with early enhancement of neurovascular functions. *Aging (Albany. NY).* **8**, 2814–2826 (2016).

229. Berger, Z. *et al.* Rapamycin alleviates toxicity of different aggregate-prone proteins. *Hum. Mol. Genet.* **15**, 433–442 (2005).

230. Ravikumar, B., Berger, Z., Vacher, C., O'Kane, C. J. & Rubinsztein, D. C. Rapamycin pre-treatment protects against apoptosis. *Hum. Mol. Genet.* **15**, 1209–1216 (2006).

231. Tain, L. S. *et al.* Rapamycin activation of 4E-BP prevents parkinsonian dopaminergic neuron loss. *Nat. Neurosci.* **12**, 1129–1135 (2009).

232. Caccamo, A., Majumder, S., Richardson, A., Strong, R. & Oddo, S. Molecular Interplay between Mammalian Target of Rapamycin (mTOR), Amyloid-β, and Tau. *J. Biol. Chem.* **285**, 13107–13120 (2010).

233. Pearl, R. *The Rate of Living*. (1928).

234. HARMAN, D. Aging: a theory based on free radical and radiation chemistry. *J. Gerontol.* **11**, 298–300 (1956).

235. Sarkar, S., Ravikumar, B., Floto, R. A. & Rubinsztein, D. C. Rapamycin and mTOR-independent autophagy inducers ameliorate toxicity of polyglutamine-expanded huntingtin and related proteinopathies. *Cell Death Differ.* **16**, 46–56 (2009).

236. Lu, C. & Thompson, C. B. Metabolic regulation of epigenetics. *Cell Metab.* **16**, 9–17 (2012).

237. Takahashi, H., McCaffery, J. M., Irizarry, R. A. & Boeke, J. D. Nucleocytosolic Acetyl-Coenzyme A Synthetase Is Required for Histone Acetylation and Global Transcription. *Mol. Cell* **23**, 207–217 (2006).

238. Wellen, K. E. *et al.* ATP-Citrate Lyase Links Cellular Metabolism to Histone Acetylation. *Science (80-.).* **324**, 1076–1080 (2009).

239. Cai, L., Sutter, B. M., Li, B. & Tu, B. P. Acetyl-CoA Induces Cell Growth and Proliferation by Promoting the Acetylation of Histones at Growth Genes. *Mol. Cell* **42**, 426–437 (2011).

240. Donohoe, D. R. *et al.* The Warburg Effect Dictates the Mechanism of Butyrate-Mediated Histone Acetylation and Cell Proliferation. *Mol. Cell* **48**, 612–626 (2012).

241. Lee, J. V. *et al.* Akt-dependent metabolic reprogramming regulates tumor cell Histone acetylation. *Cell Metab.* **20**, 306–319 (2014).

242. Moussaieff, A. *et al.* Glycolysis-Mediated Changes in Acetyl-CoA and Histone Acetylation Control the Early Differentiation of Embryonic Stem Cells. *Cell Metab.* **21**, 392–402 (2015).

243. Vogel, U., Sørensen, M., Pedersen, S., Jensen, K. F. & Kilstrup, M. Decreasing transcription elongation rate in Escherichia coli exposed to amino acid starvation. *Mol. Microbiol.* **6**, 2191–200 (1992).

244. Jona, G., Choder, M. & Gileadi, O. Glucose starvation induces a drastic reduction in the rates of both transcription and degradation of mRNA in yeast. *Biochim. Biophys. Acta* **1491**, 37–48 (2000).

245. Morin, P. & Storey, K. B. Evidence for a reduced transcriptional state during hibernation in ground squirrels. *Cryobiology* **53**, 310–318 (2006).

246. Salem, M., Silverstein, J., Rexroad, C. E., III & Yao, J. Effect of starvation on global gene expression and proteolysis in rainbow trout (Oncorhynchus mykiss). *BMC Genomics* **8**, 328 (2007).

247. Brusés, J. L. & Pilar, G. R. Effect of cycloheximide and mRNA synthesis inhibition

on death of trophically deprived ciliary ganglion neurons in culture. *J. Neurophysiol.* **74**, 2487–99 (1995).

248. Park, D. S., Farinelli, S. E. & Greene, L. A. Inhibitors of Cyclin-dependent Kinases Promote Survival of Post-mitotic Neuronally Differentiated PC12 Cells and Sympathetic Neurons. *J. Biol. Chem.* **271**, 8161–8169 (1996).

249. Park, D. S., Morris, E. J., Greene, L. A. & Geller, H. M. G1/S cell cycle blockers and inhibitors of cyclin-dependent kinases suppress camptothecin-induced neuronal apoptosis. *J. Neurosci.* **17**, 1256–70 (1997).

250. Verdaguer, E. *et al.* Inhibition of cell cycle pathway by flavopiridol promotes survival of cerebellar granule cells after an excitotoxic treatment. *J. Pharmacol. Exp. Ther.* **308**, 609–16 (2004).

251. Füllgrabe, J. *et al.* The histone H4 lysine 16 acetyltransferase hMOF regulates the outcome of autophagy. *Nature* **500**, 468–471 (2013).

252. Gong, H. *et al.* Histone modifications change with age, dietary restriction and rapamycin treatment in mouse brain. *Oncotarget* **6**, (2015).

253. Workman, J. J., Chen, H. & Nicholas Laribee, R. Saccharomyces cerevisiae TORC1 controls histone acetylation by signaling through the sit4/PP6 phosphatase to regulate sirtuin deacetylase nuclear accumulation. *Genetics* **203**, 1733–1746 (2016).

254. Sakamaki, J. ichi *et al.* Bromodomain Protein BRD4 Is a Transcriptional Repressor of Autophagy and Lysosomal Function. *Mol. Cell* **66**, 517-532.e9 (2017).

255. Swindell, W. R. Genes and gene expression modules associated with caloric restriction and aging in the laboratory mouse. *BMC Genomics* **10**, 585 (2009).

256. Kramer, N. J. *et al.* CRISPR-Cas9 screens in human cells and primary neurons identify modifiers of C9ORF72 dipeptide-repeat-protein toxicity. *Nat. Genet.* **50**, 603–612 (2018).

257. Aras, M. A., Hartnett, K. A. & Aizenman, E. Assessment of Cell Viability in Primary Neuronal Cultures. in *Current Protocols in Neuroscience* 7.18.1-7.18.15 (John Wiley & Sons, Inc., 2008). doi:10.1002/0471142301.ns0718s44

258. Li, N. *et al.* Mitochondrial complex I inhibitor rotenone induces apoptosis through enhancing mitochondrial reactive oxygen species production. *J. Biol. Chem.* **278**, 8516–25 (2003).

259. Howitz, K. T. *et al.* Small molecule activators of sirtuins extend Saccharomyces cerevisiae lifespan. *Nature* **425**, 191–196 (2003).

260. Cantó, C. *et al.* AMPK regulates energy expenditure by modulating NAD+ metabolism and SIRT1 activity. *Nature* **458**, 1056–60 (2009).

261. Saxton, R. A. & Sabatini, D. M. mTOR Signaling in Growth, Metabolism, and Disease. *Cell* **168**, 960–976 (2017).

262. Banerjee, C. *et al.* BET bromodomain inhibition as a novel strategy for reactivation of HIV-1. *J. Leukoc. Biol.* **92**, 1147–1154 (2012).

263. Deeney, J. T., Belkina, A. C., Shirihai, O. S., Corkey, B. E. & Denis, G. V. BET Bromodomain Proteins Brd2, Brd3 and Brd4 Selectively Regulate Metabolic Pathways in the Pancreatic β-Cell. *PLoS One* **11**, e0151329 (2016).

264. Sudhamalla, B., Dey, D., Breski, M., Nguyen, T. & Islam, K. Site-specific azide-acetyllysine photochemistry on epigenetic readers for interactome profiling. *Chem. Sci.* **8**, 4250–4256 (2017).

265. Sdelci, S. *et al.* MTHFD1 interaction with BRD4 links folate metabolism to transcriptional regulation. *Nat. Genet.* **51**, 990–998 (2019).

266. Piquereau, J. *et al.* The BET Bromodomain Inhibitor I-BET-151 Induces Structural and Functional Alterations of the Heart Mitochondria in Healthy Male Mice and Rats. *Int. J. Mol. Sci.* **20**, 1527 (2019).

267. Angela, M. *et al.* Fatty acid metabolic reprogramming via mTOR-mediated inductions of PPARγ directs early activation of T cells. *Nat. Commun.* **7**, 13683 (2016).

268. Wang, F. *et al.* Brd2 disruption in mice causes severe obesity without Type 2 diabetes. *Biochem. J.* **425**, 71–85 (2010).

269. Brown, J. D. *et al.* BET bromodomain proteins regulate enhancer function during adipogenesis. *Proc. Natl. Acad. Sci. U. S. A.* **115**, 2144–2149 (2018).

270. Barrow, J. J. *et al.* Bromodomain Inhibitors Correct Bioenergetic Deficiency Caused by Mitochondrial Disease Complex I Mutations. *Mol. Cell* **64**, 163–175 (2016).

271. Segatto, M. *et al.* Epigenetic targeting of bromodomain protein BRD4 counteracts cancer cachexia and prolongs survival. *Nat. Commun.* **8**, 1707 (2017).

272. Ankarcrona, M. *et al. Glutamate-Induced Neuronal Death: A Succession of Necrosis or Apoptosis Depending on Mitochondrial Function*. *Neuron* **15**, (1995).

273. Hargreaves, D. C., Horng, T. & Medzhitov, R. Control of Inducible Gene Expression by Signal-Dependent Transcriptional Elongation. *Cell* **138**, 129–145 (2009).

274. Pope, S. D. & Medzhitov, R. Emerging Principles of Gene Expression Programs and Their Regulation. *Mol. Cell* **71**, 389–397 (2018).

275. Waddington, C. H. Canalization of Development and Genetic Assimilation of Acquired Characters. *Nature* **150**, 563–565 (1942).

276. MacArthur, B. D., Ma'ayan, A. & Lemischka, I. R. Systems biology of stem cell fate and cellular reprogramming. *Nat. Rev. Mol. Cell Biol.* **10**, 672–681 (2009).

277. Huang, S., Eichler, G., Bar-Yam, Y. & Ingber, D. E. Cell Fates as High-Dimensional Attractor States of a Complex Gene Regulatory Network. *Phys. Rev. Lett.* **94**, 1–4 (2005).

278. Huang, S., Ernberg, I. & Kauffman, S. Cancer attractors: A systems view of tumors from a gene network dynamics and developmental perspective. *Semin. Cell Dev. Biol.* **20**, 869–876 (2009).

279. Huang, S. & Kauffman, S. How to escape the cancer attractor: rationale and limitations of multi-target drugs. *Semin. Cancer Biol.* **23**, 270–8 (2013).

280. Li, Q. *et al.* Dynamics inside the cancer cell attractor reveal cell heterogeneity, limits of stability, and escape. *Proc. Natl. Acad. Sci. U. S. A.* **113**, 2672–7 (2016).

281. Muñoz-Descalzo, S., de Navascues, J. & Arias, A. M. Wnt-Notch signalling: An integrated mechanism regulating transitions between cell states. *BioEssays* **34**, 110–118 (2012).

282. Guy, J., Gan, J., Selfridge, J., Cobb, S. & Bird, A. Reversal of Neurological Defects in a Mouse Model of Rett Syndrome. *Science (80-.).* **315**, 1143–1147 (2007).

283. Sztainberg, Y. *et al.* Reversal of phenotypes in MECP2 duplication mice using genetic rescue or antisense oligonucleotides. *Nature* **528**, 123–126 (2015).

284. Mei, Y. *et al.* Adult restoration of Shank3 expression rescues selective autistic-like phenotypes. *Nature* **530**, 481–484 (2016).

285. Creson, T. K. *et al.* Re-expression of SynGAP Protein in Adulthood Improves Translatable Measures of Brain Function and Behavior in a Model of Neurodevelopmental Disorders. *bioRxiv* 474965 (2018). doi:10.1101/474965

286. Kriegstein, A. R. & Dichter, M. A. Morphological classification of rat cortical neurons in cell culture. *J. Neurosci.* **3**, 1634–47 (1983).

287. Kim, D. *et al.* SIRT1 deacetylase protects against neurodegeneration in models for Alzheimer's disease and amyotrophic lateral sclerosis. *EMBO J.* **26**, 3169–79 (2007).

288. Katsimpardi, L. *et al.* Vascular and neurogenic rejuvenation of the aging mouse brain by young systemic factors. *Science* **344**, 630–4 (2014).

289. Errico, F. *et al.* Free D-aspartate regulates neuronal dendritic morphology, synaptic plasticity, gray matter volume and brain activity in mammals. *Transl. Psychiatry* **4**, e417–e417 (2014).

290. Krashia, P. *et al.* Persistent elevation of D-Aspartate enhances NMDA receptor-mediated responses in mouse substantia nigra pars compacta dopamine neurons. *Neuropharmacology* **103**, 69–78 (2016).

291. Zhou, M. *et al.* CCR5 is a suppressor for cortical plasticity and hippocampal learning and memory. *Elife* **5**, (2016).

292. Guo, N., Faller, D. V & Denis, G. V. Activation-induced nuclear translocation of RING3. *J. Cell Sci.* **113 (Pt 1**, 3085–91 (2000).

293. Kim, Y. H. *et al.* A natural compound, aristoyagonine, is identified as a potent bromodomain inhibitor by mid-throughput screening. *Biochem. Biophys. Res. Commun.* **503**, 882–887 (2018).